

CORNELL AERONAUTICAL LABORATORY, INC.  
BUFFALO, NEW YORK 14221

CAL REPORT NO. VS-2182-D-4

PROJECT SLOPE  
ANALYSIS OF THE PERFORMANCE OF  
THE LUNAR ORBITER I AND II IMAGING SYSTEMS

PREPARED BY:  
M.J. MAZUROWSKI  
T.M. HOLLADAY  
AND  
R.E. KINZLY

PHASE I FINAL REPORT  
CONTRACT NO. NAS1-5800  
15 SEPTEMBER 1967

PREPARED FOR:  
NATIONAL AERONAUTICS AND SPACE ADMINISTRATION  
LANGLEY RESEARCH CENTER, LANGLEY STATION  
HAMPTON, VIRGINIA 23365

Distribution of this report is provided in the interest of information exchange. Responsibility for the contents resides in the authors or organization that prepared it.

PRECEDING PAGE BLANK NOT FILMED.

### ABSTRACT

The results of an evaluation of the performance of the Lunar Orbiter I and II imaging systems, based upon the quality of the reconstructed photography, is presented. The evaluation procedures were developed during the earlier phases of the study and are reported elsewhere.

The performance of both imaging systems with respect to signal detail rendition was nominal. The noise level measurements yielded data that were smaller than the nominal values, but consistent with the excessive exposures attained on most of the frames analyzed. The data representing the dc signal level response did exhibit some variations, possibly caused by a nonlinear response of the ground reconstruction system or incomplete processing of the film in the spacecraft. In addition, the medium resolution photographic frames were overexposed such that most of the recorded densities are outside the range where sensitometric control is provided.

PRECEDING PAGE BLANK NOT FILMED.

## FOREWORD

This report is the result of evaluation analyses performed during the second and third phases of a continuing contract from NASA Langley Research Center; Contract No. NAS1-5800 monitored by Mr. T. Hansen.

The authors gratefully acknowledge the efforts of R. Breault, T. Gallagher, A. Gehrman, and R. Haas in several data acquisition tasks.

PRECEDING PAGE BLANK NOT FILMED.

TABLE OF CONTENTS

<u>Section</u>		<u>Page</u>
	ABSTRACT . . . . .	iii
	FOREWORD . . . . .	v
1.	INTRODUCTION . . . . .	1
2.	BACKGROUND . . . . .	3
3.	MEASURED VALUES OF THE QUALITY PARAMETERS . . . . .	11
4.	SYSTEM PERFORMANCE CRITERIA . . . . .	25
5.	CONCLUSIONS . . . . .	27
	REFERENCES . . . . .	129

LIST OF FIGURES

<u>Figure No.</u>		<u>Page</u>
1	Lunar Orbiter Photographic Quality Evaluation Flow Diagram . . . . .	28
2-4	Regression Between SO-243 Transmittance and GRE Density - Orbiter I . . . . .	29-31
5-11	Regression Between SO-243 Transmittance and GRE Density - Orbiter II . . . . .	32-38
12	Hurter-Driffield Response Data and Fitted Para- metric Function - Orbiter I High Level Analysis . .	39
13-19	Hurter-Driffield Response Data and Fitted Para- metric Function - Orbiter II . . . . .	40-46
20	Edge Sharpness Response - Orbiter I . . . . .	47
21	Edge Sharpness Response - Orbiter II . . . . .	48
22-25	Scanner-Communications-GRS MTF - Orbiter I . .	49-52
26	Scanner-Communications-GRS MTF - Orbiter II . .	53
27	Medium Resolution Frame 144 - Orbiter I . . . . .	54
28	Selected Crater Shadow Edges - MRF 144 . . . . .	55
29-38	Medium Resolution Imaging System MTF - Orbiter I . . . . .	56-65
39	Medium Resolution Imaging System MTF - Orbiter II . . . . .	66
40	High Resolution Imaging System MTF - Orbiter II . . . . .	67
41-44	Standard Deviation in Measurement of Brightness Longitude - Orbiter I . . . . .	68-71
45-70	Standard Deviation in Measurement of Brightness Longitude - Orbiter II . . . . .	72-97

LIST OF FIGURES (Cont.)

<u>Figure No.</u>		<u>Page</u>
71-74	Signal-to-Noise Ratio for Cone Detection - Orbiter I . . . . .	98-101
75-100	Signal-to-Noise Ratio for Cone Detection - Orbiter II . . . . .	102-127

LIST OF TABLES

<u>Table No.</u>		<u>Page</u>
1A	Mission I Frames Analyzed . . . . .	7
1B	Mission II Frames Analyzed . . . . .	8
2	Relative Log Exposure for Reticule No. 8 . . . . .	13
3A	Average GRE Density Levels - Mission I . . . . .	15
3B	Average GRE Density Levels - Mission II . . . . .	16
4A	Measured Values of Total Noise Power - Mission I Evaluation . . . . .	17
4B	Measured Values of Total Noise Power - Mission II Evaluation . . . . .	18

## 1. INTRODUCTION

The results of an analysis of the quality of the monoscopic photographs received from the Lunar Orbiter I and II spacecraft are presented in this report. They include the measured values of the quality parameters specified in the Phase I Final Report<sup>(1)</sup> and the associated values for the system performance criteria described in the Phase II Final Report<sup>(2)</sup>. This document does not contain a detailed description of the techniques used or a complete discussion of the intermediate results of the analysis. Such descriptions and results can be found in the Phase II Final Report. The purpose of the report is to provide the reader with the results of the mission analyses.

The remainder of this report consists of three sections: a presentation of background information, a description of the measured quality parameters, and a presentation of the resulting system performance criteria. The background section serves to remind the reader of the general classification of quality parameters and the functions or quantities which were selected in each of the classes to describe the quality of the Lunar Orbiter Photographs. In addition, it describes several minor differences in the analysis procedures between Lunar Orbiter I and Lunar Orbiter II.

PRECEDING PAGE BLANK NOT FILMED.

## 2. BACKGROUND

Quality parameters usually can be divided into three general classes; namely, factors which describe signal level, noise level, and signal detail rendition. In order to describe the quality of a Lunar Orbiter photograph, one or more parameters from each of these three classes had to be selected and techniques established whereby these parameters could be measured from the reconstructed GRE film. This was done during the Phase I effort<sup>(1)</sup>.

The factor describing signal level must relate the input dc signal level (exposure on the spacecraft film) to the output signal level (GRE film density). Because of the nonlinear response of the spacecraft film, it is convenient to separate the total response into two functions describing signal level. These are the Hurter-Driffield response curve for the spacecraft film and the linear response characteristic relating the transmittance of the spacecraft film to the recorded GRE density. The step tablet in the pre-exposed edge data array provides a convenient source of data for the measurement of the total response. Measurements are made of average density of each of the nine steps in the step tablet and the corresponding relative exposures obtained from data supplied by the Eastman Kodak Company. The separation of the total response into the two selected functions is accomplished by utilizing "nominal" transmittance values obtained from independent measurements made using a sample of bimat processed film acquired from the same roll which supplied the actual flight film. The relationship between SO-243 transmittance and GRE density is determined by employing statistical fitting techniques on these transmittance values and measured GRE densities. Finally, using the resulting response, measured GRE densities are converted to transmittance or density on the spacecraft film and combined with the relative exposure values to yield a Hurter-Driffield response curve.

A single quantity was chosen to describe the noise level of the system. This quantity is the total noise power observed in the GRE image within that spatial frequency occupied by the signal; namely,  $\pm 20$  lines/mm at the GRE film scale. Since the noise power introduced by the spacecraft film and by the GRE film are both functions of density, the total noise power is measured in the region of the average density of the GRE image. In order to measure the total noise power, one of the uniform steps of the step tablet in the pre-exposed edge data array is selected. The variance of the density trace obtained by scanning the selected area with an appropriate microdensitometer aperture can be computed to establish the total noise power. Although the details of the data acquisition and reduction techniques are not to be given in this report, it should be mentioned that additional numerical filtering techniques are employed to remove the scan line structure from the microdensitometer trace and to limit the observed density fluctuations to the desired bandwidth.

The most complete way to describe the signal detail rendition of a system is to employ a factor called the modulation transfer function. In the case of the Lunar Orbiter photographic system, a nonlinear element in the system, namely the spacecraft film, indicated that a two-step evaluation procedure is desirable. In this procedure, which is detailed in the Phase II Final Report<sup>(2)</sup>, two separate modulation transfer functions are measured; one describing the signal detail rendition of the camera system, and the other describing the signal detail rendition of the communications link. These are referred to as the camera system modulation transfer function and the scanner-communications-GRS modulation transfer function, respectively. All techniques for measuring modulation transfer functions employ a test object whose spatial frequency content is known and can be compared to the resulting frequency content of the image of this object. The shadow-to-sunlight edge, interior to the crater, provides the test object used to evaluate a camera system modulation transfer function. The evaluation of the scanner-communications-GRS modulation function on the other hand is made using an edge of the step tablet in the pre-exposed edge data array. Microdensitometer traces are made across the selected

test objects on the reconstructed GRE film and combined with auxiliary data to evaluate the corresponding modulation transfer function using numerical computation techniques. The use of this two-step evaluation procedure requires the ability to convert GRE density to relative exposure on the spacecraft film. If the photography is so overexposed that any of the exposures lie outside the range of sensitometric control, the procedure becomes inaccurate or impossible to use. An alternative approximate technique which ignores the nonlinearity on the imaging system was developed in the Phase II effort<sup>(2)</sup> for use in such circumstances. Due to the overexposure of the medium resolution photography of Lunar Orbiter I, this procedure is employed in the evaluation of that photography. Although the exposure of the photographs of Lunar Orbiter II was improved, sensitometric conversion problems still prevented the use of the two-step procedure and the alternative approximate technique is also used in this evaluation. In addition to these departures, a minor difference in the data processing procedures existed between Lunar Orbiter I and II. Numerical filtering techniques are employed to eliminate the scan line structure from the microdensitometer traces obtained scanning the GRE film of Mission I, while for Mission II, an electronic filter incorporated in the microdensitometer circuitry is utilized for this purpose. The response of both filters is equivalent and can be found in the Phase III Final Report<sup>(3)</sup>. In all cases, removal of the noise power in the edge traces at frequencies below the scan line frequency is accomplished by employing hand smoothing techniques.

The flow diagram presented in Fig. 1 summarizes the evaluation of photographic quality, including the measurement of the quality parameters described above. It should be noted that the quality parameters are inputs to computational programs which evaluate the system performance criteria. These criteria consist of a signal-to-noise ratio for detecting a right circular cone on the lunar surface and the variance of the measurement of the brightness longitude (or slope) for a uniform square area on the lunar surface.

The nature of the measurement techniques used to evaluate the quality parameters necessitates that statistical procedures be used. Consequently, several microdensitometer scans are made across shadow-to-sunlight edges and the corresponding imaging system modulation transfer functions determined. The average of these individual measurements of the transfer function represent the measured value of this quality parameter. As the number of the individual measurements increases, the confidence which one has in the average values increases. In the Phase II effort<sup>(2)</sup>, it was concluded that about 25 measurements of each of the individual transfer functions would be required to attain the desired reliability in the corresponding average values. Studies concerning the required number of individual measurements of total noise power indicated that about seven measurements are reasonable. In a similar fashion, when measuring the signal level quality parameters, the average density of each of the nine steps of the step tablet of pre-exposed edge data array is evaluated using the steps from 10 or more of the frame-lets in the frame being analyzed. An analysis employing the number of measurements described above constitutes a detailed or "high level" analysis. In such analyses, the resulting quality parameters will have been measured to a sufficient accuracy so that the reliability of the resulting system performance criteria is approximately 6% to 11%.

The evaluation of the photographic performance of Lunar Orbiter I is confined to the medium resolution (8 meter) photography since the high resolution photography is obviously badly blurred by image motion. The evaluation was divided into two levels. In a high level analysis, the number of measurements made for each photograph to estimate the performance within 6% to 11% accuracy is described above. In a low level analysis, the number of measurements made for each of the quality parameters is reduced. The purpose of this analysis is to establish whether the additional frames analyzed at this level would vary significantly from those already analyzed at the high level, if they were analyzed at the high level also. In answering this question, the same quality parameters which were measured for the frames analyzed at the high level are also measured for the additional frames under examination. Since the number of individual measurements which are averaged to determine the quality parameter is reduced, the reliability

attained in the quality parameters is decreased. The following reductions in the quantity of data employed in the analysis are made. In measuring signal level, the number of individual step tablets employed in the analysis is reduced from 15 to approximately 5. The total noise power is determined from two microdensitometer scans rather than seven, and the total system frequency response is determined from approximately 6 to 12 scans across the shadow-to-sunlight edges rather than the 25 employed in the high level analysis.

The analysis of the Mission I photographs employed 10 medium resolution frames, four of these frames were analyzed at the high level, and the additional 6 frames were analyzed at the low level. One frame was chosen from each of the 10 sites photographed by Lunar Orbiter I. Table 1A presents some of the associated information for each of the selected frames. The required microdensitometer scans were made from one of the two original GRE films recorded at the DSIF site.

Table 1A  
MISSION I FRAMES ANALYZED

MRF NO.	SITE	PHASE ANGLE	ANALYSIS LEVEL
61	A-1	60.9	HIGH
75	A-2	65.4	LOW
85	A-3	69.2	HIGH
108	A-4	68.4	LOW
125	A-5	68.5	LOW
144	A-6	54.1	HIGH
164	A-7	58.3	LOW
179	A-8	59.2	LOW
191	A-9.2a	63.6	LOW
207	A-9.2b	62.2	HIGH

The analysis of the Mission II photographs employed 13 medium resolution frames and 13 high resolution frames. One of each type of frame was chosen from each of the 13 sites photographed by Lunar Orbiter II. The structure of the analysis was altered to increase the effectiveness of the performance evaluation. Since no significant difference in the imaging system modulation transfer function was observed among the measurements made in the evaluation of Mission I, it was decided to evaluate the system modulation transfer function at each end of Mission II in order to save the time which would be required to obtain edge traces from all 26 frames to be analyzed. If no significant difference in response were noted, it would be assumed that the system response remained constant at the average of the two samples throughout the mission. The analysis of the remaining quality parameters (signal and noise level) was made on each frame at the high level so that, in effect, there was no low level analysis in the evaluation of Mission II photography. Table 1B presents some of the associated information for each of the selected frames. The required microdensitometer scans were made from one of the two original GRE films recorded at the DSIF site.

Table 1B  
MISSION II FRAMES ANALYZED

HRF & MRF NO.	SITE	PHASE ANGLE
13	P-1	73.0
39	P-2	67.8
46	P-3a	75.6
63	P-4	77.7
69	P-5	69.0
88	P-6	61.1
99	P-7a	70.2
124	P-8b	61.7
141	P-9	66.1
157	P-10b	75.5
174	P-11b	61.5
183	P-12a	72.8
208	P-13b	70.4

The combined results obtained from our evaluation of the photographic performance of Lunar Orbiters I and II are presented in the following two sections. The measured values of the various quality parameters are presented according to classification in Section 3 and the resulting values of the system performance criteria are given in Section 4. The final section presents the conclusions obtained from our evaluation.

### 3. MEASURED VALUES OF THE QUALITY PARAMETERS

The values measured for the quality parameters selected to represent the quality of the Lunar Orbiter photographs are presented in this section for each of the 10 medium resolution frames used in the analysis of Mission I and for each of the 26 frames used in the analysis of Mission II.

As indicated in the introduction, two functions were selected as quality parameters to represent the manner in which the dc signal level is transmitted by the complete Lunar Orbiter imaging system. These functions are the Hurter-Driffield response curve for the SO-243 film in the spacecraft and the relationship between the transmittance of the SO-243 film and the density recorded on the GRE film. Measurements are made of the density of each of the nine steps in the step tablet in several of the framelets composing each frame. The individual measurements for each framelet of the frame are averaged to determine an average density for each of the nine steps in the step tablet. The resulting average densities are combined with nominal values for the transmittance of steps on the spacecraft film to establish the relationship between the transmittance and the recorded GRE density for each frame. Least square techniques are then employed to compute the relationship between the data. While under nominal conditions this relationship is expected to be linear as the Mission I data indicates, most of the results of the Mission II measurements show that a quadratic regression analysis yields significantly lower residual errors than did a linear regression analysis.

Figs. 2 through 4 contain the results of the measurements for the 10 Mission I frames analyzed. Figs. 5 through 11 contain the results of the measurements for the 26 frames analyzed from the Mission II data. In addition to the nine points corresponding to the measurements of average density made for each of the nine steps of the step tablet, the figures include  $\pm$  sigma error bars representing the deviation of the individual measurements made on several framelets in each frame, and the fitted

regression indicated by the solid line. As noted, with the exception of MRF 61, 144, and 207 from Mission I and MRF 46, MRF 174, and HRF 99 from Mission II, the results do not exhibit a linear characteristic.

Several effects can produce a nonlinear characteristic. This would occur if (1) the measured values of the average GRE densities were incorrect due to measurement errors or kinescope flare light, (2) the actual values of transmittance of each step on the spacecraft film were not equal to their "nominal" values because of radiation exposure, processing variations or variations in the exposure of the edge print camera, and (3) the transmittance to density response were, in fact, truly nonlinear. Subsequent analysis of the voltage signals received at the GRE for three of the frames employed in the Mission II evaluation indicated that the primary source of the nonlinear response was the GRE equipment. The secondary source of the nonlinearity can most probably be attributed to the fact that the processing of the SO-243 film in the spacecraft was not performed under nominal conditions. In the analysis of the Mission I data, the GRE response was assumed to be linear, while in the Mission II analysis, the nonlinearity was wholly attributed to the GRE. The actual effect in both cases is small, however, and produces no significant difference in the final evaluation of system performance.

Since the GRE density is the only quantity which can be measured directly from the Lunar Orbiter photographs, it is reasonable to assume that the fitted equation would be used to predict SO-243 transmittance from known values of GRE density. Therefore, the GRE density can be regarded as an independent variable, while the SO-243 transmittance is the dependent variable. Consequently, the least squares technique is used to compute the quadratic regression of SO-243 transmittance on GRE density in the form

$$T = b_0 + b_1 D + b_2 D^2 \quad (1)$$

The resulting values of  $b_0$ ,  $b_1$ , and  $b_2$  completely specify the quality parameter. In the case of the Mission I data analysis, the term  $b_2$  was set equal to zero, thus forcing a linear regression analysis.

Once the response from the transmittance of the SO-243 film to GRE density has been determined, this relationship can be used to convert the measured values of GRE density for each of the steps of the step tablet to the corresponding values of SO-243 transmittance. To evaluate the second quality parameter associated with signal level; namely, the Hurter-Driffield response curve of the spacecraft film (i. e., SO-243 film), it is only necessary to convert the values of transmittance to density and plot these values as a function of the log of the relative exposure of each of the steps in the step tablet. When a relative exposure of 1.0 is arbitrarily assigned to the first step, viz., log exposure of 0.0, the log exposure of the remaining steps can be computed by employing the known change in log exposure between steps for the reticle used on producing the flight film. In the case of the Lunar Orbiter I and II, reticle No. 8 was used in the edge print camera. Table 2 presents the relative log exposure for each of the steps in the step tablet. These values are combined with the values of SO-243 density determined

Table 2  
RELATIVE LOG EXPOSURE FOR  
RETICLE NO. 8

STEP NO.	RELATIVE * LOG (E)
1	0.00
2	0.13
3	0.27
4	0.40
5	0.56
6	0.77
7	0.94
8	1.10
9	1.26

\* BASED UPON THE  $\Delta(\text{LOG } E)$  INCREMENTS SPECIFIED IN L-020495-KU, 6 MAY 1966.

from the measured values of GRE density using the relationships for each of the frames given in the previous figures. The resulting Hurter-Driffield response curves are shown in Figs. 12 through 19\*. It is convenient to express response curves in terms of an analytic expression given by

$$D_{243} = C_1 + C_2 \operatorname{erf} \left\{ C_3 \log_{10} (C_4 + C_5 E) \right\} \quad (2)$$

where

$$\operatorname{erf}(x) = \frac{1}{\sqrt{\pi}} \int_{-\infty}^x e^{-t^2/2} dt$$

and  $E$  is the exposure. This analytic function is fitted to the data using nonlinear parametric estimation techniques which minimize the sum of squares deviation. This technique was applied to each of the frames shown in Figs. 12 through 19 and the resulting parametric form is represented by the solid line in each part of the figure. The dashed curve is the same parametric form fitted to data obtained from a sample of bimat processed film taken from the rolls which provided the flight film for Lunar Orbiters I and II. This curve, therefore, represents what may be considered the nominal curve for each mission.

In addition to evaluating the spacecraft film transmittance-to-GRE density characteristics and the Hurter-Driffield response of the spacecraft film, there is one other measurement that is made in the evaluation procedures which is part of the analysis of the signal level quality of the imaging system. The measurements described above related the output signal (GRE density) to a relative input signal. To specify the absolute operation point of the system, it is convenient to measure the average density in the reconstructed photograph. We estimate this density by measuring the average density of flat areas near the nadir in the reconstructed photograph\*\*. Tables

---

\* The Mission I results are presented only for the four frames analyzed at the high level. The low level analysis results are quite similar and somewhat uninteresting.

\*\* Typical examples of selected areas are given in the photograph presented in Fig. 28 and are labeled with the letters A through G.

3A and 3B present the results of Mission I and II, respectively. Included in the table is the number of the gray level in the step tablet which has the closest density to the measured value for the flat surface in the scene. Those cases where the measured value is less than that for Step 9 are indicated by the letters "OE" for overexposed.

Table 3A  
AVERAGE GRE DENSITY LEVELS - MISSION I

MRF NO.	GRE DENSITY FOR FLAT AREA NEAR NADIR	CLOSEST GRAY LEVEL IN STEP TABLET
61	$0.69 \pm 0.03$	OE
75	$0.33 \pm 0.01$	OE
85	$0.69 \pm 0.02$	OE
108	$0.59 \pm 0.03$	OE
125	$0.70 \pm 0.02$	9
144	$0.57 \pm 0.01$	OE
164	$0.54 \pm 0.02$	OE
179	$0.67 \pm 0.02$	9
191	$0.82 \pm 0.03$	9
207	$0.96 \pm 0.03$	6

OE: OVEREXPOSED - GRE DENSITY BELOW STEP 9

Another quality parameter selected for the Lunar Orbiter photographs, describing the noise level in the system, is the total noise power observed in the GRE image within the spatial frequency band occupied by the signal. This quality parameter is measured by scanning uniformly exposed areas on the GRE film with the microdensitometer. The most convenient areas are the uniform steps or gray levels in the step tablet. Apart from the scan line structure in the GRE image, the variations in the microdensitometer trace are produced by the noise added to the signal originating on the spacecraft film. The total noise power can be evaluated by computing the variance of the observed density fluctuations after the scan lines have been removed. Since the noise power contributed by the spacecraft film

Table 3B  
 AVERAGE GRE DENSITY LEVELS - MISSION II

MRF NO.	GRE DENSITY FOR FLAT AREAS NEAR NADIR	CLOSEST GRAY LEVEL IN STEP TABLET
13	0.78	8
39	0.86	7
46	0.96	6
63	0.68	9
69	0.66	9
88	0.85	8
99	0.75	9
124	0.43	0E
141	0.63	0E
157	0.70	9
174	0.58	9
183	0.59	0E
208	0.78	7
HRF NO.		
13	1.04	6
39	1.76	5
46	1.35	5
63	1.12	6
69	0.90	7
88	1.32	6
99	1.54	5
124	1.13	6
141	1.30	6
157	1.15	6
174	1.02	6
183	1.11	6
208	1.80	4

0E: OVEREXPOSED - GRE DENSITY BELOW STEP 9

and by the reconstructing film are both dependent upon the signal level, the gray level of the step tablet chosen to evaluate the total noise power indicated previously in Tables 3A and 3B is selected so that its density (in the GRE image) is close to the density produced by a flat region of the lunar surface near the nadir in the frame being analyzed. This criterion was selected since this density should be reasonably close to the average density of the photograph. Since the value of the total noise power is independent of the direction in which the film is scanned, traces are made perpendicular to the scan line in the GRE image. Scans were made across the appropriate step of the step tablet in approximately seven framelets for each of the frames analyzed at the high level in Mission I and all the frames analyzed in Mission II. The average total noise power determined from the individual measurements on each framelet represents the value of this quality parameter. Tables 4A and 4B contain the results of the measurements for each of the frames analyzed in Mission I and Mission II, respectively. The standard deviation associated with the measured value of total noise power

Table 4A  
MEASURED VALUES OF TOTAL  
NOISE POWER - MISSION I

	MRF NO.	TOTAL NOISE POWER •	STANDARD DEVIATION	EQUIVALENT PERCENT
HIGH LEVEL	61	0.001795	0.000196	10.9
	85	0.001590	0.000123	7.7
	144	0.001106	0.000089	8.0
	207	0.001523	0.000078	5.1
LOW LEVEL	75	0.000913	NA	NA
	108	0.001429	NA	NA
	125	0.002048	NA	NA
	164	0.001064	NA	NA
	179	0.001305	NA	NA
	191	0.001982	NA	NA

NA - NOT APPLICABLE  
• IN UNITS OF DENSITY<sup>2</sup> ON GRE FILM

Table 4B  
MEASURED VALUES OF TOTAL NOISE POWER MISSION II

FRAME	TOTAL NOISE POWER •	STANDARD DEVIATION •	EQUIVALENT PERCENT
MRF 13	0.001333	0.0001641	12.3
MRF 39	0.002340	0.0001287	5.5
MRF 46	0.006167	0.0004662	7.6
MRF 63	0.001025	0.0000689	6.7
MRF 69	0.000986	0.0001066	10.8
MRF 88	0.001707	0.0002096	12.3
MRF 99	0.001472	0.0001763	12.0
MRF 124	0.000499	0.0000381	7.6
MRF 141	0.001193	0.0001364	11.4
MRF 157	0.000909	0.0000833	9.2
MRF 174	0.000749	0.0000620	8.3
MRF 183	0.000895	0.0000792	8.8
MRF 208	0.003334	0.0002620	7.8
HRF 13	0.004724	0.0004672	9.9
HRF 39	0.008944	0.0006520	7.3
HRF 46	0.009369	0.001063	11.4
HRF 63	0.006453	0.001134	17.6
HRF 69	0.002517	0.0004533	18.0
HRF 88	0.007347	0.0004122	5.6
HRF 99	0.01043	0.0008062	7.7
HRF 124	0.005230	0.0004451	8.5
HRF 141	0.005429	0.0006982	12.9
HRF 157	0.005741	0.0004087	7.1
HRF 174	0.005356	0.0006336	11.8
HRF 183	0.004154	0.0008496	20.4
HRF 208	0.01238	0.0004135	3.3

• IN UNITS OF DENSITY<sup>2</sup> ON GRE FILM

is also presented in the tables\*. This quantity is based upon the observed deviation of the individual measurements made on each framelet and represents the variation in the total noise power which could be expected if the computations were to be repeated. As a convenience, the percentage corresponding to the standard deviation is also shown.

\* Because of the reduction in the number of measurements in the low level analysis of the Mission I frames, the deviation cannot be reliably evaluated from the data and is not presented in the table.

The final quality parameter selected for the Lunar Orbiter photographs described the signal detail rendition of the imaging system. This parameter includes the effect of the scanner-communications-GRS modulation transfer function and the camera system modulation transfer function. To measure transfer functions, a test object must be selected which has sufficient detail to be degraded by the system. The amount of degradation is then measured by comparing the spectrum of the image to that of the object for the test target selected. The edges in the pre-exposed edge data array provide convenient targets for evaluation of the detail rendition of the combined scanner-communications-GRS system since these edges are printed onto the film independently of either lens in the spacecraft. An edge is selected between one of the steps of the step tablet in the array and the background region. This edge is scanned by the microdensitometer using a narrow slit aperture and the resultant density trace employed to evaluate the combined scanner-communications-GRS modulation transfer function. In addition to this trace, the initial sharpness of the edge target selected must be known. If the edge were extremely sharp, this additional information could be eliminated. In the present case, however, the initial sharpness of the edge is measured by employing a sample of bimat processed spacecraft film containing the edge data and obtained from the same roll of film which actually supplied the film for the mission. From the results obtained in the Phase II study, it was concluded that the edges of Steps 5, 6 and 7 provided the most likely candidates for evaluating the transfer function. Consequently, the sharpness of these edges were evaluated from the bimat processed film sample of Mission I. About 10 edge traces (samples) are required for reasonable precision of this sharpness measurement. The resulting sharpness response functions from the Mission I evaluation are presented in Fig. 20. From this figure, we see that the edges of Steps 5 and 6 are equally sharp and consequently both were employed in evaluating the scanner-communications-GRS modulation transfer function. Since the edge of Step 7 was eliminated in the Mission I evaluation, only the sharpness of the edges of Steps 5 and 6 was measured in the Mission II evaluation and shown in Fig. 21.

An error analysis made during the Phase II study indicated that the established procedure would estimate the modulation transfer function accurately at spatial frequencies below that corresponding to the 50% sharpness response point for the edge targets selected. From the previous two figures, we see that this limit is about 60 lines/mm in the Mission I and II evaluations.

To evaluate the transfer function, the edges of Steps 5 and 6 were scanned in at least 25 of the framelets composing the frames selected for a high level analysis from Mission I and the individual transfer functions measured from each of the edge traces were averaged. The results of these measurements are shown in Figs. 22 to 25. Included in each figure is the number of edges used and a 95% confidence band shown by dashed lines. It is evident, from the results, that the performance of the portion of the imaging system from the scanner to the reconstructed imagery did not change during the course of the mission. Consequently, in the Mission II evaluation a different measurement procedure was employed. Instead of evaluating the transfer function for each frame analyzed (i. e., 13 high and 13 medium resolution frames), the evaluation was only made twice; once for a frame at the beginning of the mission (#13) and once for a frame near the end of the mission (#183). Since there is no apparent difference in the transfer functions below the 60 line/mm limit between the beginning and end of the mission, these results were averaged to determine the value of the scanner-communications-GRS modulation transfer function for the entire mission as shown in Fig. 26.

In addition to the gray levels and the associated edges which were used above, the pre-exposed data array also contains a series of square wave test patterns. These patterns could have been employed to evaluate the scanner-communications-GRS transfer function instead of the edges, however, they have several disadvantages. Most important is the fact that the lowest spatial frequency square wave patterns is 32 lines/mm, whereas the region of lower frequencies is of primary importance in the performance evaluation. The acquisition and reduction of the square wave data, although straightforward, is not as easily automated as the

procedures employing an edge trace. To show that equivalent results are obtained from both methods, an analysis of the scanner-communications-GRS MTF was made from both the high and low contrast square wave patterns in medium resolution frame 61 of Lunar Orbiter I. It was assumed that the test patterns were essentially undegraded on the reticle in the edge print camera and that they are degraded by the edge print camera in the process of exposing the reticle onto the spacecraft film. This degradation can be measured in the form of an effective frequency response much like the sharpness of the edges was evaluated above. The square wave test patterns on the bimat processed sample of spacecraft were scanned with a micro-densitometer on six framelets and the normalized square wave response evaluated from the resulting traces\*. In a similar fashion, the square wave patterns were scanned in six framelets of the reconstructed image of MRF 61 and a normalized square wave response determined. In this case, the response includes the effects of both the edge print camera and the scanner through the reconstruction portion of the Lunar Orbiter imaging system. It is a straightforward process to convert square wave response to sine wave response or transfer function<sup>(4)</sup>. The effect of the edge print camera can be removed by dividing the latter transfer function by the former in analogy to the correction for edge sharpness used earlier. This procedure was followed for the bar patterns of 32, 40, 50, 63 and 80 lines/mm. The measured responses are shown as triangles in Fig. 22 which includes the results of the edge analysis described earlier. The results begin to deviate considerably at 50 lines/mm, however, this is sufficiently close to the 60 lines/mm limit of accuracy established by the sharpness of the edge test objects to be expected.

The second transfer function which describes signal detail rendition is the camera system modulation transfer function. The target selected to evaluate this transfer function is the shadow-to-sunlight edge interior

---

\* To evaluate the normalized response, the initial modulation of the square waves on the reticle must be known. Since this information was not available, the initial modulation was assumed to be constant for all the bar objects regardless of frequency and was estimated by extrapolation of the measured modulations to zero spatial frequency.

to a crater. This edge is affected by both the camera system and the scanner-communications-GRS system. Therefore, to evaluate the camera system modulation transfer function alone, the edge must be corrected for the effect of the combined scanner-communications-GRS system by employing the modulation transfer function measured above. This evaluation procedure requires that the measured edge trace be converted from GRE density to relative exposure on the spacecraft film. Due to the overexposure of most of the medium resolution frames on both Missions I and II, the recorded GRE densities of the image are below the density of the last step of the step tablet. This condition also exists for high resolution frame 13 of Mission II. Consequently, sensitometry or photometric calibration does not exist for conversion of GRE density to relative exposure. As a result of this situation, the measured GRE density values for the shadow-to-sunlight crater edge cannot be reliably converted to camera exposure and therefore the established data reduction techniques cannot be employed.

Fortunately, however, an alternative method was developed during the Phase II program for performing the required analysis. This method requires that the test object (i. e., the shadow-to-sunlight edge) be a relatively low contrast object<sup>\*</sup>. In this case, the nonlinearity of the spacecraft film can be ignored. The excessive exposure of the photographic frames, in addition to placing the GRE densities in a region where sensitometry is not available, also has the effect of compressing the density range across the selected test target, reducing its contrast. In this case, the effective modulation transfer function for the entire imaging system (that is, the combined camera system and scanner-communications-GRS system) can be evaluated by employing the smoothed shadow-to-sunlit edge trace in the same data reduction programs used previously to evaluate the scanner-communications-GRS modulation transfer function.

---

\* The analysis of even high contrast objects by means of the alternative method described here yields results which are found to have sufficient accuracy for the analysis of the system performance.

In the Mission I high level analysis and in the Mission II evaluation, approximately 25 craters were selected near the center of each of the frames analyzed and the corresponding shadow-to-sunlit edges scanned, employing a narrow slit in the sun plane direction (i. e., normal to the shadow-to-sunlit edge). Fig. 27 is a reproduction of medium resolution frame 144 which is one of the four frames analyzed at the high level in Mission I. The craters selected in the frame are indicated by the circles in the enlarged section of the frame presented in Fig. 28. The resulting edge traces were processed to remove the scan line structure and hand smoothed to reduce the noise within the signal band. The modulation transfer function for the entire imaging system is determined by differentiating and taking a Fourier transform. The individual measurements of modulation transfer function from the edge interior to each of the craters selected in a frame are averaged to determine the desired quality parameters. As in the case for the evaluation of the scanner-communications-GRS modulation transfer function, the structure of the evaluation was different for Mission I and Mission II photography.

In the Mission I evaluation, the transfer function was measured for each of the frames analyzed except that at least 25 samples (i. e., different crater shadow-to-sunlight edges) were used in the frame analyzed at the high level and about 10 samples for those analyzed at the low level. Figs. 29 through 38 present the results. In the Mission II evaluation, the transfer function was measured for both the high resolution system and the medium resolution system in one frame at the beginning, and in one frame at the end of the mission using about 20 samples in each frame. Again, because there is no significant difference between the two results, they were combined to yield the result in Fig. 39 for the medium resolution system and in Fig. 40 for the high resolution system.

#### 4. SYSTEM PERFORMANCE CRITERIA

The system performance criteria are evaluated by using the measured values of the quality parameters reported in Section 2. These criteria are designed to aid in evaluating the performance of the Lunar Orbiter photographic system from the camera exposure to the density recorded on the GRE film. Two criteria were developed under the Phase II effort<sup>(2)</sup>. One criterion is the variance in the measurement of brightness longitude or slope angle for a uniform square area inclined toward, or away from, the sun. The amount of inclination and the size of the area are incidental parameters which may be varied to develop different values of this criterion. It is a function of all of the quality parameters in each of the three classes; namely, noise level, signal level, and signal detail rendition. In the case of the signal level quality parameters, this criterion is dependent upon the absolute sensitometry of the system; that is, the GRE density corresponding to the absolute exposure on the spacecraft film. Due to the excessive exposure on most of Mission I frames and on some of the medium resolution frames in Mission II, however, the sensitometry was not available to convert densities to exposure. In this case, the relative exposure on Step 9 was selected to be representative of the exposure for a flat surface near nadir in the photograph. Actually, the exposure would be greater than this. The lack of sensitometry, however, requires the use of such an approximation, and this choice is reasonable. The values for the expected variance in the measurement of the brightness longitude for both Missions are presented in Figs. 41 through 70. The values of this criterion were computed for the range of brightness longitude between  $\pm 15^\circ$  where the positive values correspond to areas sloped away from the sun and for various values of target size ranging from 8 resolution elements to 1 resolution element. It should be noted that for those frames which were overexposed, the values of these numbers are exceedingly large which would be expected on the basis of the results in the Phase II Final Report<sup>(2)</sup>.

The other system performance criterion is based upon the signal-to-noise ratio of a right circular cone sitting on a flat surface near nadir in the photograph. Two cone geometries are analyzed, cones having a base to height ratio of 4:1 and cones having a base to height ratio of 14:1. The base diameter of the cone is a variable which can be changed to compute various values for this criterion. Again, the value of the signal-to-noise ratio is a function of all the quality parameters measured in each of the three classes. In addition, the value of this criterion also depends upon the relationship between absolute exposure and recorded density on the GRE film. The approximate procedure described above to establish absolute exposure was again employed in evaluating the signal-to-noise ratio for those frames which were overexposed. This approximation would tend to produce higher signal-to-noise ratios than actually obtained in those cases where the cone target does not cast a shadow (phase angle less than  $63.4^\circ$ ) at the 4:1 base-to-height ratio. The results for each of the frames analyzed in both missions are presented in Figs. 71 through 100.

## 5. CONCLUSIONS

It can be concluded from the results of the analysis of both Lunar Orbiter I and II data, that the system performance with respect to signal detail rendition was nominal. The data obtained from the 6 frames from Mission I analyzed at the low level (i. e. , a small number of measurements) does not indicate any difference in performance from those frames analyzed at the high level.

The noise level measurements made for both missions yielded data that were smaller than the nominal value, but consistent with the excessive exposures attained on most of the frames analyzed. The observed over-exposure was such that most of the recorded GRE densities were outside of the range where sensitometric control was provided, the problem being more severe for the Mission I data.

The systems did not perform nominally with respect to signal level in that the GRE response was not linear and the processing in the spacecraft was not complete.

For most of the frames analyzed, the signal-to-noise ratio was only slightly affected by the excessive exposures because both the signal power and noise power were decreased. In those cases where the test cone will cast a shadow, such as frame 85 from Mission I and all Mission II frames except 88, 124 and 174, the signal-to-noise ratio is increased above the nominal value by the overexposure.

The estimate of the variance in the measurement of the brightness longitude for the square target areas shows a larger value than expected, primarily due to the excessive exposure. In addition, since the majority of GRE densities are outside of the region where sensitometric control is available, these densities cannot be reliably converted to relative or absolute camera exposures. Consequently, the Lunar Orbiter I and some of the Lunar Orbiter II photographs will have little value for determining the brightness longitude as a function of position on the lunar surface by means of photoclinoetry.

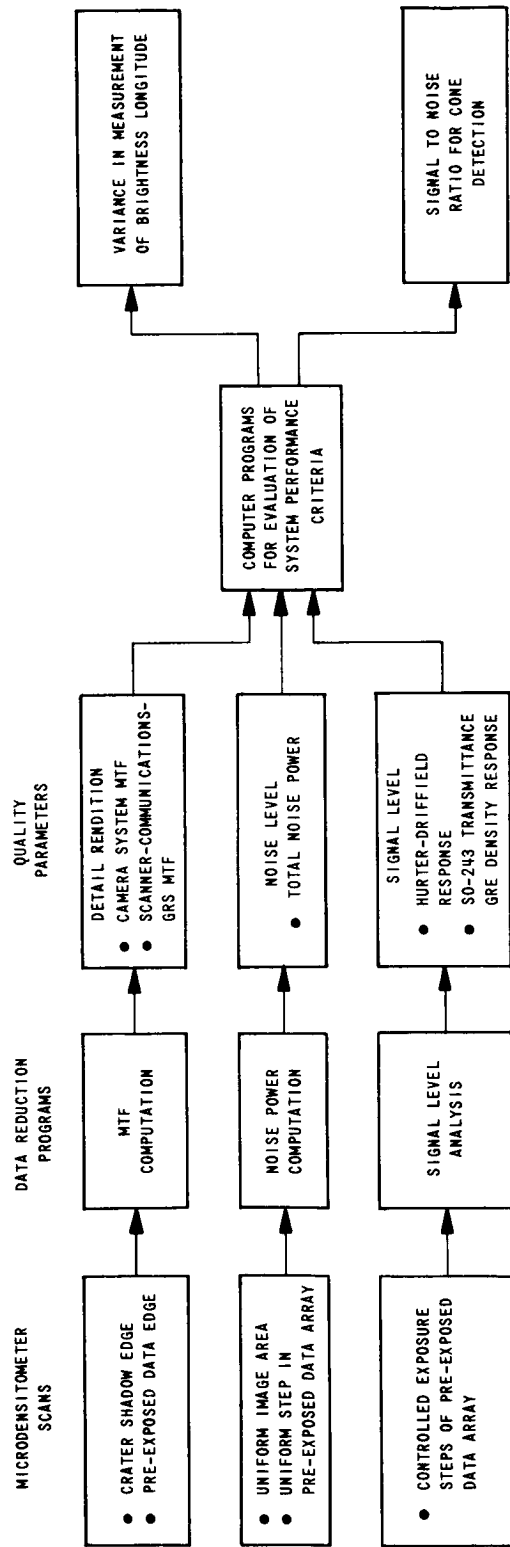
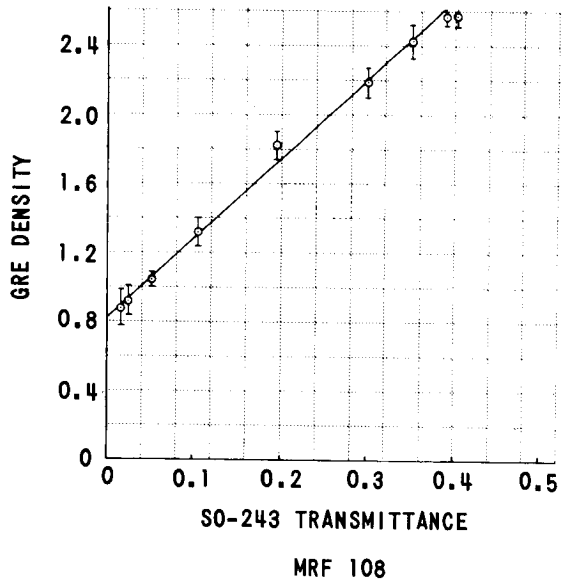
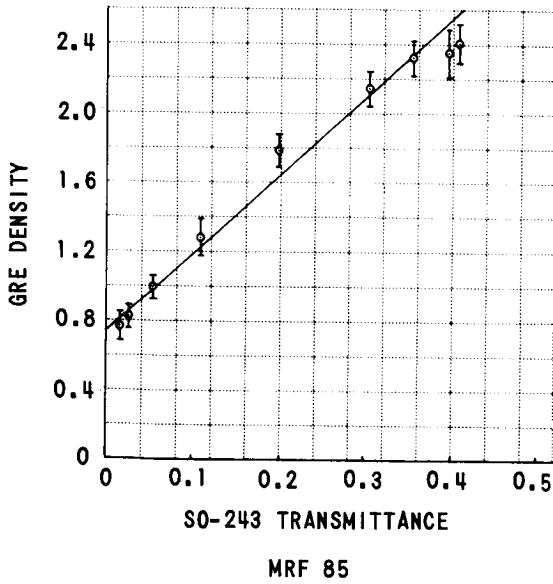
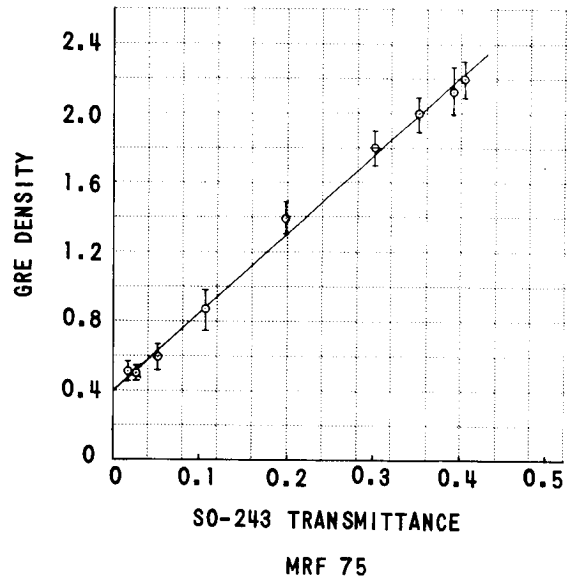
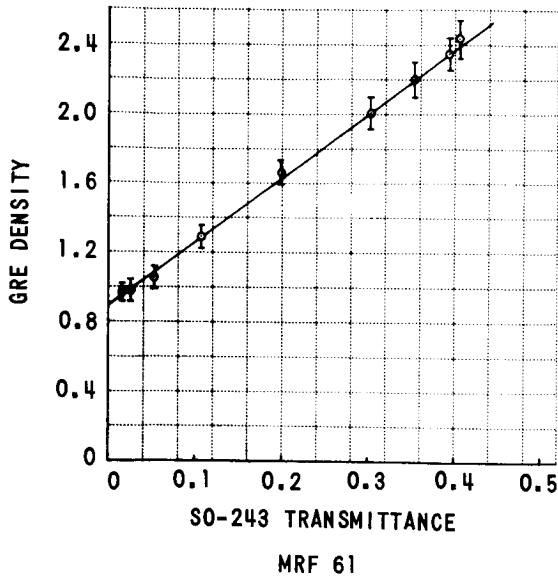
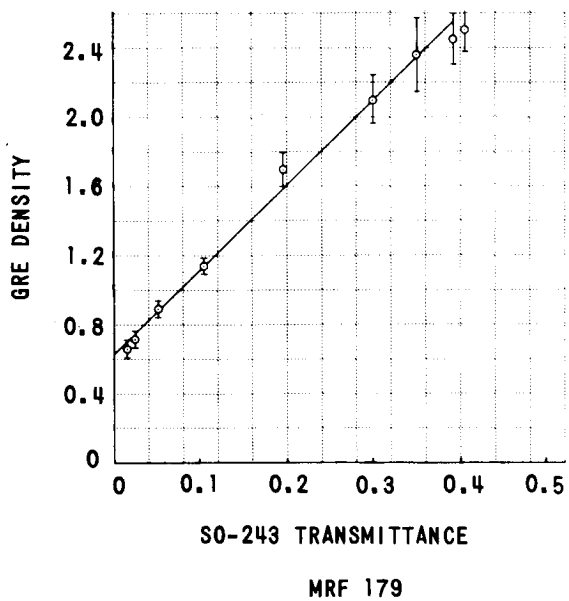
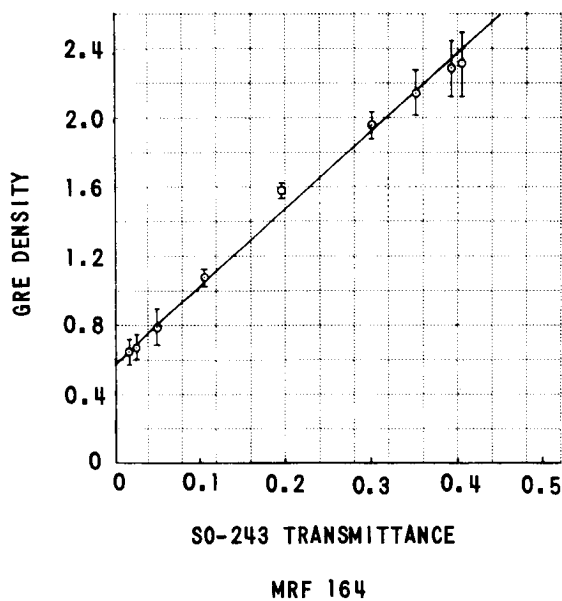
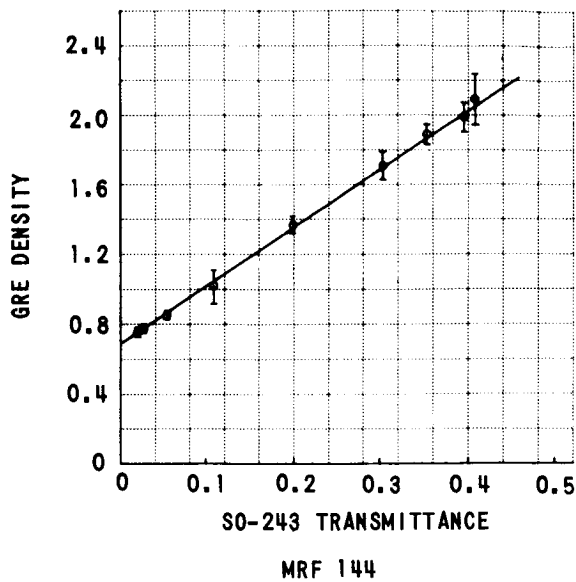
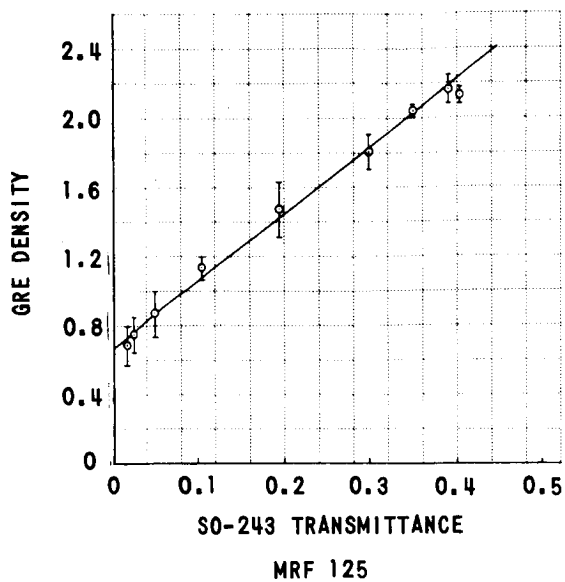


Figure 1 LUNAR ORBITER PHOTOGRAPHIC QUALITY EVALUATION FLOW DIAGRAM



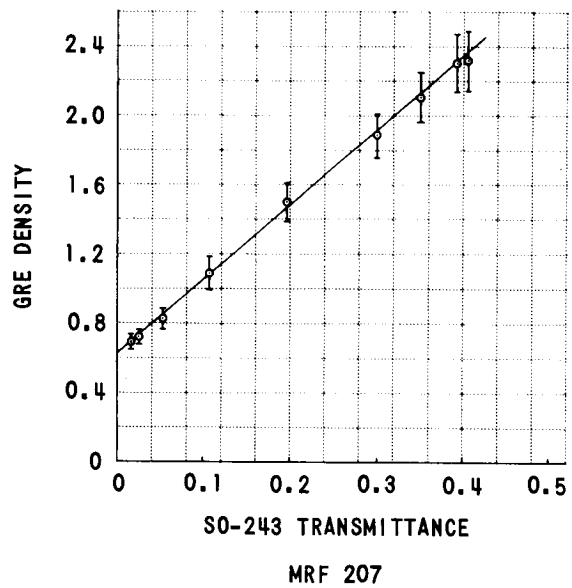
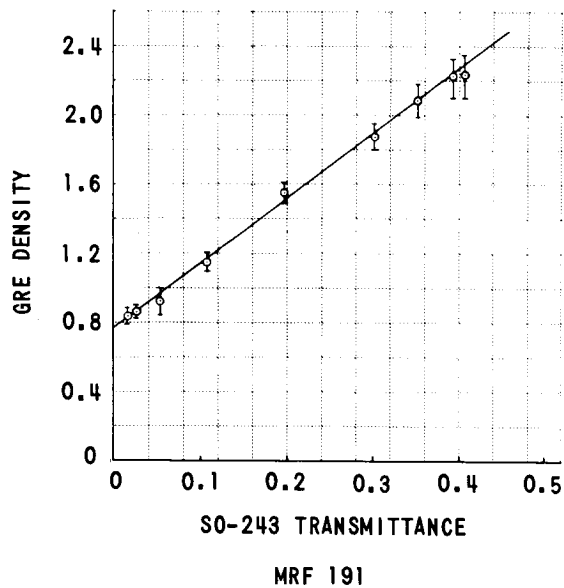
THE SOLID LINE IS THE COMPUTED REGRESSION OF SO-243 TRANSMITTANCE ON GRE DENSITY AND THE ERROR BARS INDICATE THE  $\pm$  ONE SIGMA SPREAD OF THE INDIVIDUAL MEASUREMENTS OF GRE DENSITY USING SEVERAL FRAMELETS IN EACH FRAME

Figure 2 REGRESSION BETWEEN SO-243 TRANSMITTANCE AND GRE DENSITY - ORBITER I



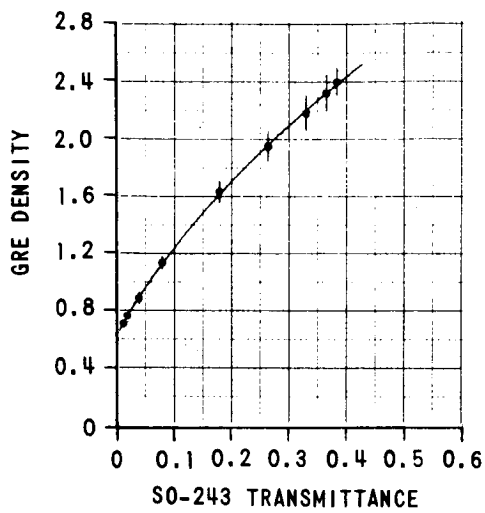
THE SOLID LINE IS THE COMPUTED REGRESSION OF SO-243 TRANSMITTANCE ON GRE DENSITY AND THE ERROR BARS INDICATE THE  $\pm$  ONE SIGMA SPREAD OF THE INDIVIDUAL MEASUREMENTS OF GRE DENSITY USING SEVERAL FRAMELETS IN EACH FRAME

Figure 3 REGRESSION BETWEEN SO-243 TRANSMITTANCE AND GRE DENSITY - ORBITER I

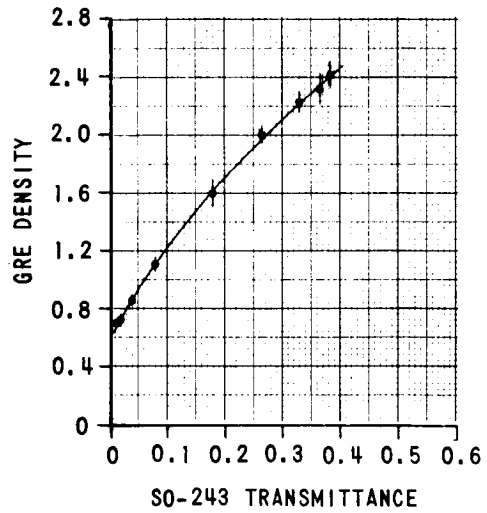


THE SOLID LINE IS THE COMPUTED REGRESSION OF SO-243 TRANSMITTANCE ON GRE DENSITY AND THE ERROR BARS INDICATE THE  $\pm$  ONE SIGMA SPREAD OF THE INDIVIDUAL MEASUREMENTS OF GRE DENSITY USING SEVERAL FRAMELETS IN EACH FRAME

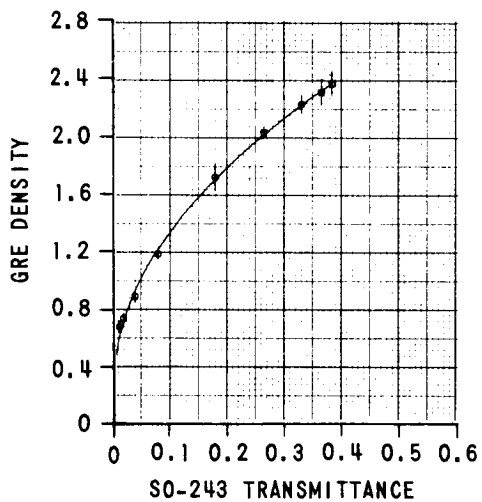
Figure 4 REGRESSION BETWEEN SO-243 TRANSMITTANCE AND GRE DENSITY - ORBITER I



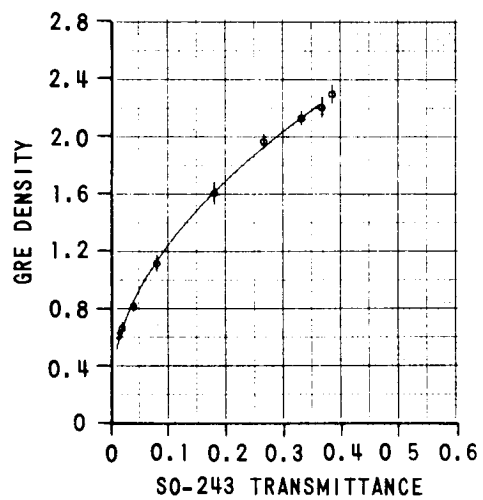
HRF 13



MRF 13



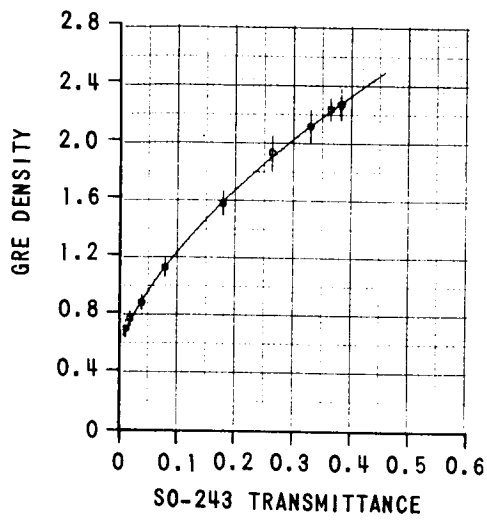
HRF 39



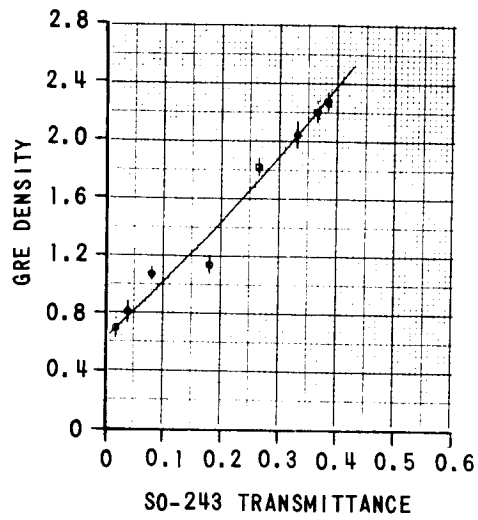
MRF 39

THE SOLID LINE IS THE COMPUTED REGRESSION OF SO-243 TRANSMITTANCE ON GRE DENSITY AND THE ERROR BARS INDICATE THE  $\pm$  ONE SIGMA SPREAD OF THE INDIVIDUAL MEASUREMENTS OF GRE DENSITY USING SEVERAL FRAMELETS IN EACH FRAME

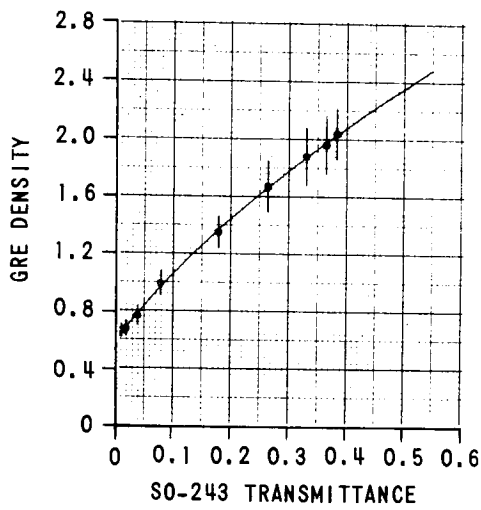
Figure 5 REGRESSION BETWEEN SO-243 TRANSMITTANCE AND GRE DENSITY-ORBITER II



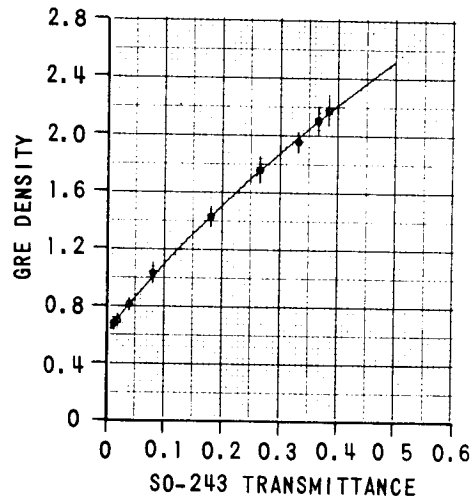
HRF 46



MRF 46



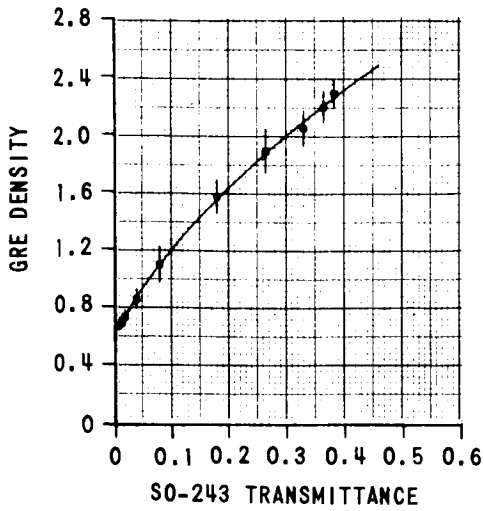
HRF 63



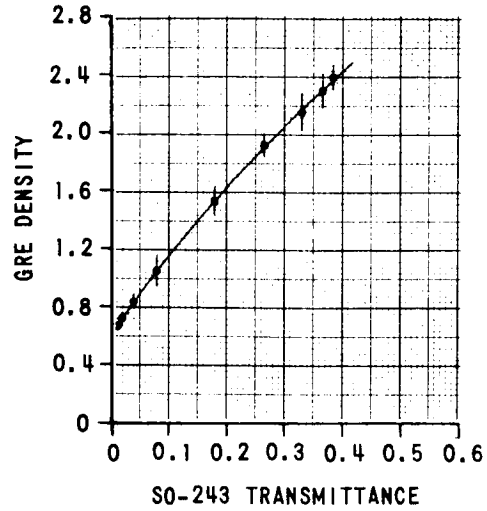
MRF 63

THE SOLID LINE IS THE COMPUTED REGRESSION OF SO-243 TRANSMITTANCE ON GRE DENSITY AND THE ERROR BARS INDICATE THE  $\pm$  ONE SIGMA SPREAD OF THE INDIVIDUAL MEASUREMENTS OF GRE DENSITY USING SEVERAL FRAMELETS IN EACH FRAME

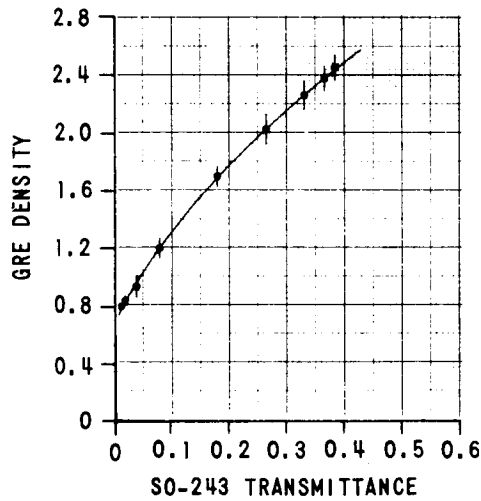
Figure 6 REGRESSION BETWEEN SO-243 TRANSMITTANCE AND GRE DENSITY-ORBITER II



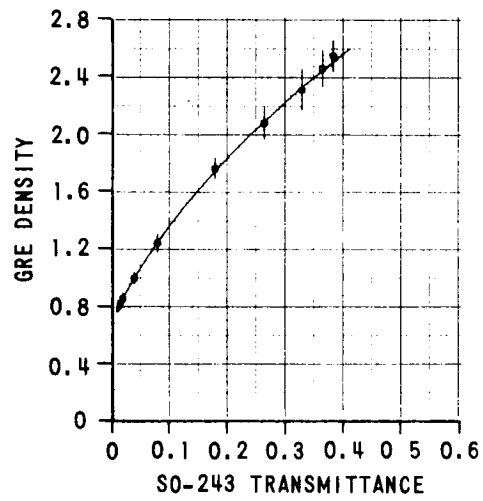
HRF 69



MRF 69



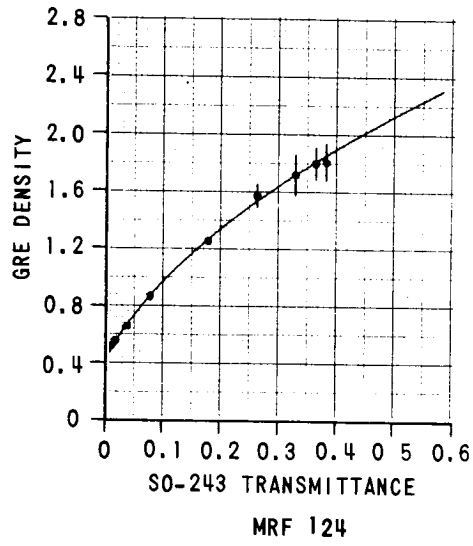
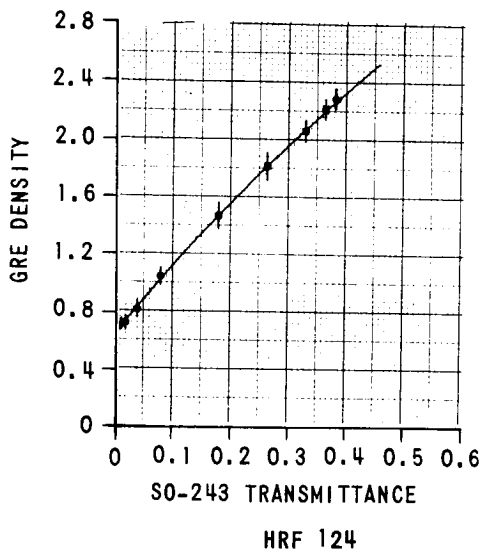
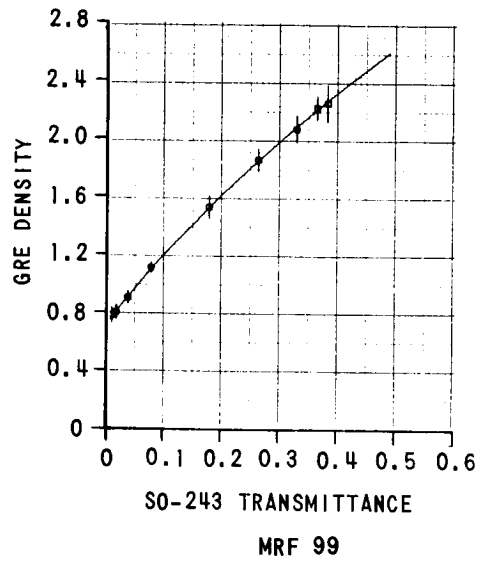
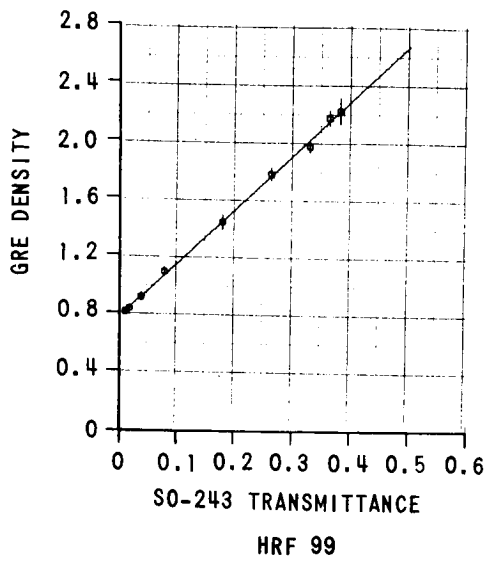
HRF 88



MRF 88

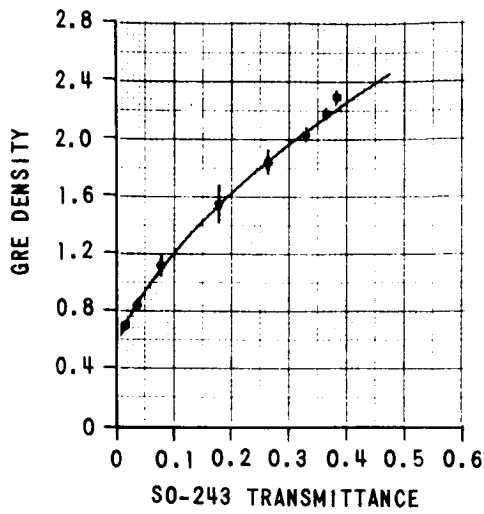
THE SOLID LINE IS THE COMPUTED REGRESSION OF SO-243 TRANSMITTANCE ON GRE DENSITY AND THE ERROR BARS INDICATE THE  $\pm$  ONE SIGMA SPREAD OF THE INDIVIDUAL MEASUREMENTS OF GRE DENSITY USING SEVERAL FRAMELETS IN EACH FRAME

Figure 7 REGRESSION BETWEEN SO-243 TRANSMITTANCE AND GRE DENSITY-ORBITER II

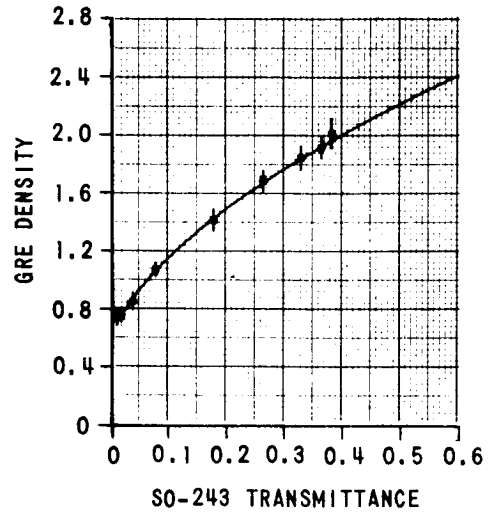


THE SOLID LINE IS THE COMPUTED REGRESSION OF SO-243 TRANSMITTANCE ON GRE DENSITY AND THE ERROR BARS INDICATE THE  $\pm$  ONE SIGMA SPREAD OF THE INDIVIDUAL MEASUREMENTS OF GRE DENSITY USING SEVERAL FRAMELETS IN EACH FRAME

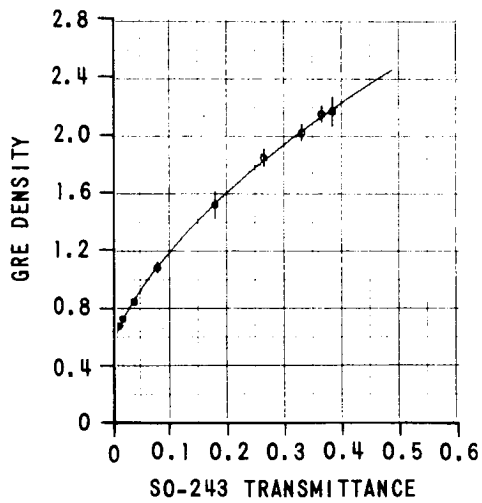
Figure 8 REGRESSION BETWEEN SO-243 TRANSMITTANCE AND GRE DENSITY-ORBITER II



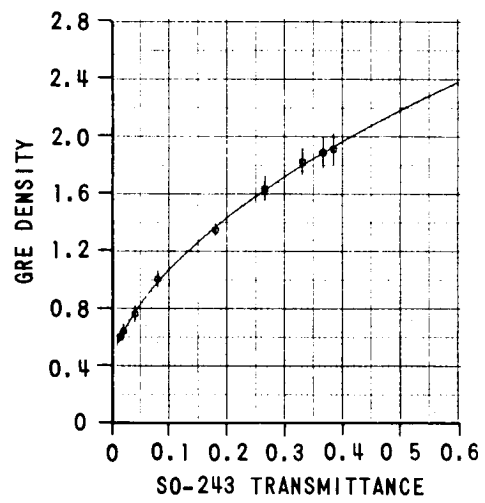
HRF 141



MRF 141



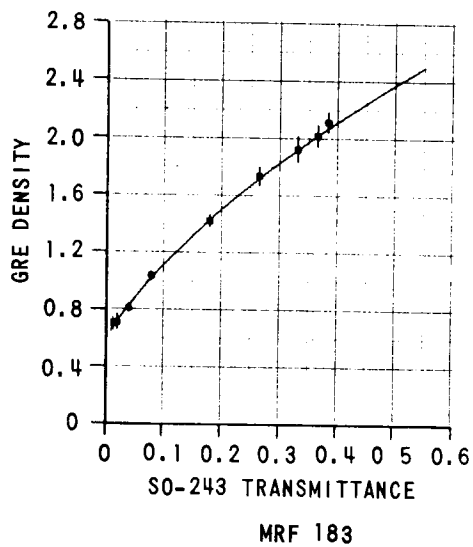
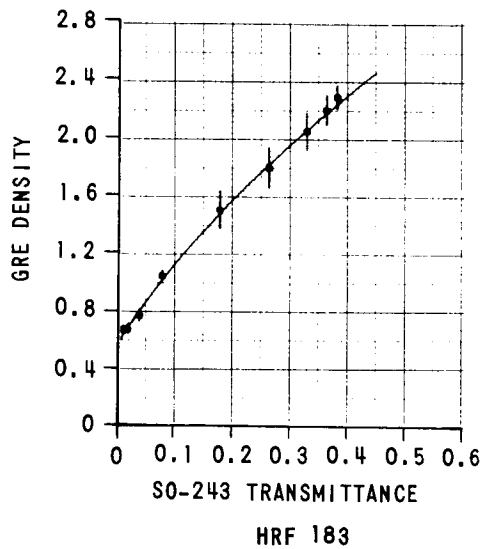
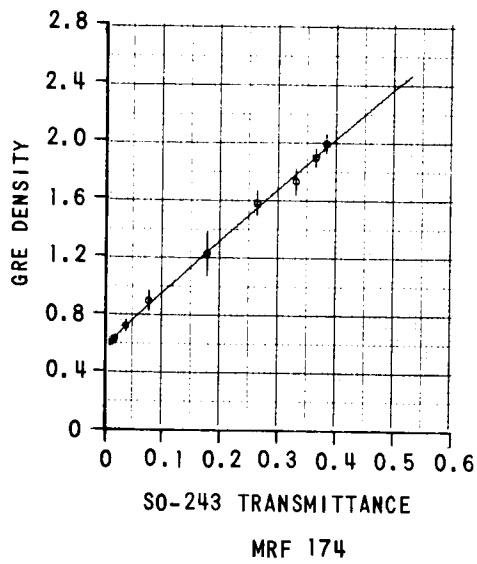
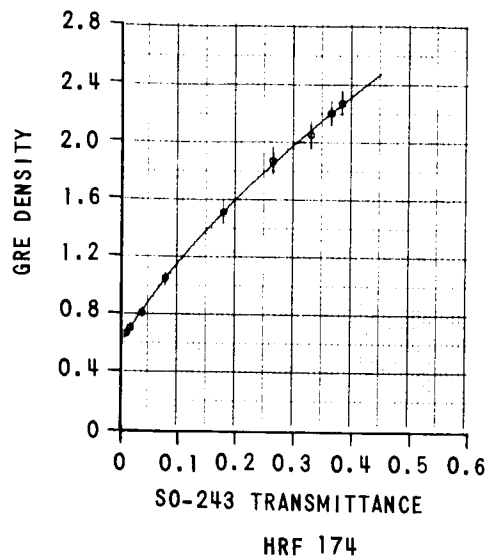
HRF 157



MRF 157

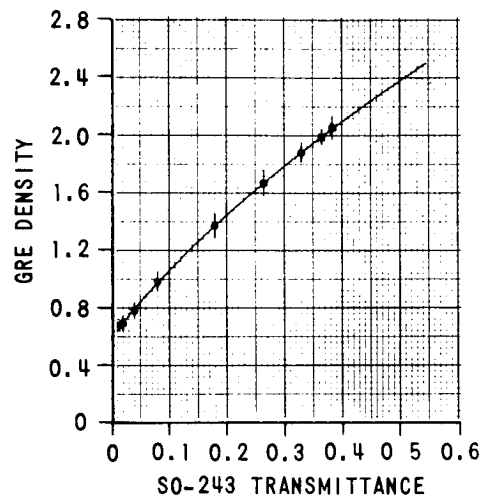
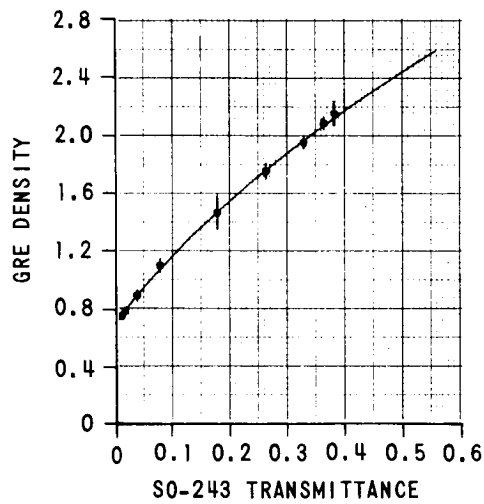
THE SOLID LINE IS THE COMPUTED REGRESSION OF SO-243 TRANSMITTANCE ON GRE DENSITY AND THE ERROR BARS INDICATE THE  $\pm$  ONE SIGMA SPREAD OF THE INDIVIDUAL MEASUREMENTS OF GRE DENSITY USING SEVERAL FRAMELETS IN EACH FRAME

Figure 9 REGRESSION BETWEEN SO-243 TRANSMITTANCE AND GRE DENSITY-ORBITER II



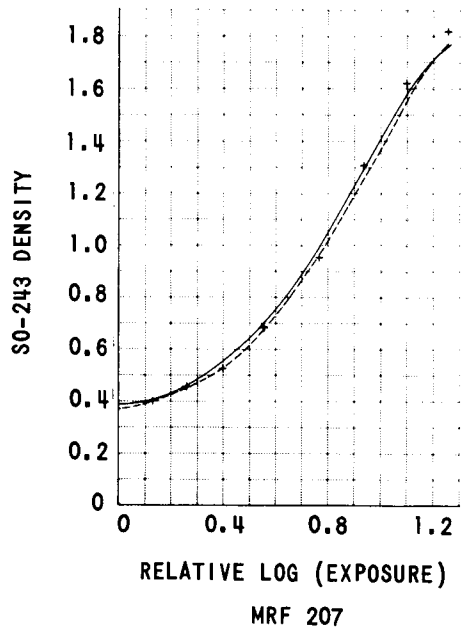
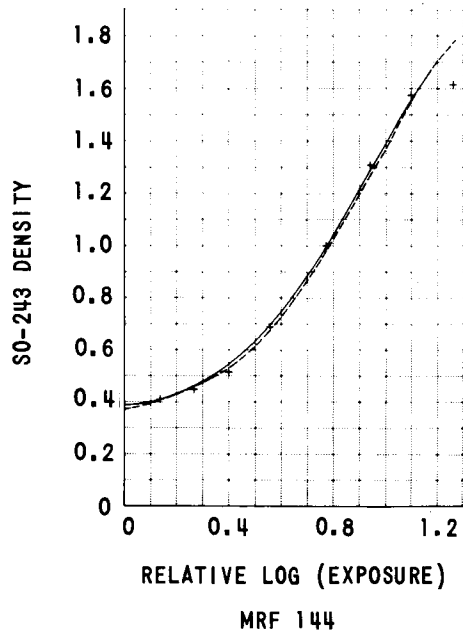
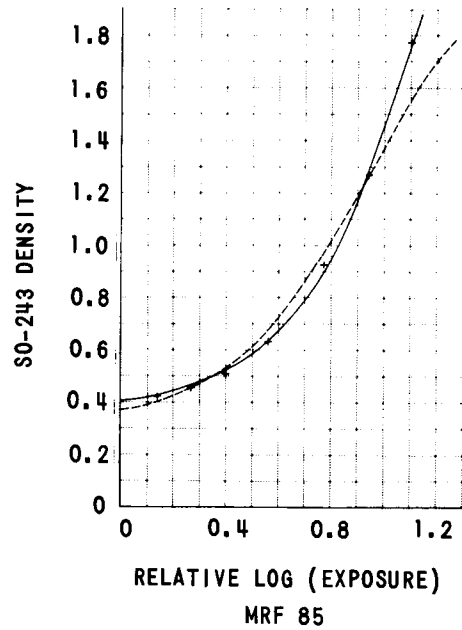
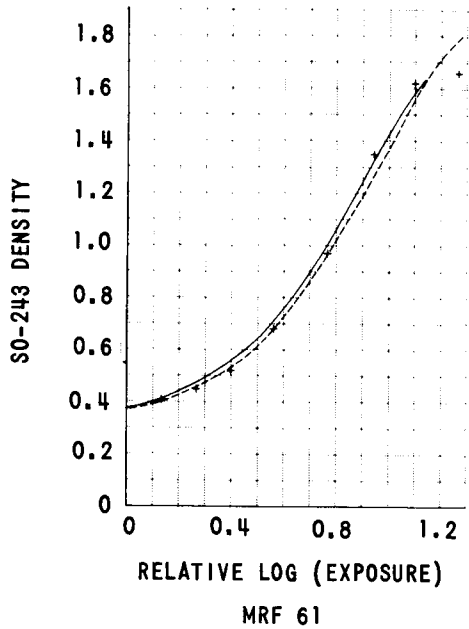
THE SOLID LINE IS THE COMPUTED REGRESSION OF SO-243 TRANSMITTANCE ON GRE DENSITY AND THE ERROR BARS INDICATE THE  $\pm$  ONE SIGMA SPREAD OF THE INDIVIDUAL MEASUREMENTS OF GRE DENSITY USING SEVERAL FRAMELETS IN EACH FRAME

Figure 10 REGRESSION BETWEEN SO-243 TRANSMITTANCE AND GRE DENSITY-ORBITER II



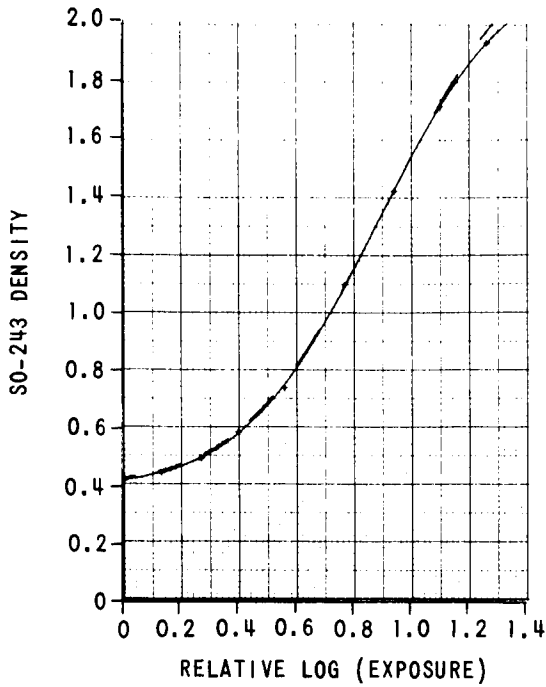
THE SOLID LINE IS THE COMPUTED REGRESSION OF SO-243 TRANSMITTANCE ON GRE DENSITY AND THE ERROR BARS INDICATE THE  $\pm$  ONE SIGMA SPREAD OF THE INDIVIDUAL MEASUREMENTS OF GRE DENSITY USING SEVERAL FRAMELETS IN EACH FRAME

Figure 11 REGRESSION BETWEEN SO-243 TRANSMITTANCE AND GRE DENSITY-ORBITER II

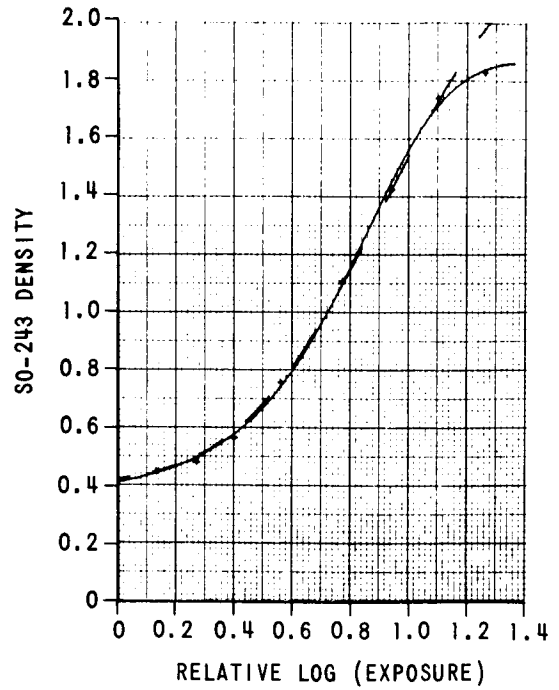


THE SYMBOLS (+) ARE THE MEASURED VALUES OF GRE DENSITY CONVERTED TO SPACECRAFT FILM DENSITY USING THE CORRESPONDING LINEAR RELATIONSHIPS. THE DASHED CURVE (---) IS THE PARAMETRIC FUNCTION FITTED TO THE DATA OBTAINED USING A SAMPLE OF BIMAT PROCESSED FILM TAKEN FROM THE ROLL WHICH PROVIDED THE FLIGHT FILM FOR LUNAR ORBITER I.

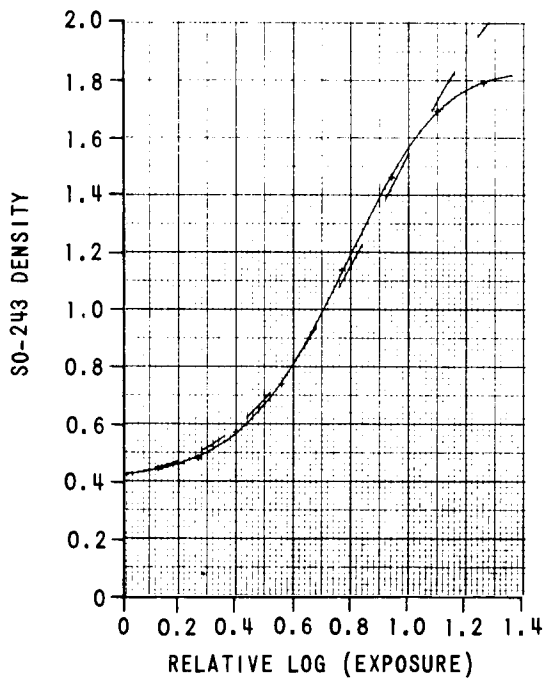
Figure 12 HURTER-DRIFFIELD RESPONSE DATA AND FILTERED PARAMETRIC FUNCTION-ORBITER I HIGH LEVEL ANALYSIS



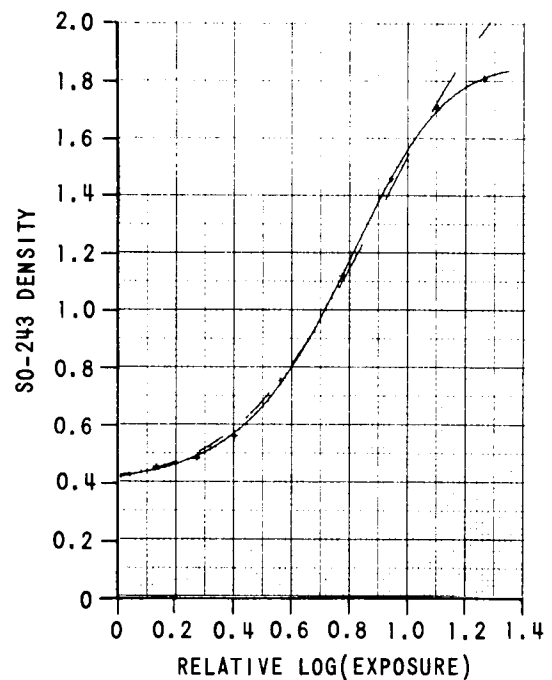
HRF 13



MRF 13



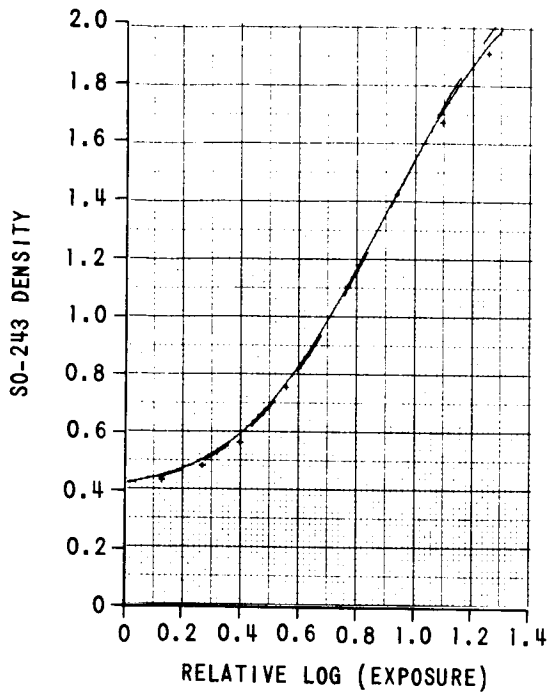
HRF 39



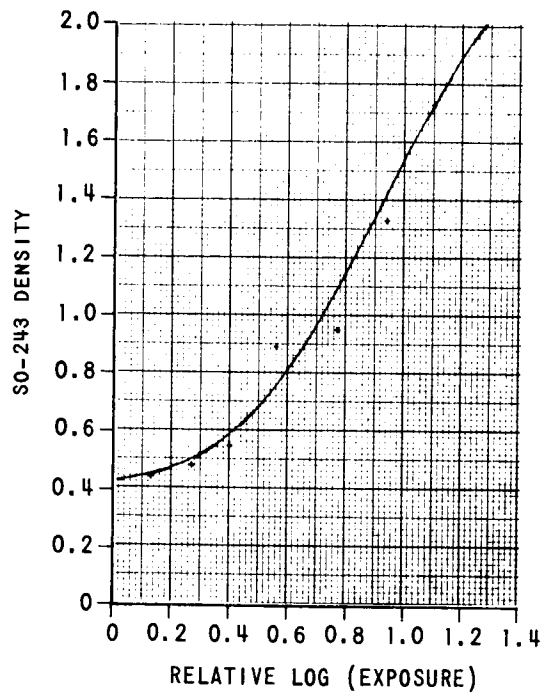
MRF 39

THE SYMBOLS (+) ARE THE MEASURED VALUES OF GRE DENSITY CONVERTED TO SPACECRAFT FILM DENSITY USING THE CORRESPONDING RELATIONSHIPS SHOWN IN FIGURE 5. THE DASHED CURVE (-----) IS THE PARAMETRIC FUNCTION FITTED TO THE DATA OBTAINED USING A SAMPLE OF BIMAT PROCESSED FILM TAKEN FROM THE ROLL WHICH PROVIDED THE FLIGHT FILM FOR LUNAR ORBITER II.

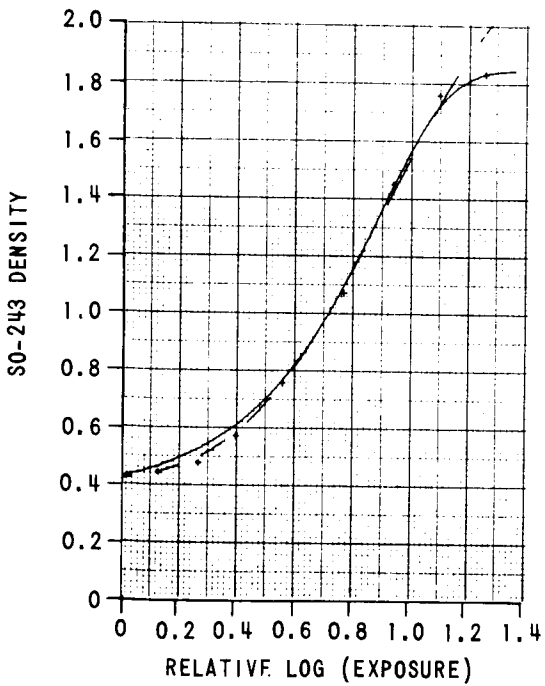
Figure 13 HURTER-DRIFFIELD RESPONSE DATA AND FITTED PARAMETRIC FUNCTION-ORBITER II



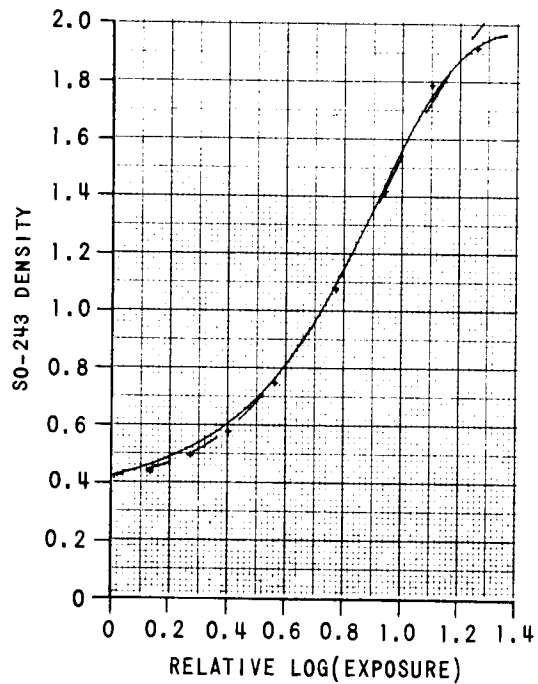
HRF 46



MRF 46



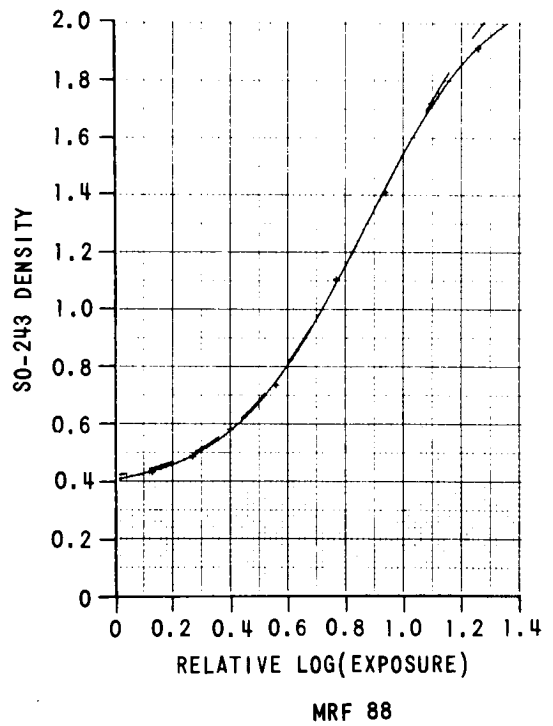
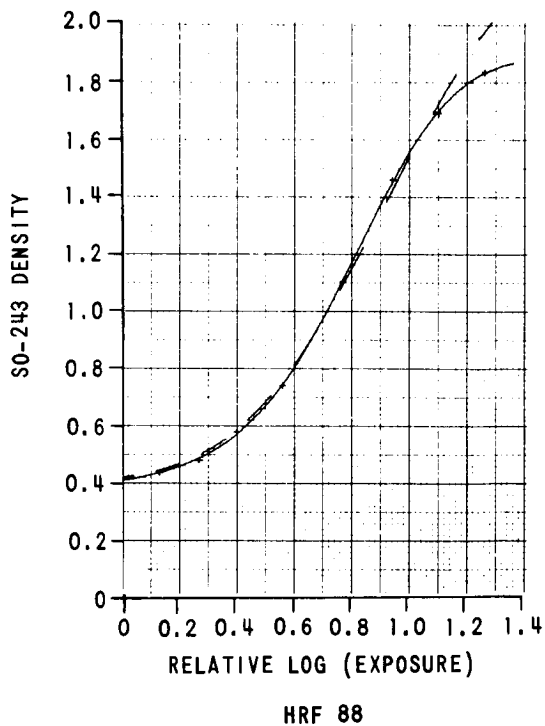
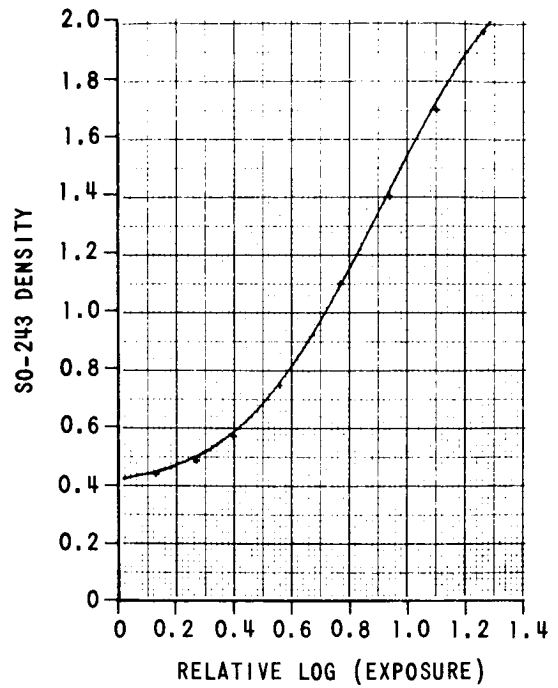
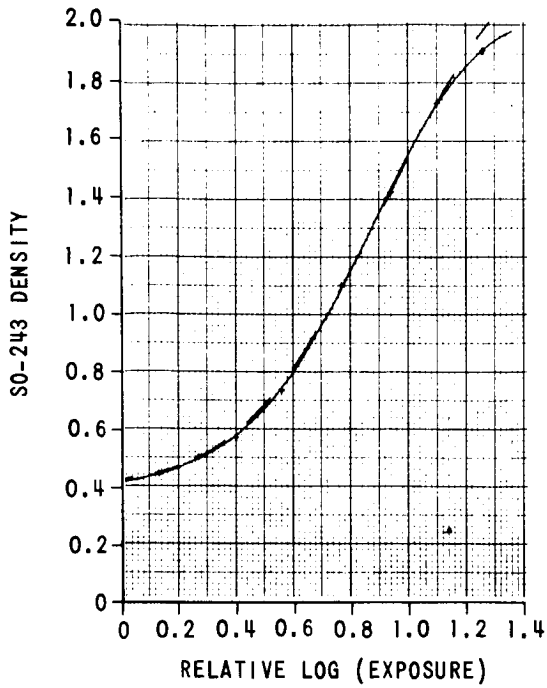
HRF 63



MRF 63

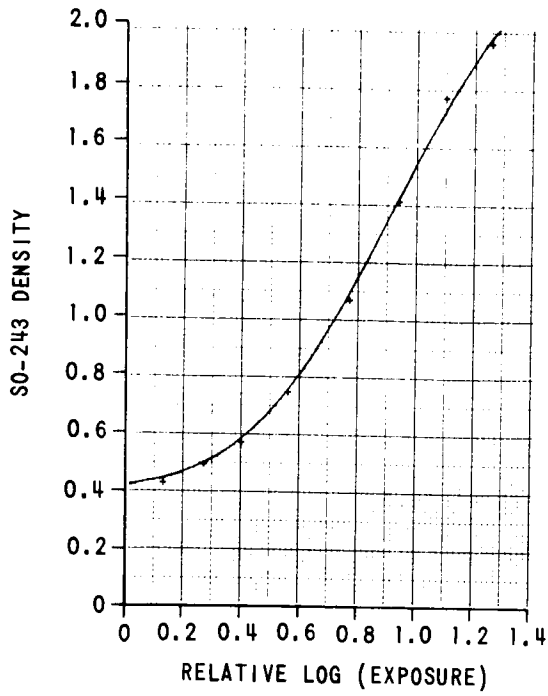
THE SYMBOLS (+) ARE THE MEASURED VALUES OF GRE DENSITY CONVERTED TO SPACECRAFT FILM DENSITY USING THE CORRESPONDING RELATIONSHIPS SHOWN IN FIGURE 6. THE DASHED CURVE (-----) IS THE PARAMETRIC FUNCTION FITTED TO THE DATA OBTAINED USING A SAMPLE OF BIMAT PROCESSED FILM TAKEN FROM THE ROLL WHICH PROVIDED THE FLIGHT FILM FOR LUNAR ORBITER II.

Figure 14 HURTER-DRIFFIELD RESPONSE DATA AND FITTED PARAMETRIC FUNCTION-ORBITER II

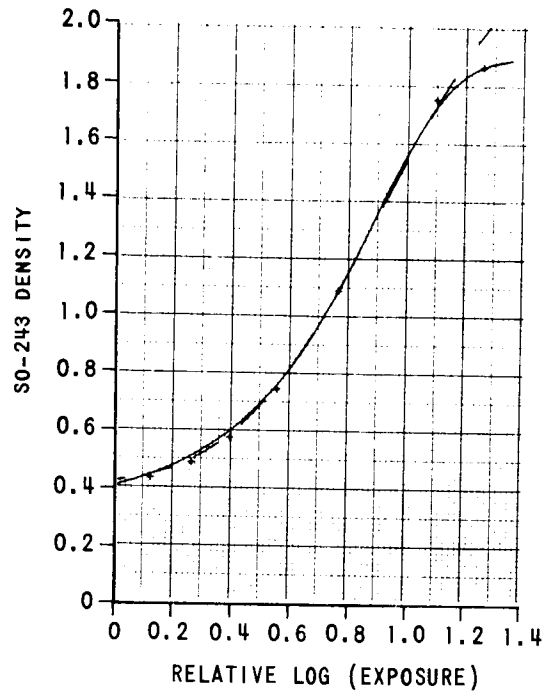


THE SYMBOLS (+) ARE THE MEASURED VALUES OF GRE DENSITY CONVERTED TO SPACECRAFT FILM DENSITY USING THE CORRESPONDING RELATIONSHIPS SHOWN IN FIGURE 7. THE DASHED CURVE (-----) IS THE PARAMETRIC FUNCTION FITTED TO THE DATA OBTAINED USING A SAMPLE OF BIMAT PROCESSED FILM TAKEN FROM THE ROLL WHICH PROVIDED THE FLIGHT FILM FOR LUNAR ORBITER II.

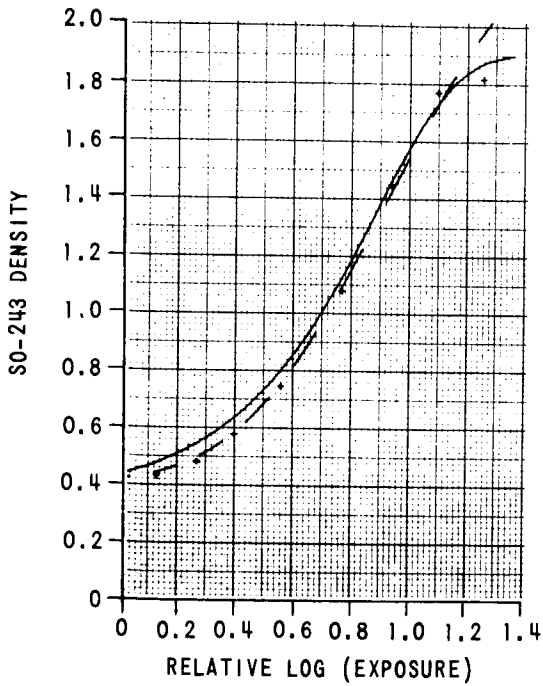
Figure 15 HURTER-DRIFFIELD RESPONSE DATA AND FITTED PARAMETRIC FUNCTION-ORBITER II



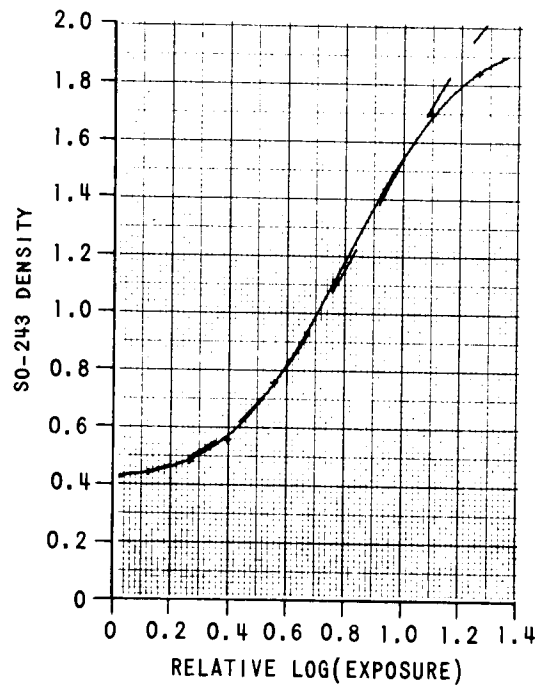
HRF 99



MRF 99



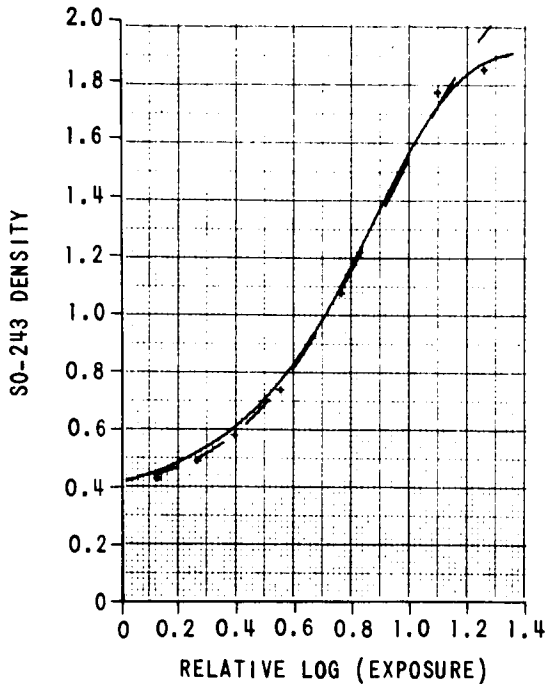
HRF 124



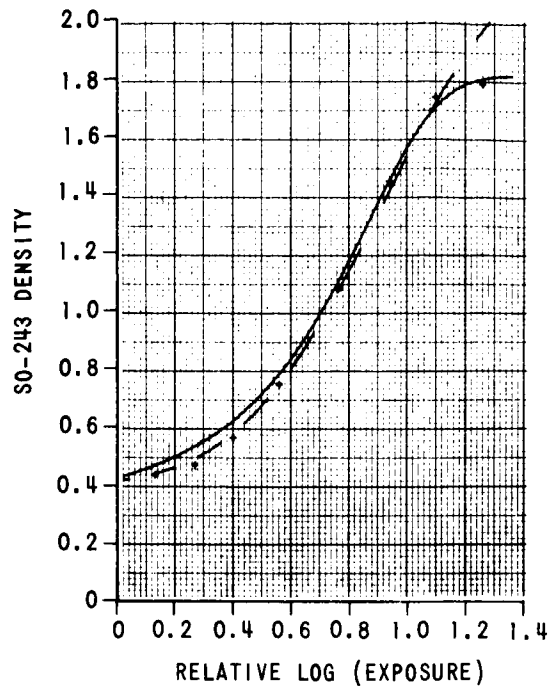
MRF 124

THE SYMBOLS (+) ARE THE MEASURED VALUES OF GRE DENSITY CONVERTED TO SPACECRAFT FILM DENSITY USING THE CORRESPONDING RELATIONSHIPS SHOWN IN FIGURE 8. THE DASHED CURVE (-----) IS THE PARAMETRIC FUNCTION FITTED TO THE DATA OBTAINED USING A SAMPLE OF BIMAT PROCESSED FILM TAKEN FROM THE ROLL WHICH PROVIDED THE FLIGHT FILM FOR LUNAR ORBITER II.

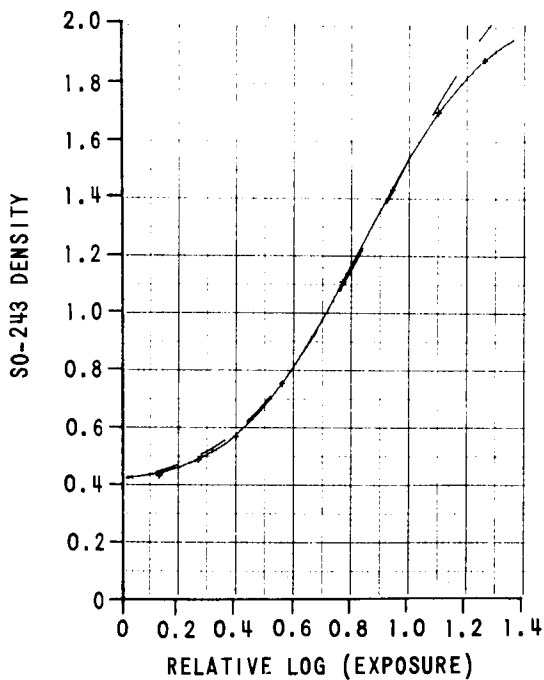
Figure 16 HURTER-DRIFFIELD RESPONSE DATA AND FITTED PARAMETRIC FUNCTION-ORBITER II



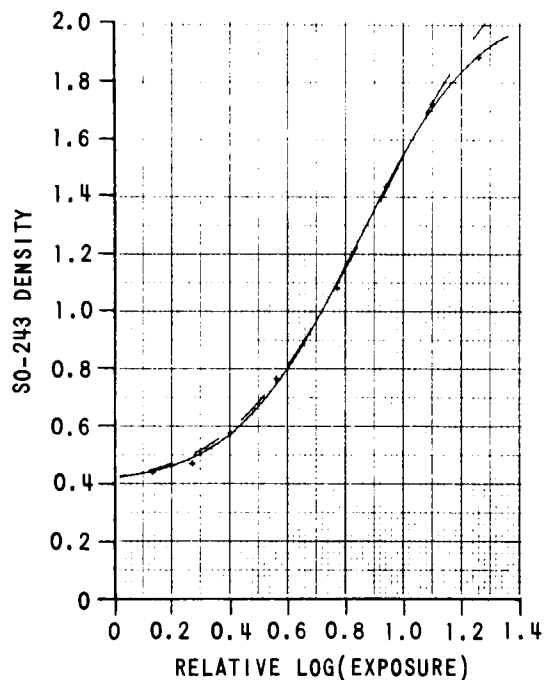
HRF 141



MRF 141



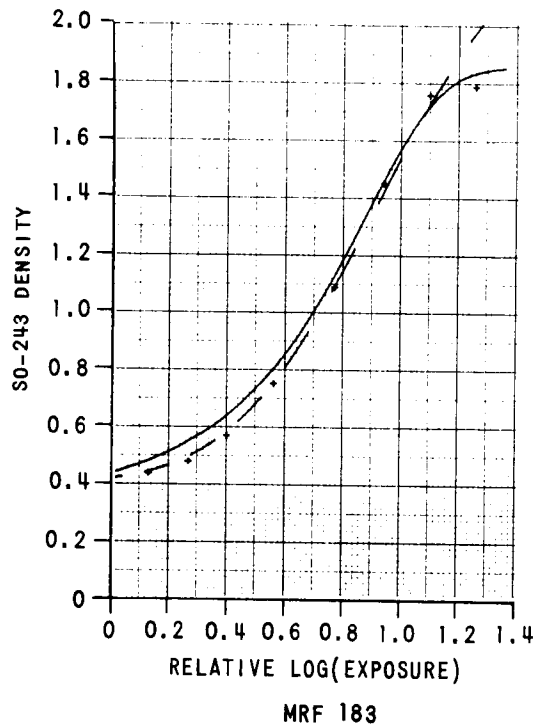
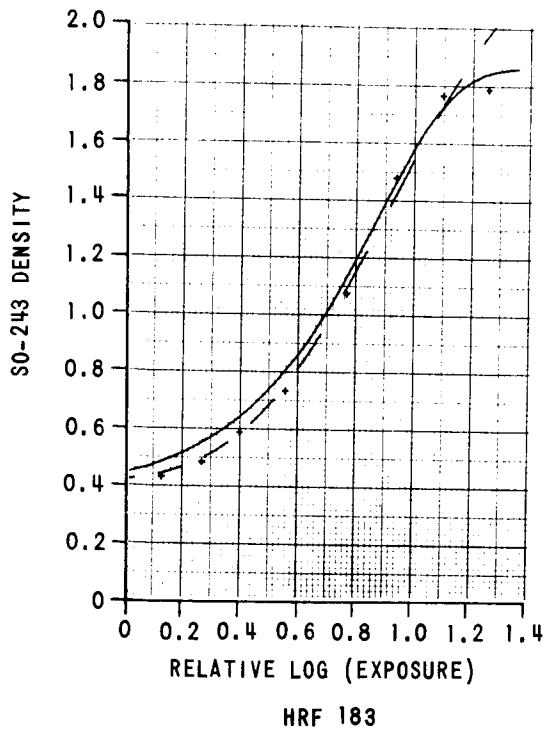
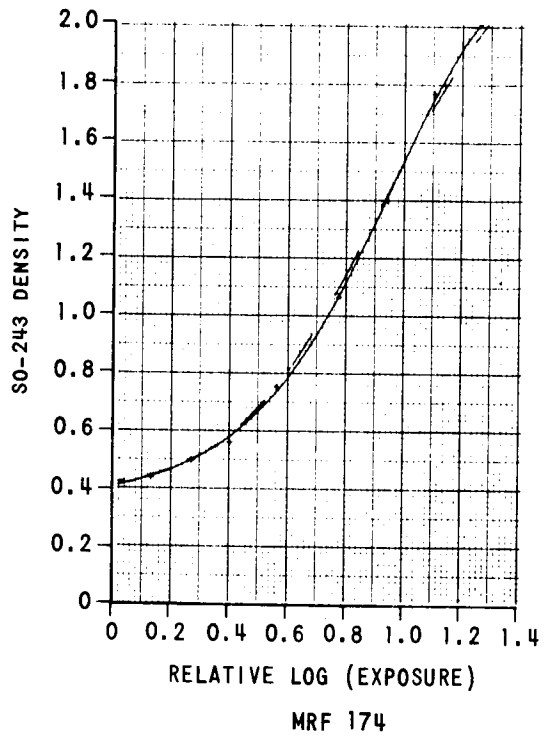
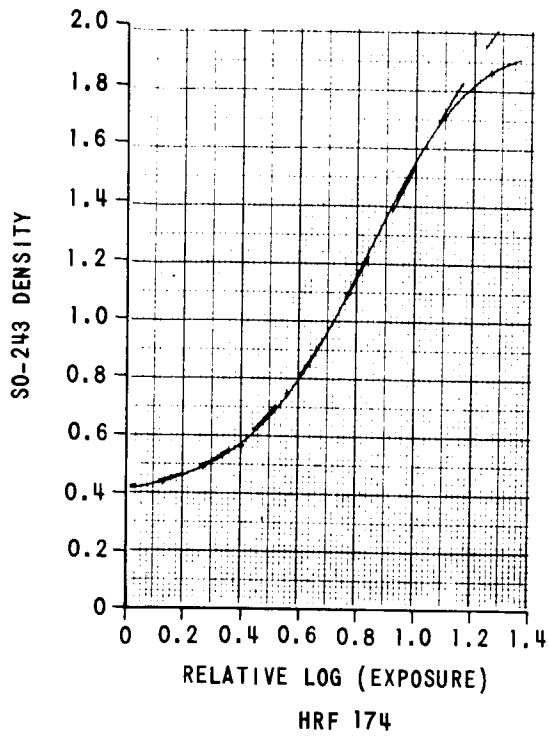
HRF 157



MRF 157

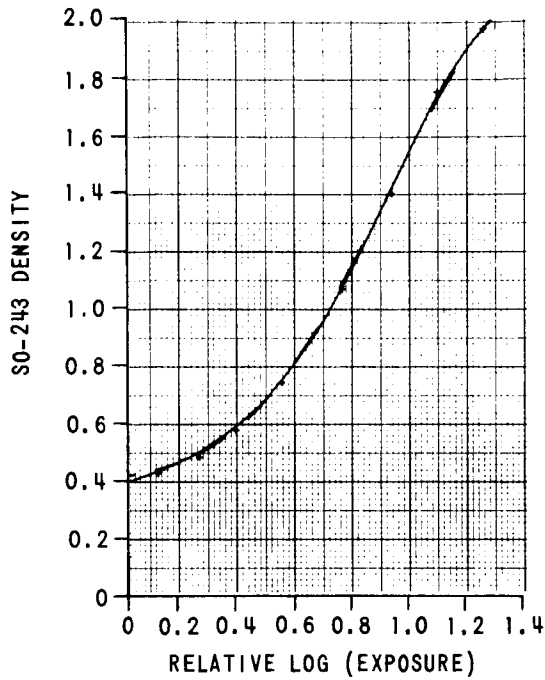
THE SYMBOLS (+) ARE THE MEASURED VALUES OF GRE DENSITY CONVERTED TO SPACECRAFT FILM DENSITY USING THE CORRESPONDING RELATIONSHIPS SHOWN IN FIGURE 9. THE DASHED CURVE (-----) IS THE PARAMETRIC FUNCTION FITTED TO THE DATA OBTAINED USING A SAMPLE OF BIMAT PROCESSED FILM TAKEN FROM THE ROLL WHICH PROVIDED THE FLIGHT FILM FOR LUNAR ORBITER II.

Figure 17 HURTER-DRIFFIELD RESPONSE DATA AND FITTED PARAMETRIC FUNCTION-ORBITER II

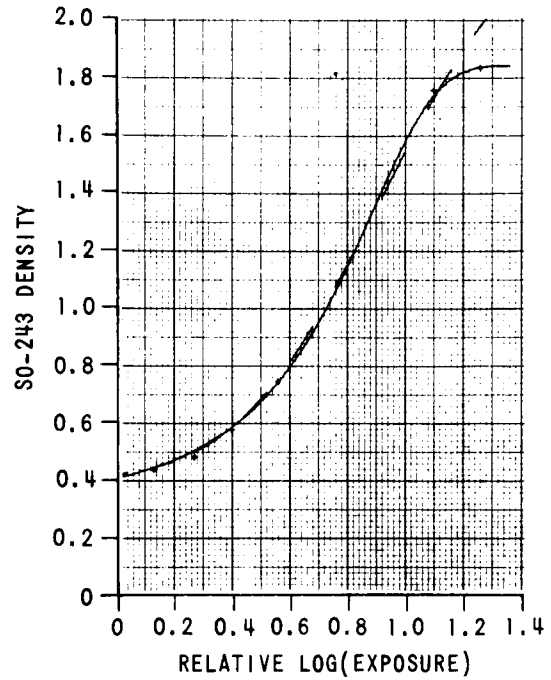


THE SYMBOLS (+) ARE THE MEASURED VALUES OF GRE DENSITY CONVERTED TO SPACECRAFT FILM DENSITY USING THE CORRESPONDING RELATIONSHIPS SHOWN IN FIGURE 10. THE DASHED CURVE (-----) IS THE PARAMETRIC FUNCTION FITTED TO THE DATA OBTAINED USING A SAMPLE OF BIMAT PROCESSED FILM TAKEN FROM THE ROLL WHICH PROVIDED THE FLIGHT FILM FOR LUNAR ORBITER II.

Figure 18 HURTER-DRIFFIELD RESPONSE DATA AND FITTED PARAMETRIC FUNCTION-ORBITER II



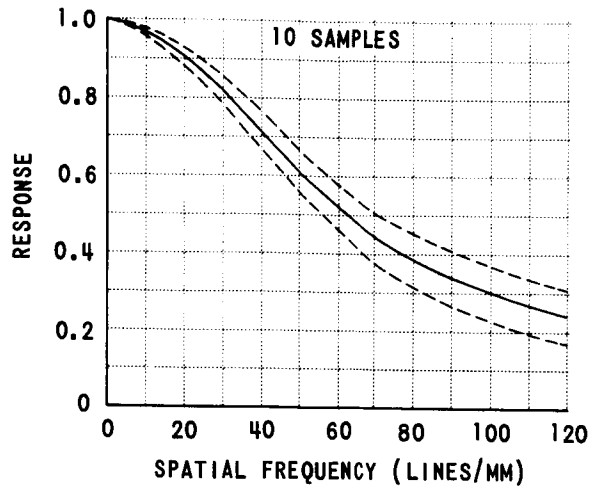
HRF 208



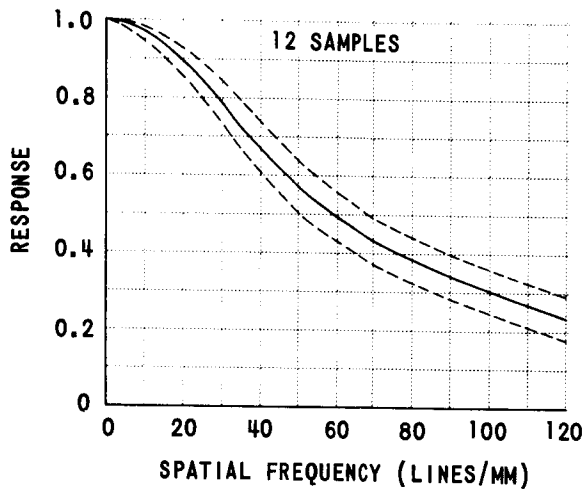
MRF 208

THE SYMBOLS (+) ARE THE MEASURED VALUES OF GRE DENSITY CONVERTED TO SPACECRAFT FILM DENSITY USING THE CORRESPONDING RELATIONSHIPS SHOWN IN FIGURE 11. THE DASHED CURVE (-----) IS THE PARAMETRIC FUNCTION FITTED TO THE DATA OBTAINED USING A SAMPLE OF BIMAT PROCESSED FILM TAKEN FROM THE ROLL WHICH PROVIDED THE FLIGHT FILM FOR LUNAR ORBITER II.

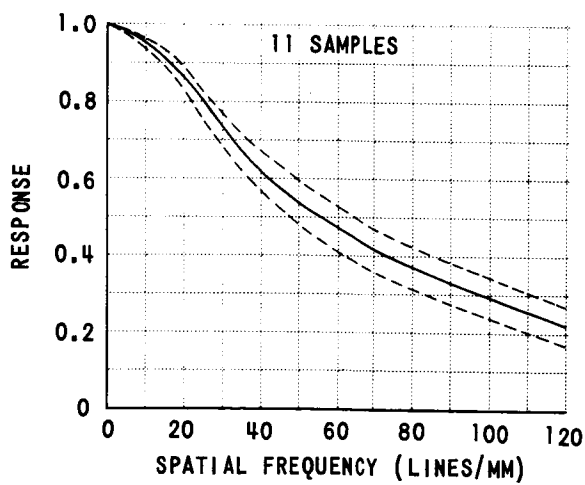
Figure 19 HURTER-DRIFFIELD RESPONSE DATA AND FITTED PARAMETRIC FUNCTION-ORBITER II



(a) EDGE OF STEP 5

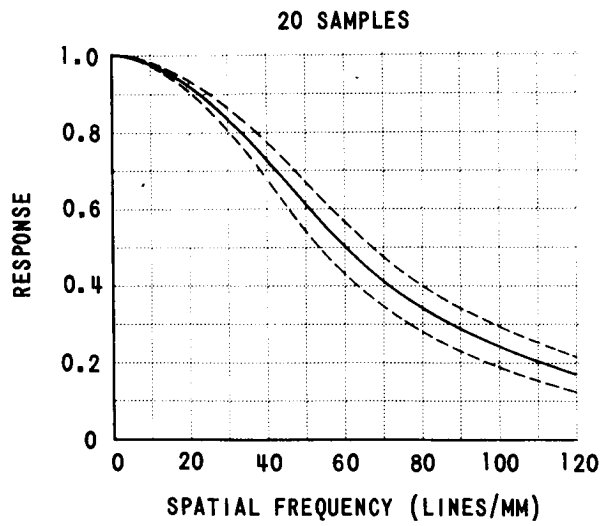


(b) EDGE OF STEP 6

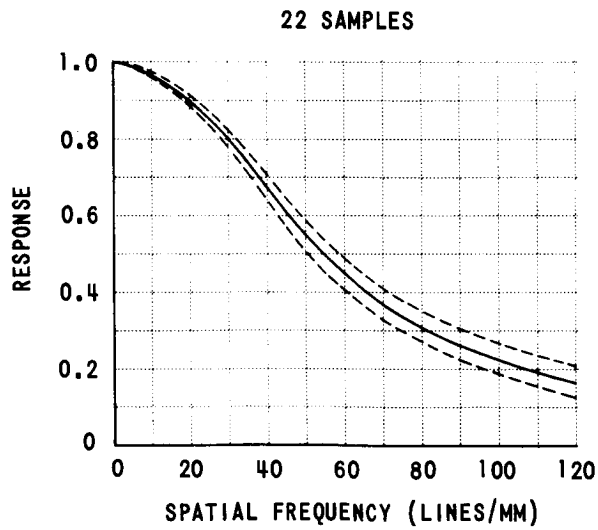


(c) EDGE OF STEP 7

Figure 20 EDGE SHARPNESS RESPONSE - ORBITER I



(a) EDGE OF STEP 5



(b) EDGE OF STEP 6

Figure 21 EDGE SHARPNESS RESPONSE-ORBITER II

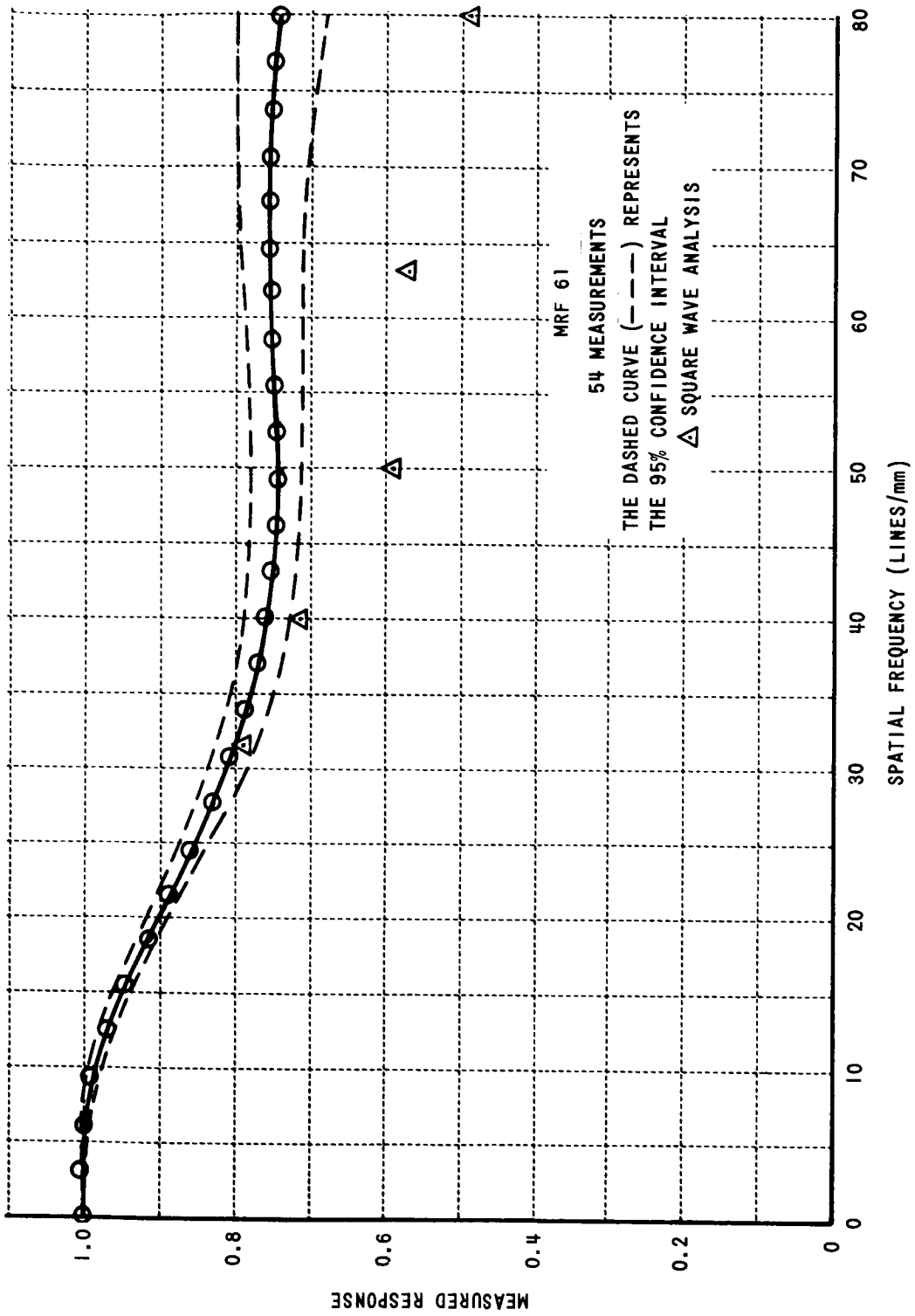


Figure 22 SCANNER-COMMUNICATIONS-GRS MTF-ORBITER I

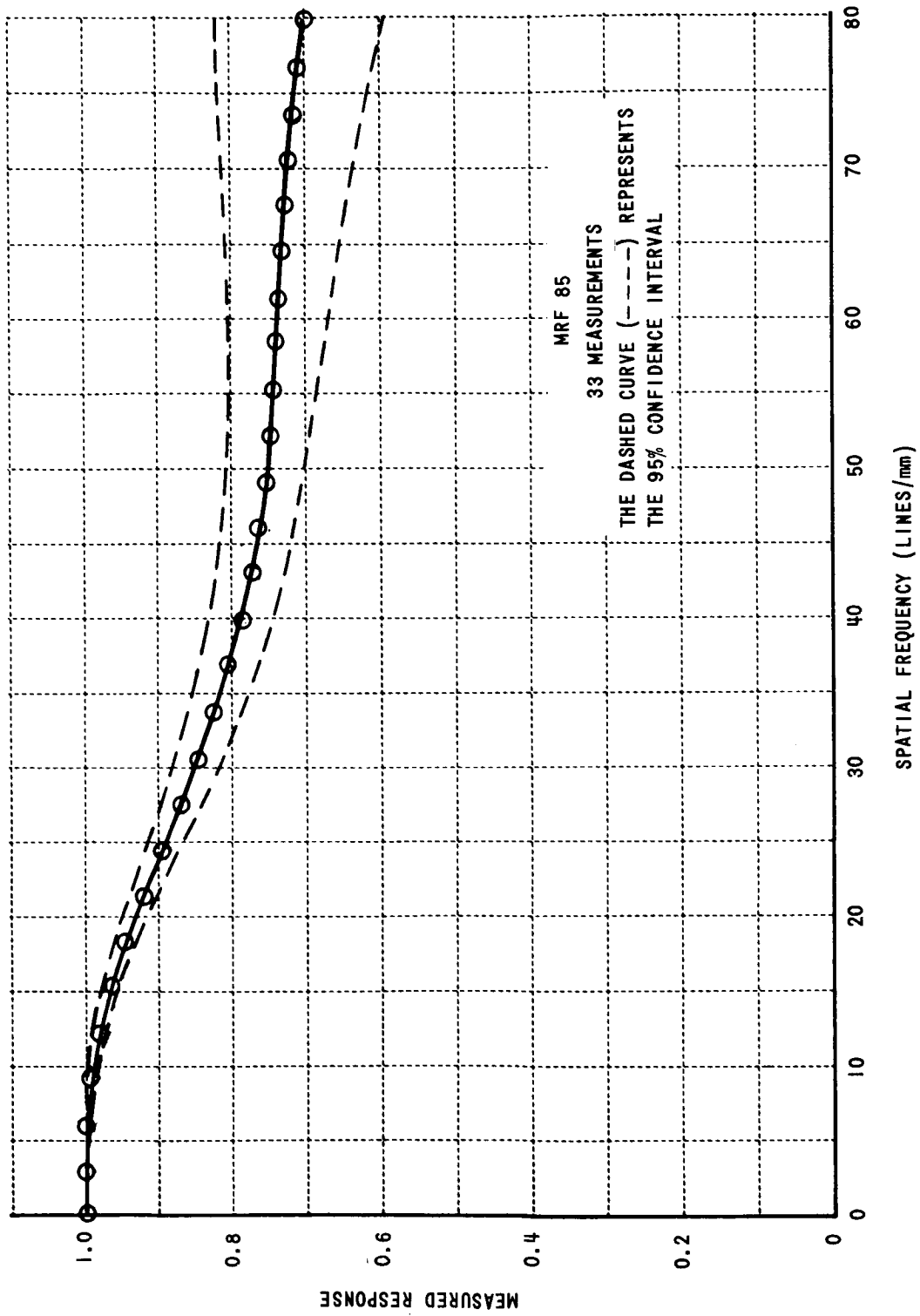


Figure 23 SCANNER-COMMUNICATIONS-GRS MTF-ORBITER I

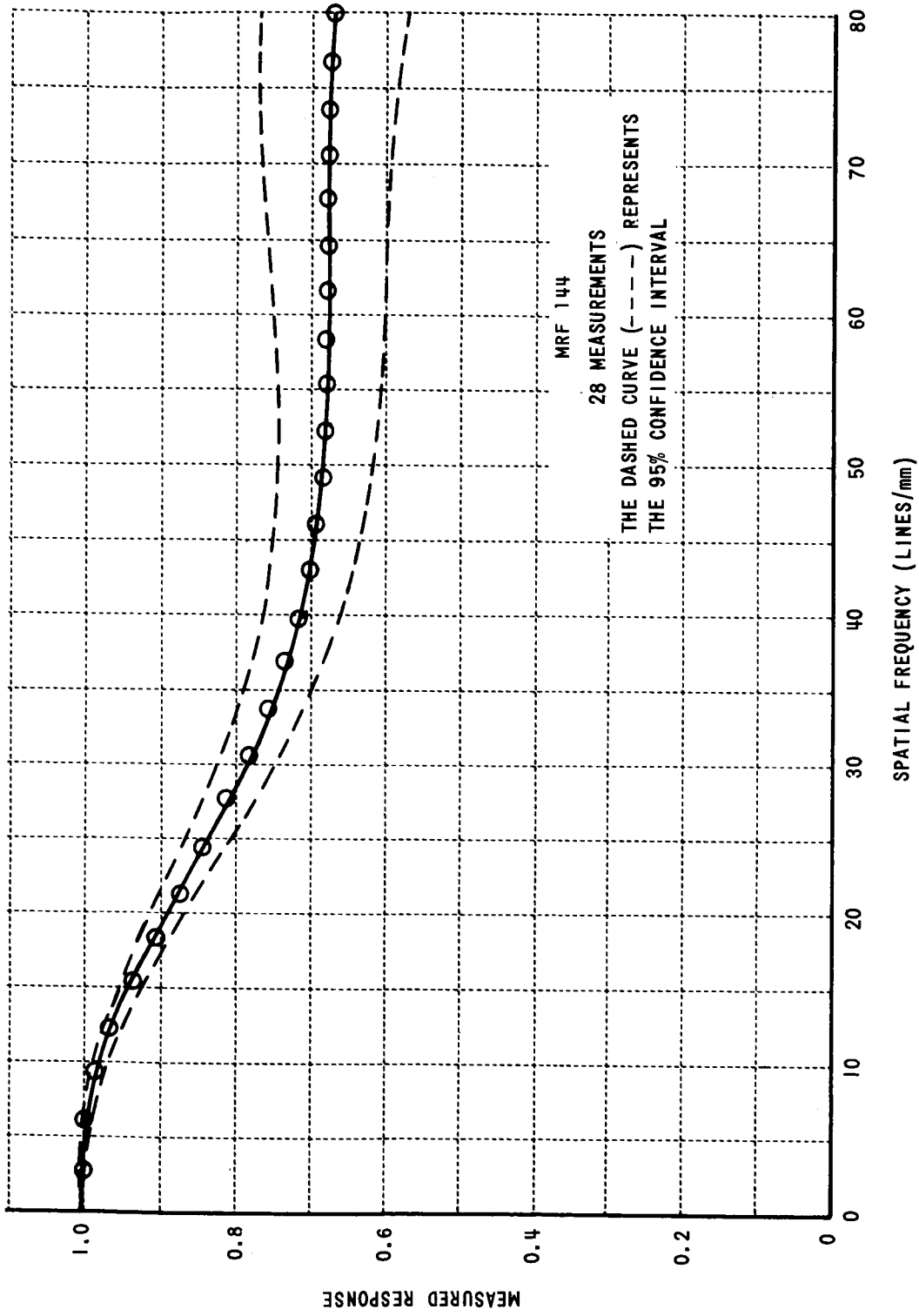


Figure 24 SCANNER-COMMUNICATIONS-GRS MTF-ORBITER I

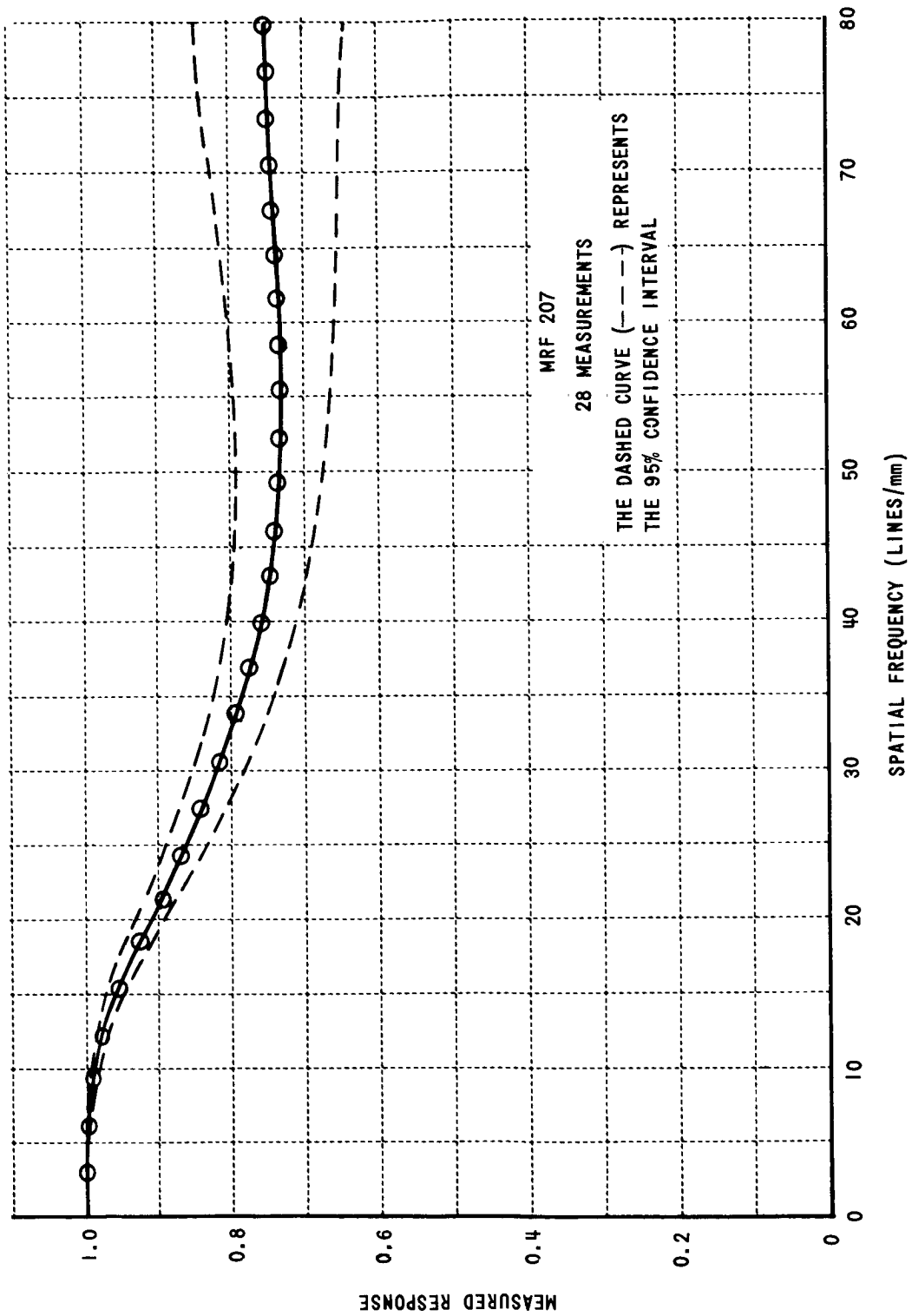


Figure 25 SCANNER-COMMUNICATIONS-GRS MTF-ORBITER I

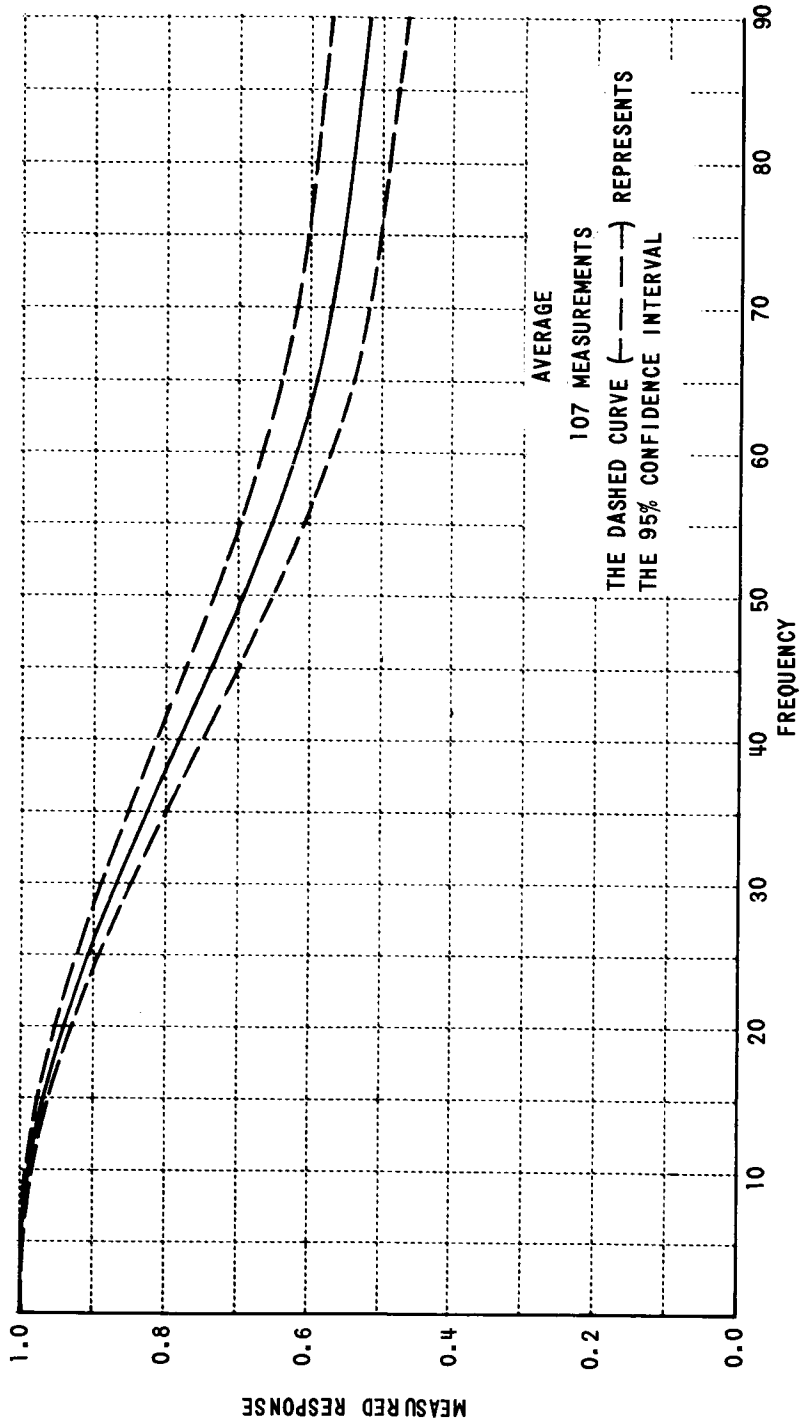


Figure 26 SCANNER-COMMUNICATIONS-GRS MTF-ORBITER II

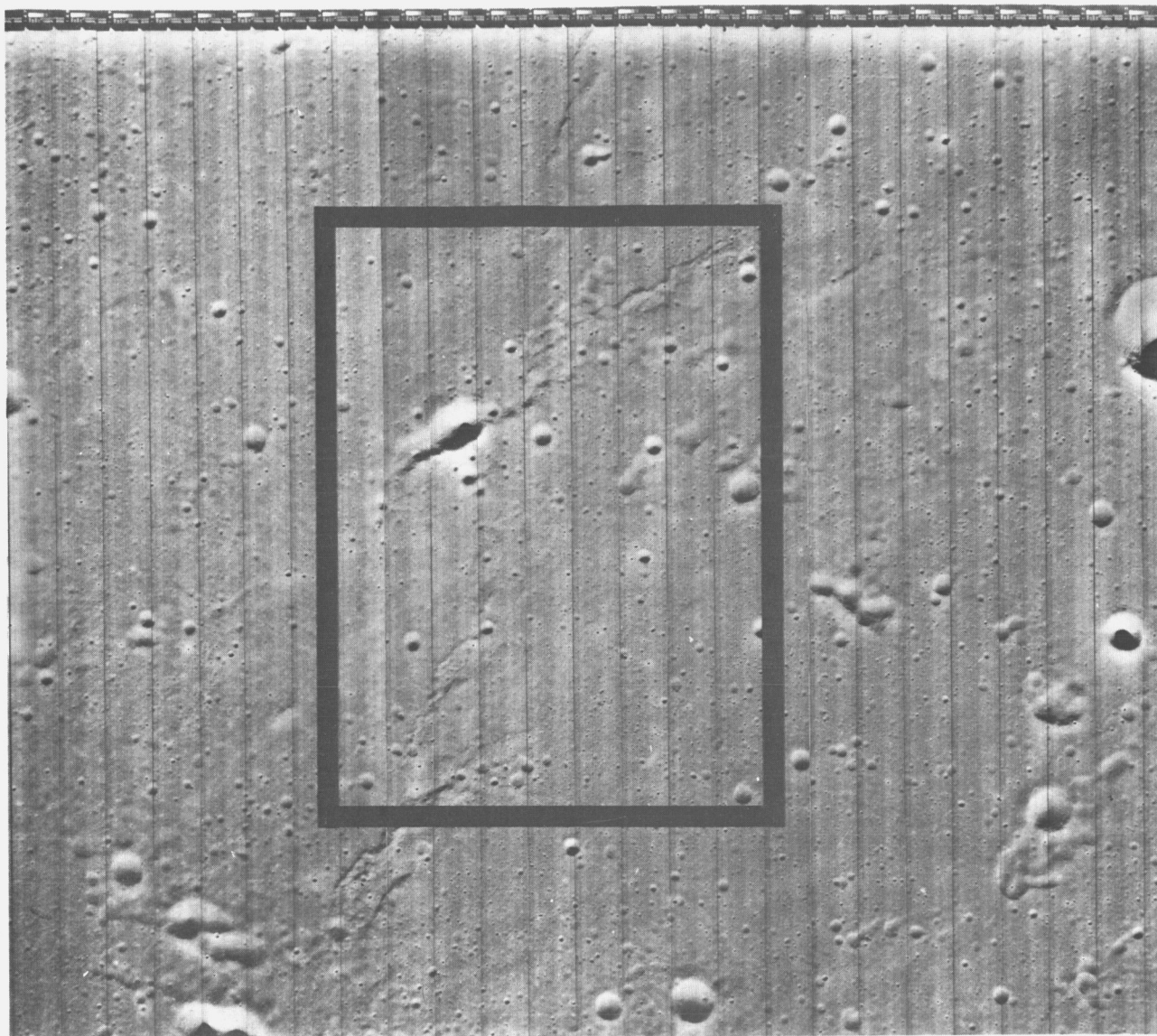
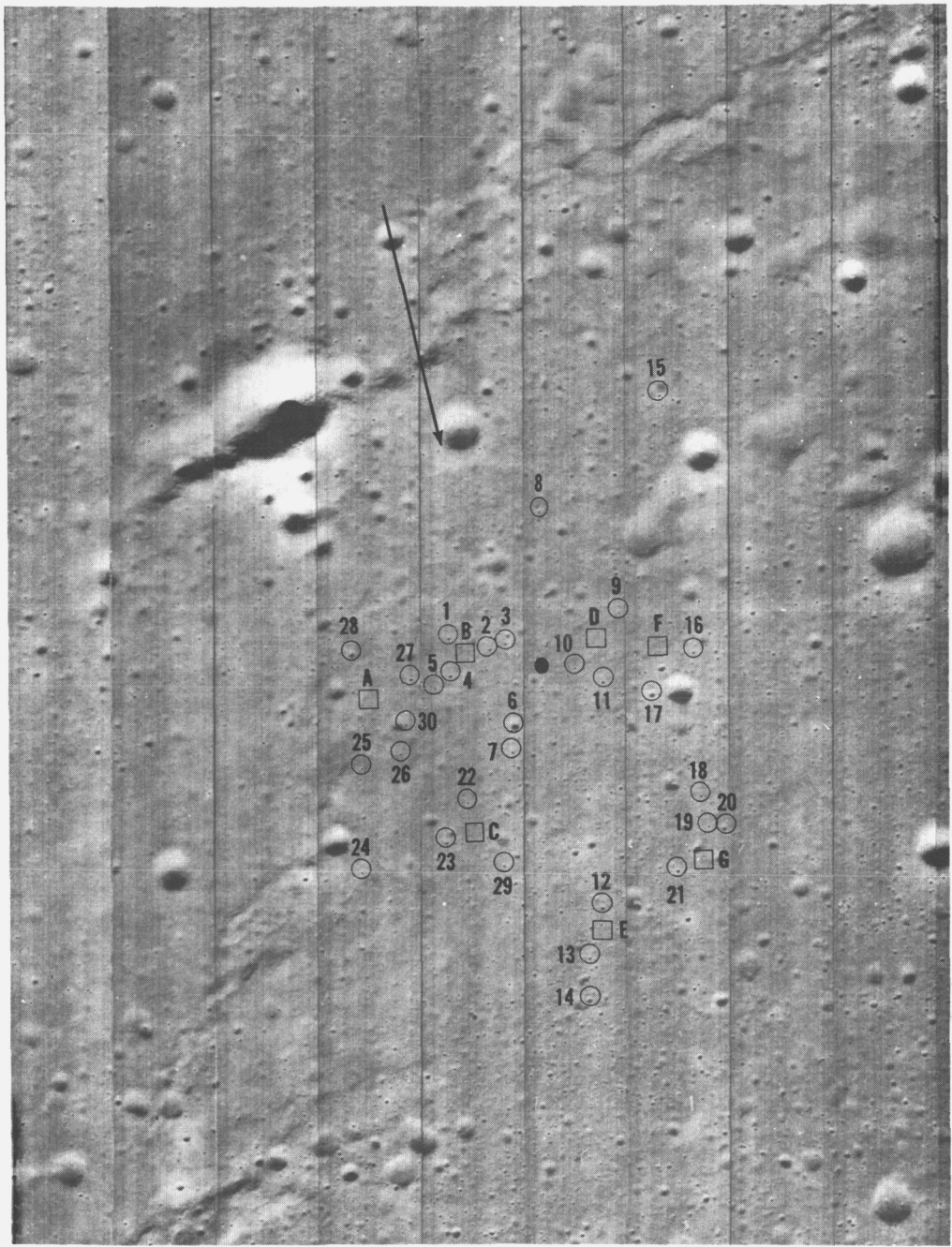


Figure 27 MEDIUM RESOLUTION FRAME 85-ORBITER I



- NADIR
  - UNIFORM AREAS TO MEASURE DENSITY FOR FLAT SURFACE
- SELECTED CRATER EDGES
  - DIRECTION OF INCIDENT SUNLIGHT

Figure 28 SELECTED CRATER SHADOW EDGES-MRF 85

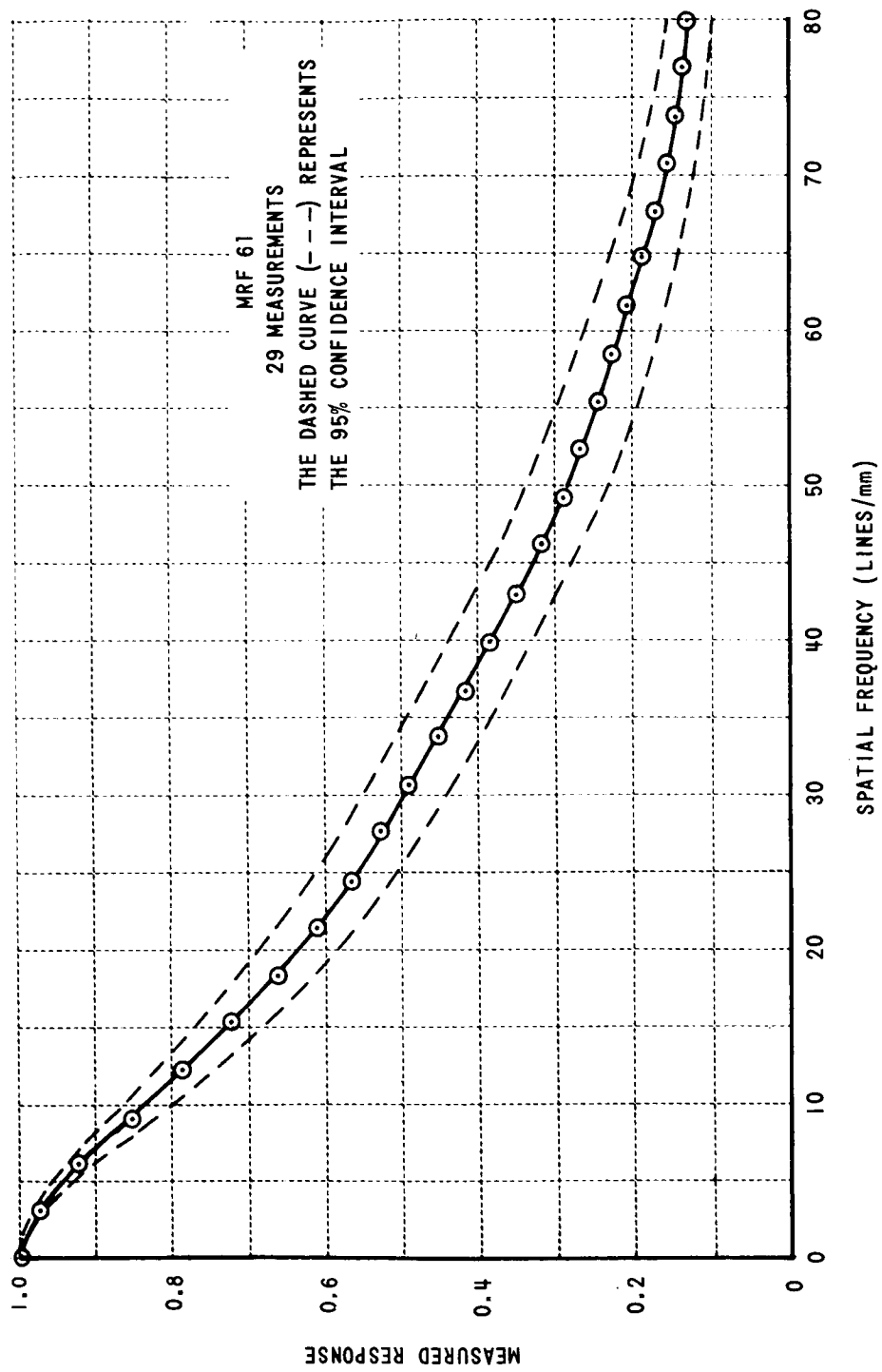


Figure 29 MEDIUM RESOLUTION IMAGING SYSTEM MTF-ORBITER I

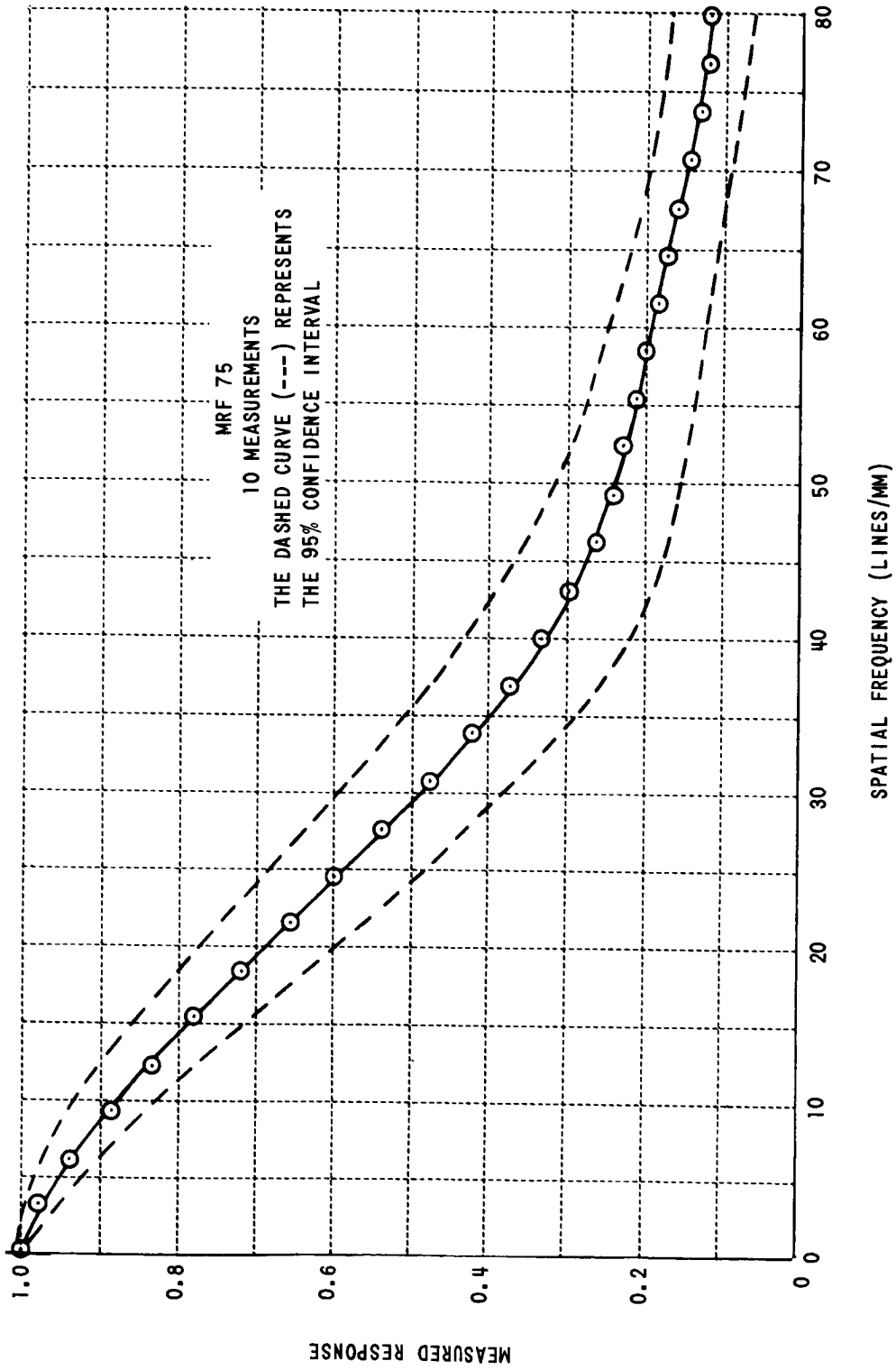


Figure 30 MEDIUM RESOLUTION IMAGING SYSTEM MTF-ORBITER I

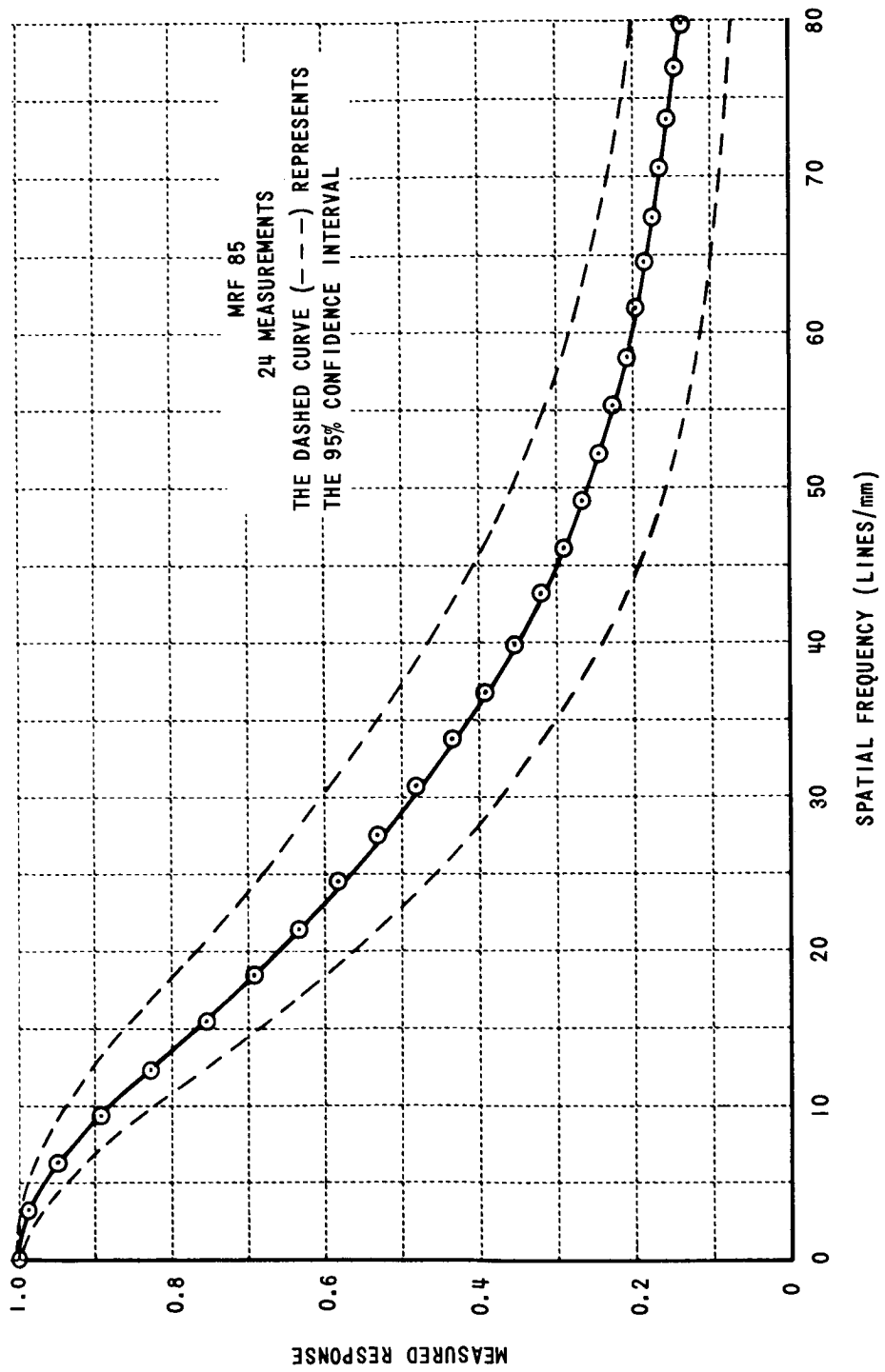


Figure 31 MEDIUM RESOLUTION IMAGING SYSTEM MTF-ORBITER I

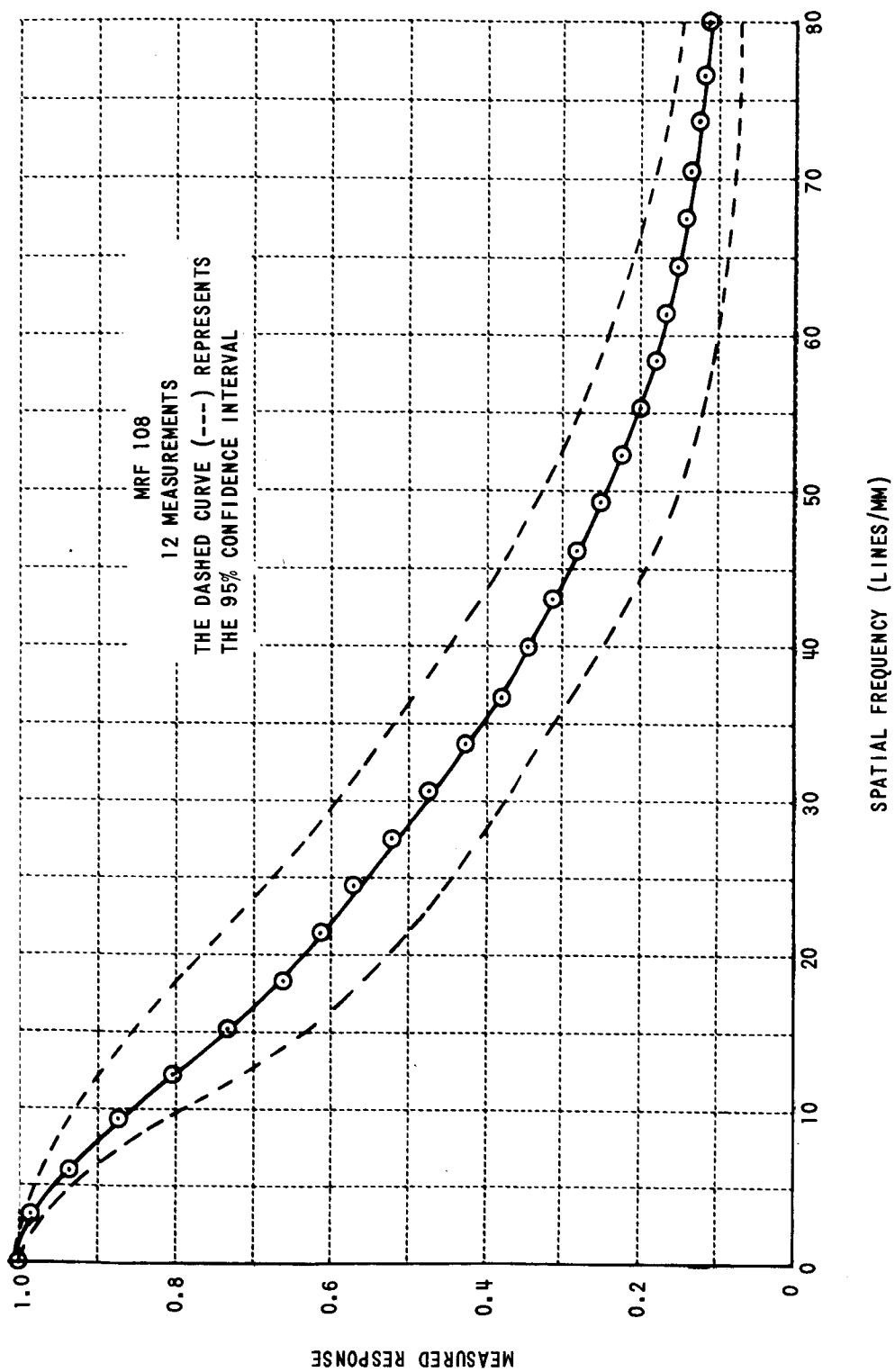


Figure 32 MEDIUM RESOLUTION IMAGING SYSTEM MTF-ORBITER I

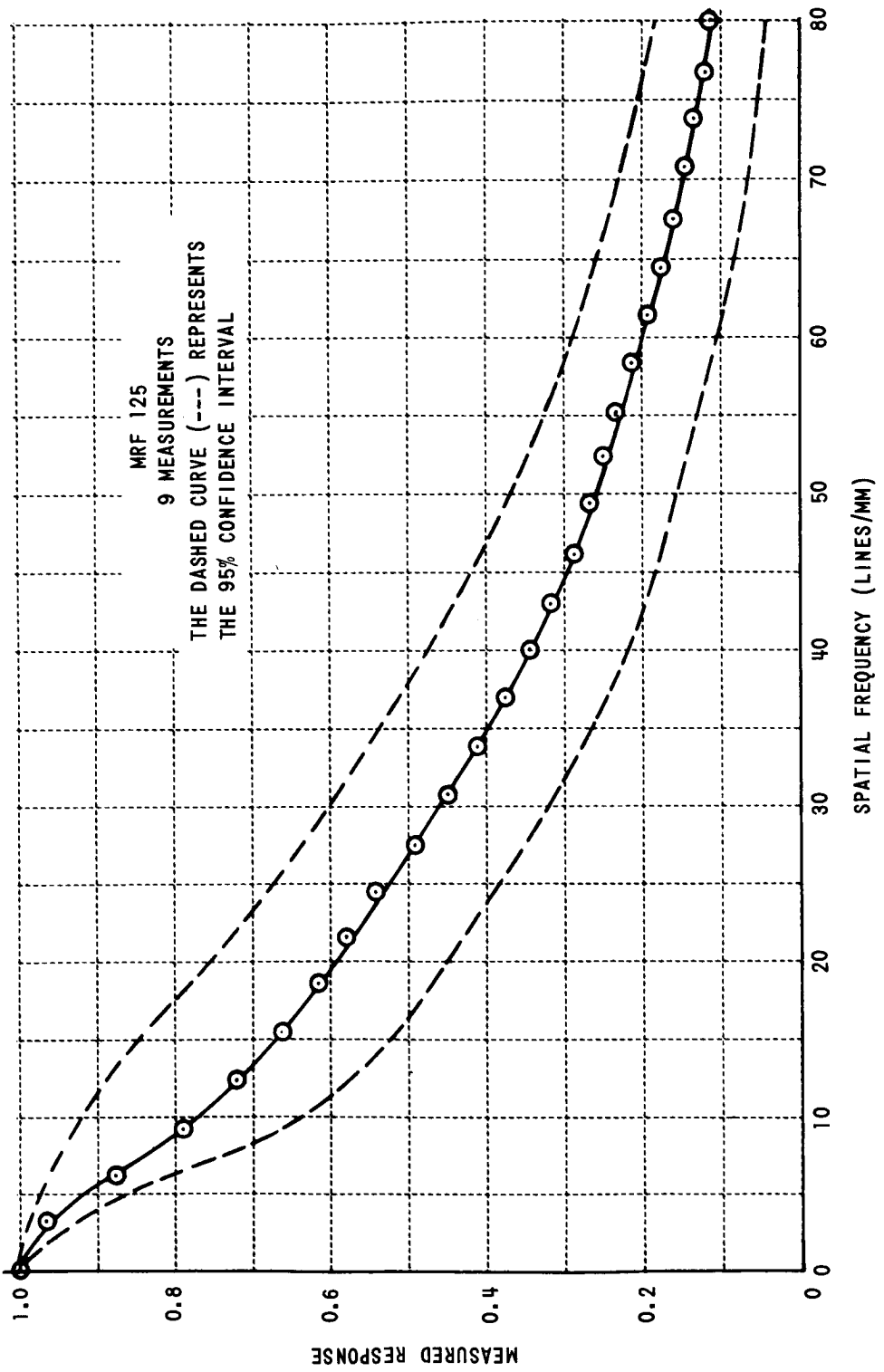


Figure 33 MEDIUM RESOLUTION IMAGING SYSTEM MTF-ORBITER I

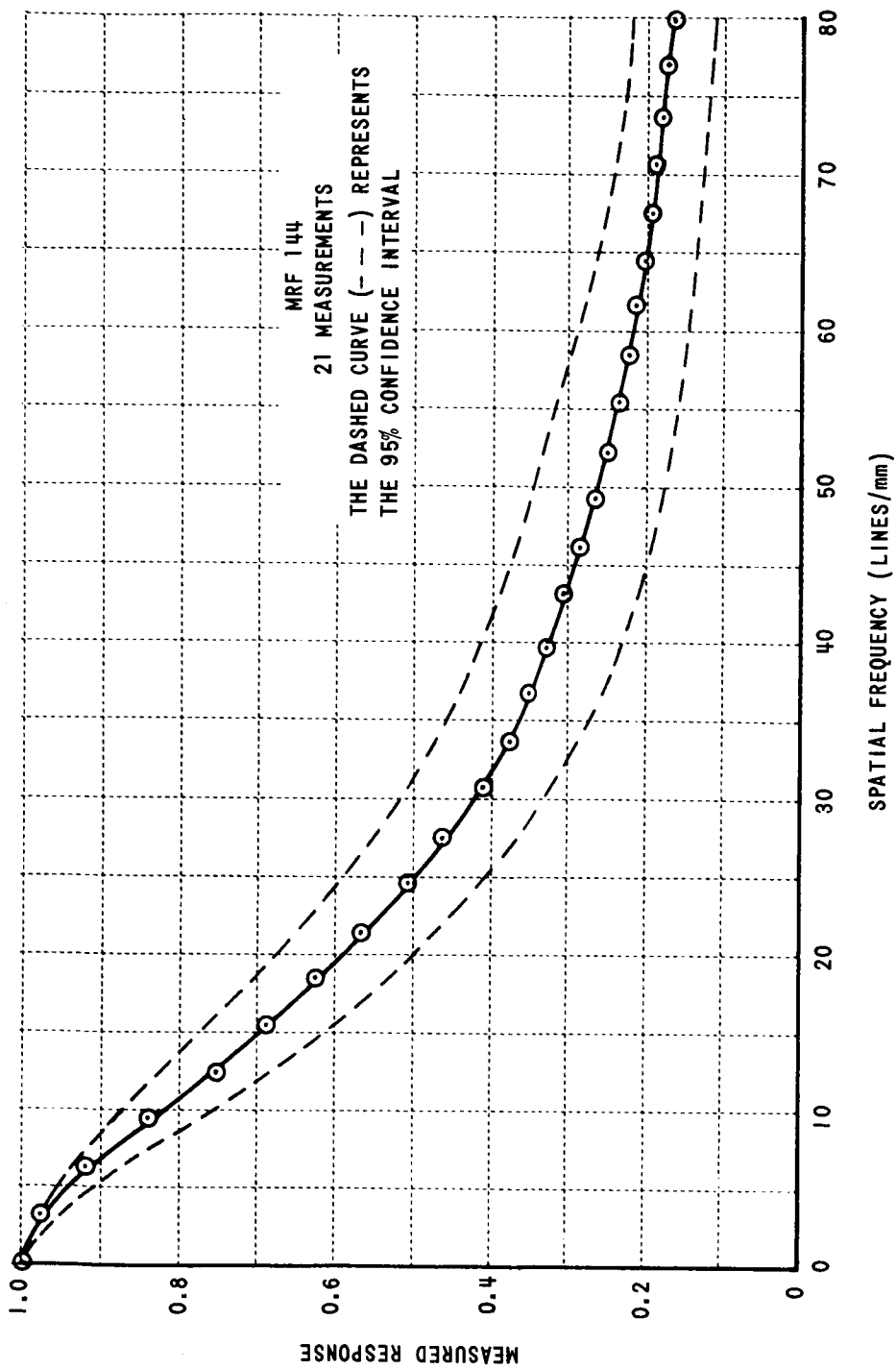


Figure 34 MEDIUM RESOLUTION IMAGING SYSTEM MTF-ORBITER I

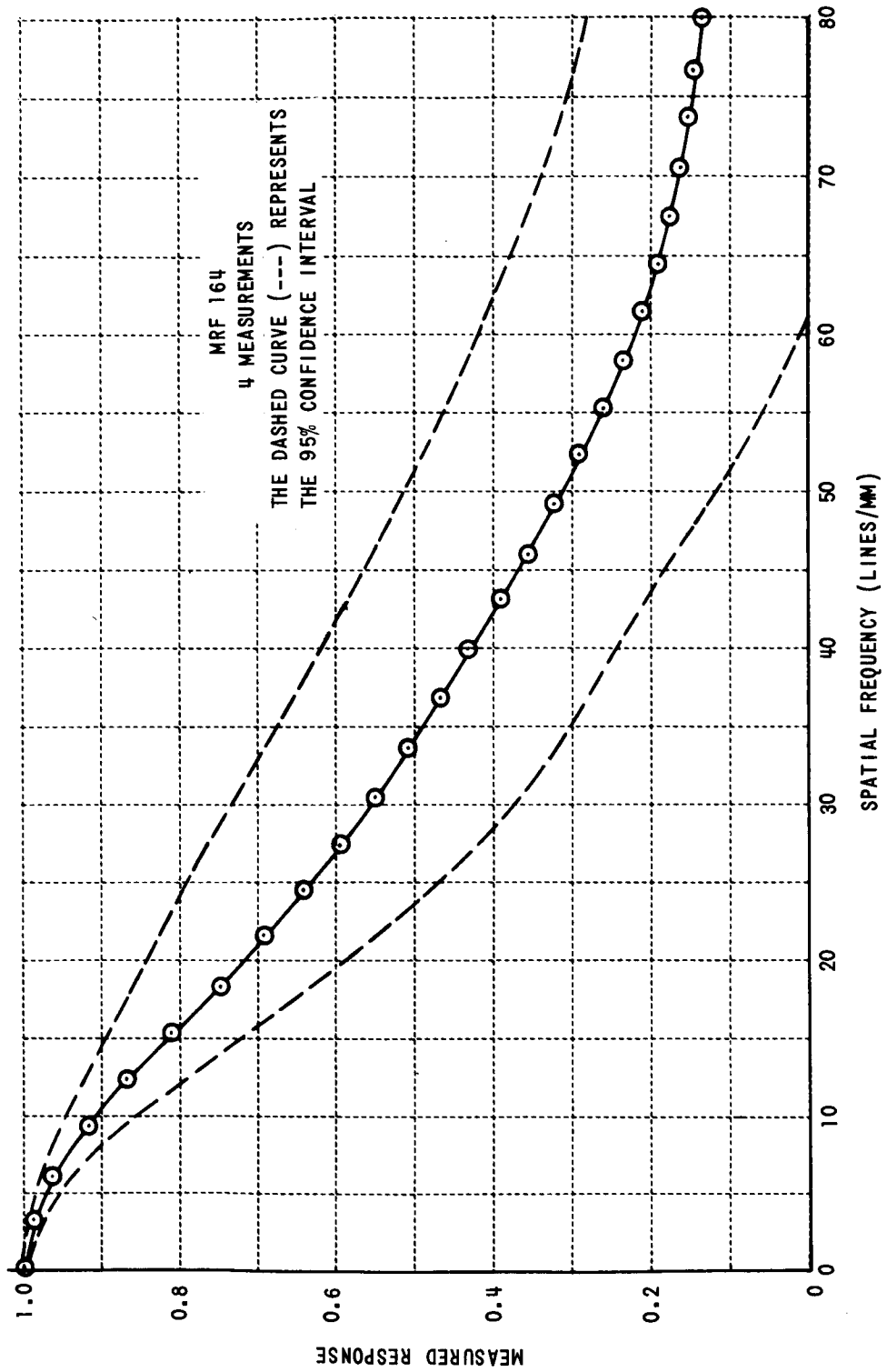


Figure 35 MEDIUM RESOLUTION IMAGING SYSTEM MTF-ORBITER I

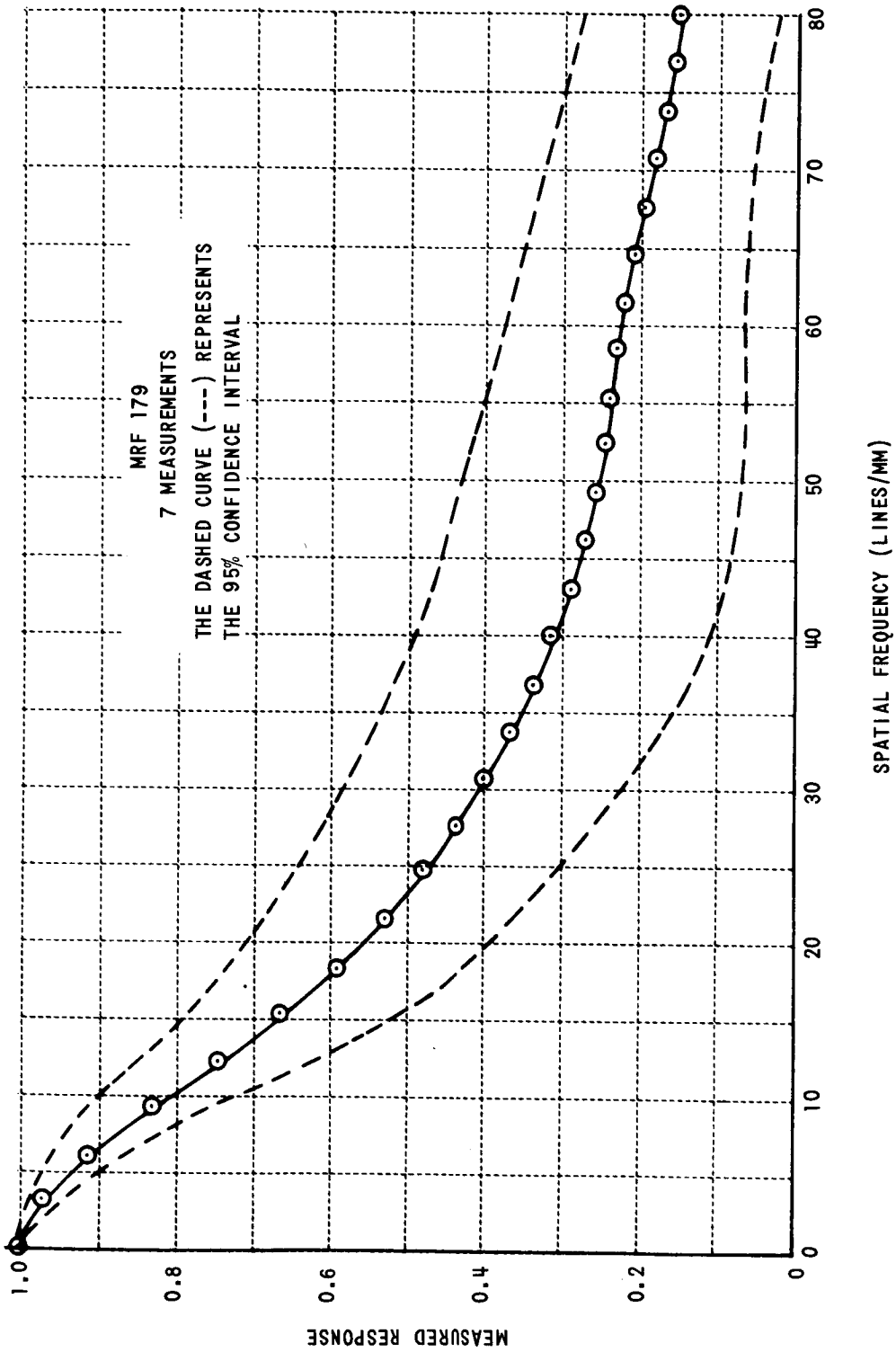


Figure 36 MEDIUM RESOLUTION IMAGING SYSTEM MTF-ORBITER I

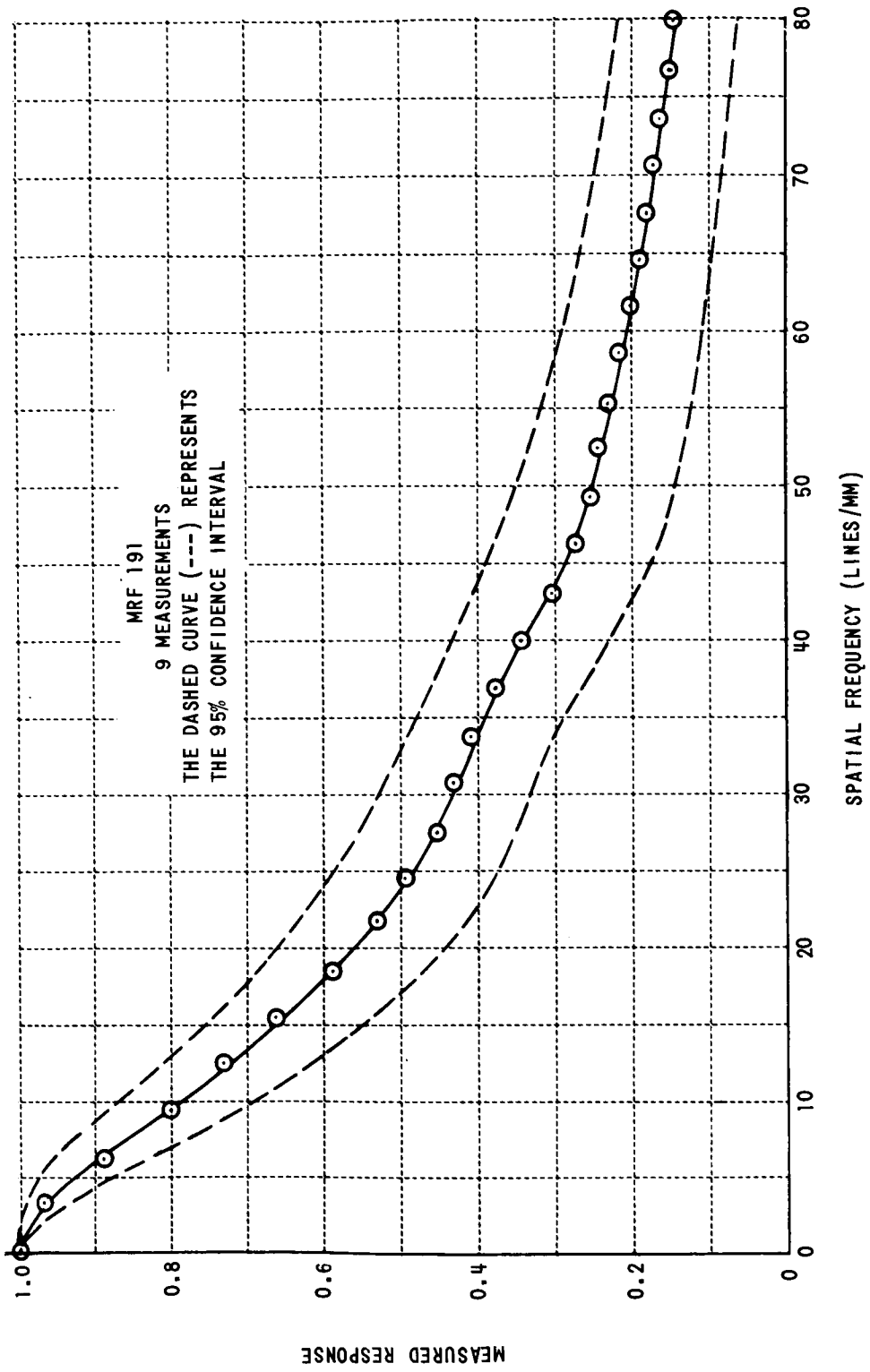


Figure 37 MEDIUM RESOLUTION IMAGING SYSTEM MTF-ORBITER I

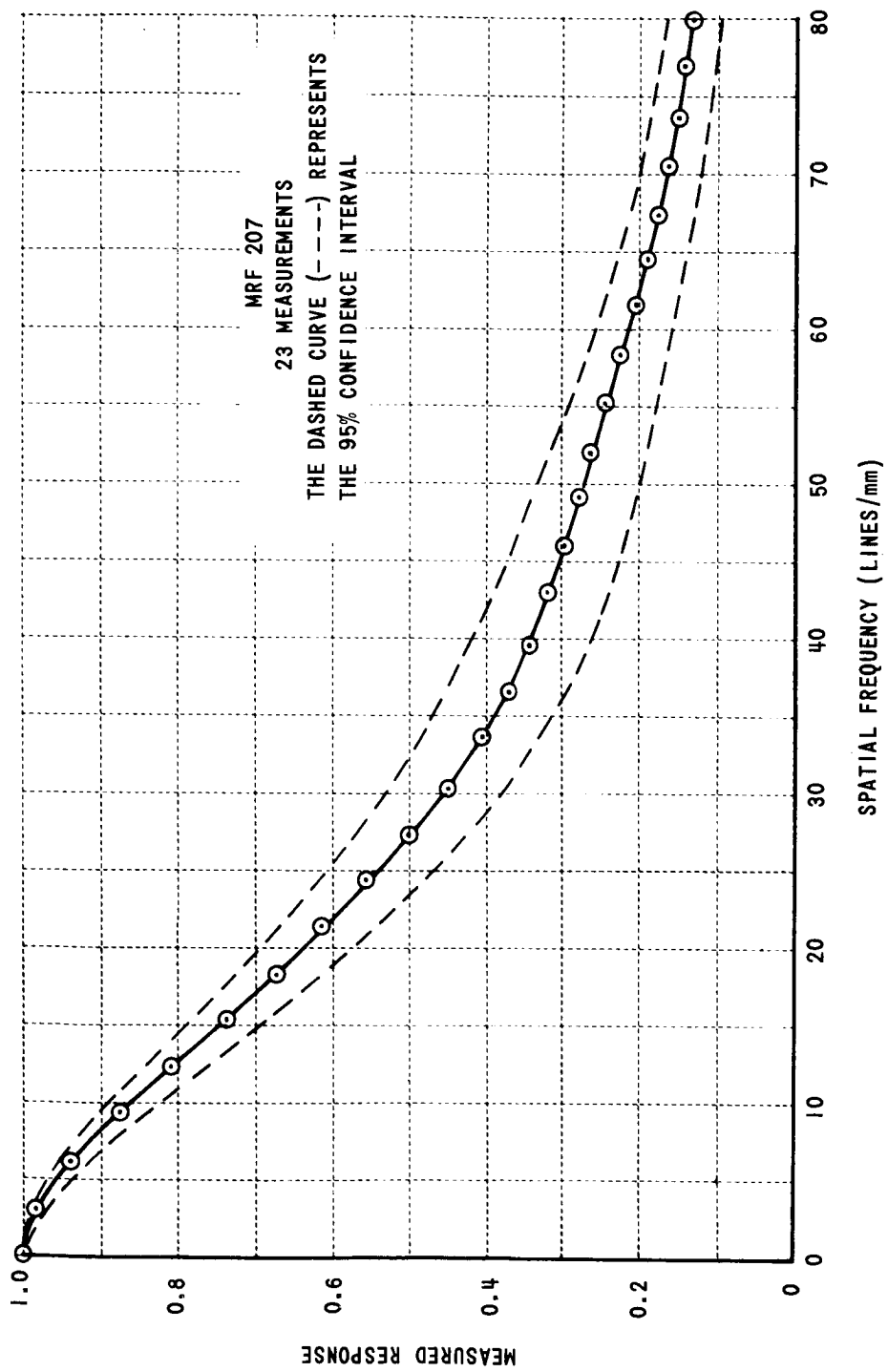


Figure 38 MEDIUM RESOLUTION IMAGING SYSTEM MTF-ORBITER I

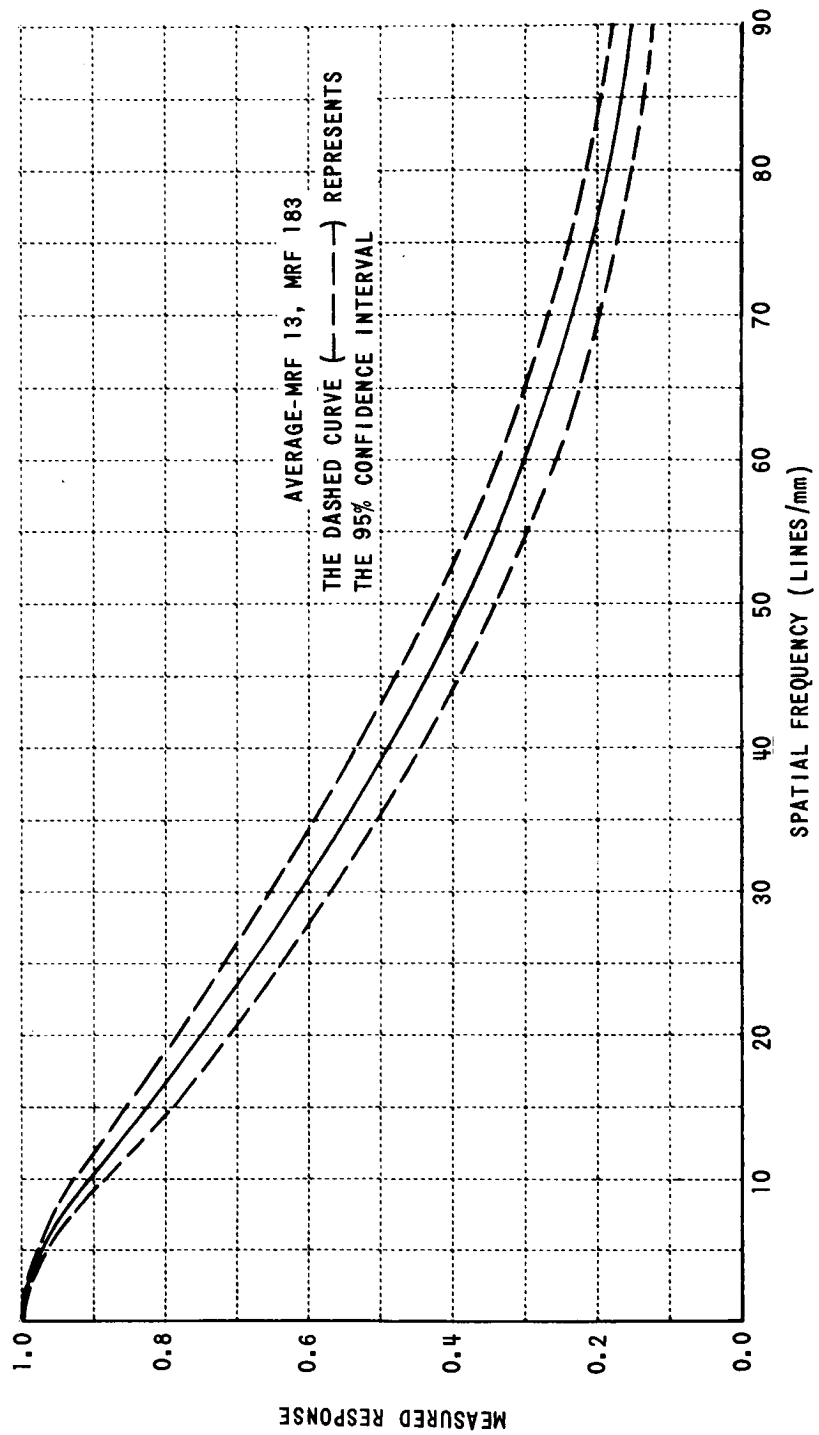


Figure 39 MEDIUM RESOLUTION IMAGING SYSTEM MTF - ORBITER II

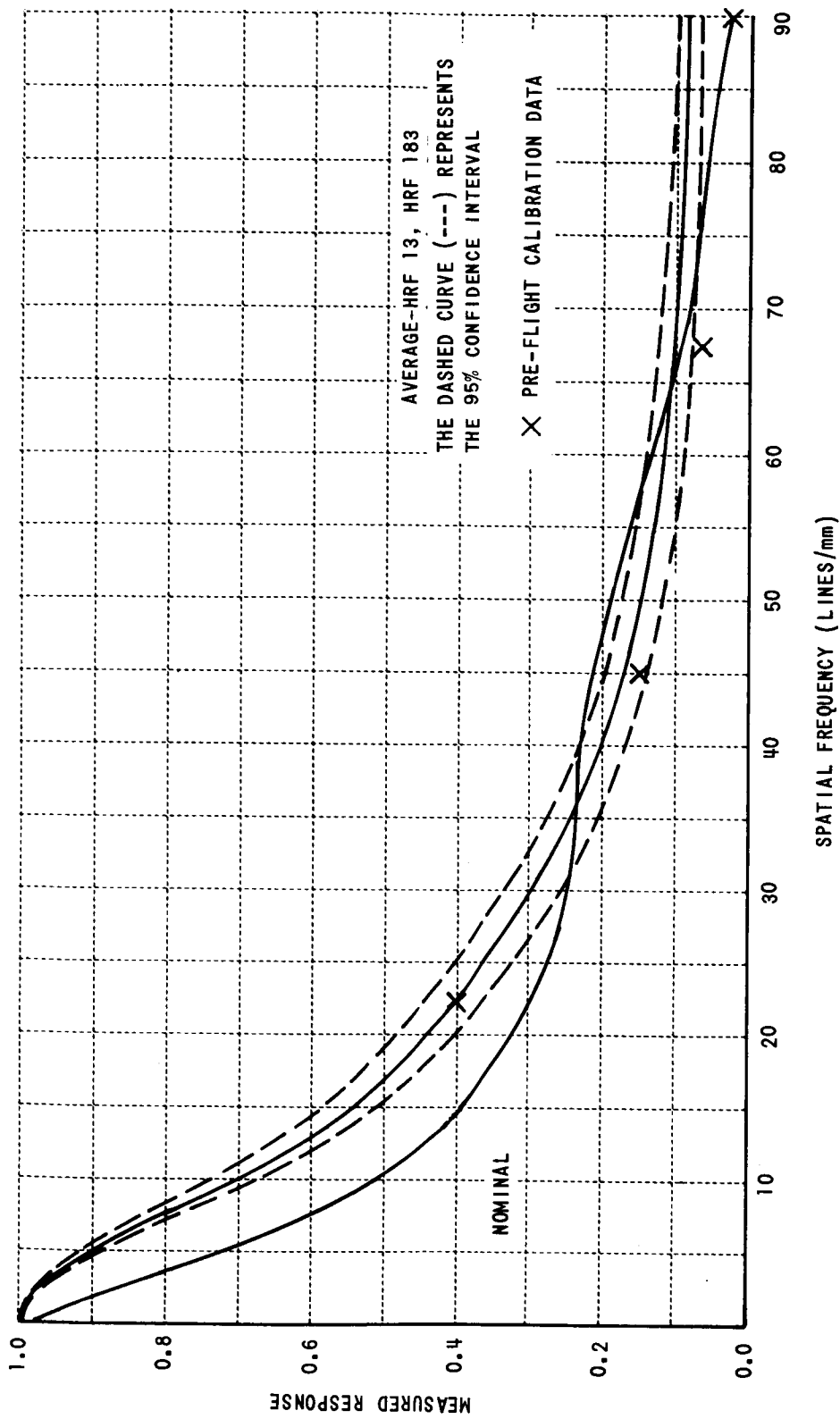


Figure 40 HIGH RESOLUTION IMAGING SYSTEM MTF - ORBITER II

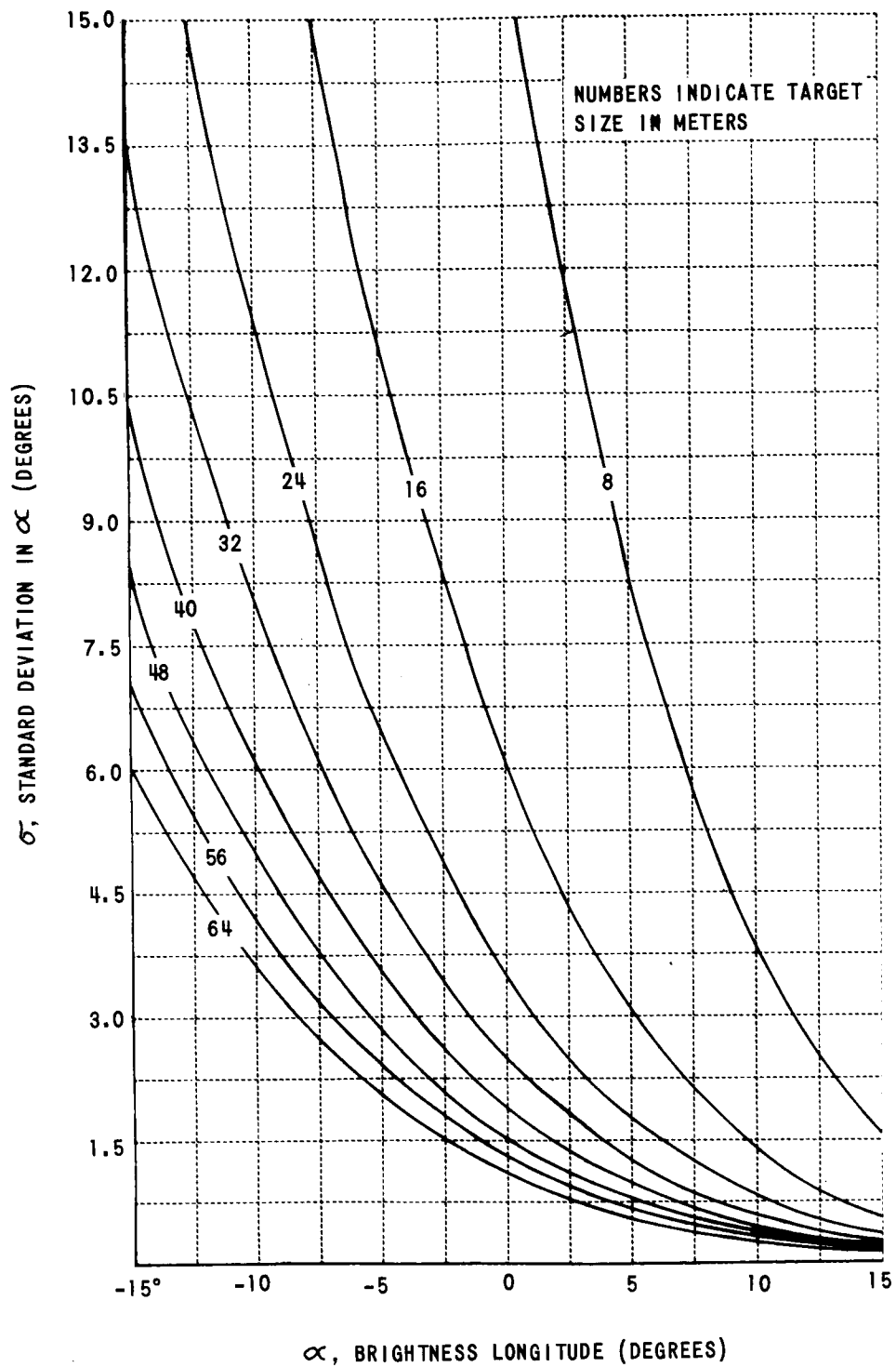


Figure 41 STANDARD DEVIATION IN MEASUREMENT OF BRIGHTNESS LONGITUDE - ORBITER I, MRF 61

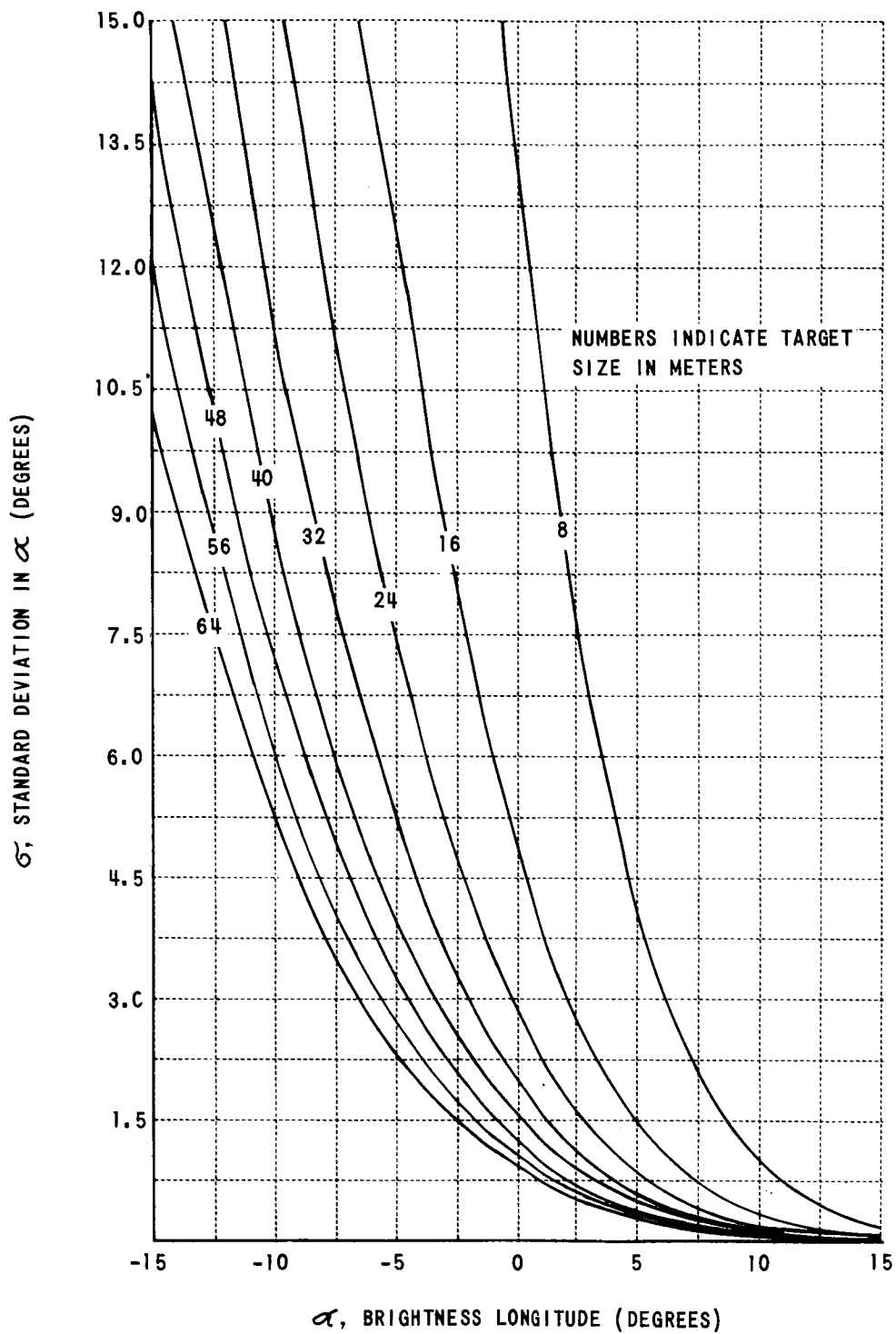


Figure 42 STANDARD DEVIATION IN MEASUREMENT OF BRIGHTNESS LONGITUDE - ORBITER I, MRF 85

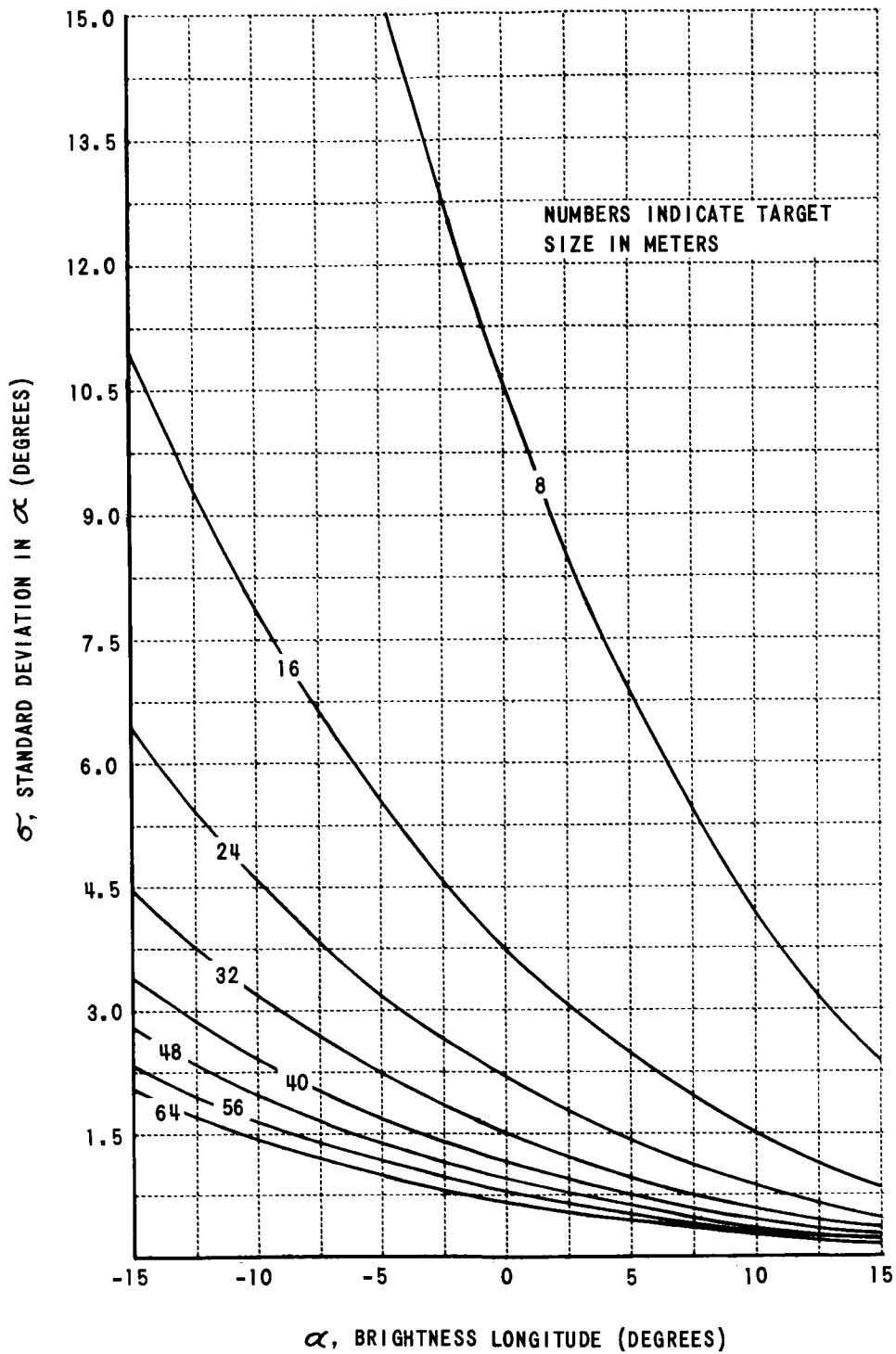


Figure 43 STANDARD DEVIATION IN MEASUREMENT OF BRIGHTNESS LONGITUDE - ORBITER I, MRF 144

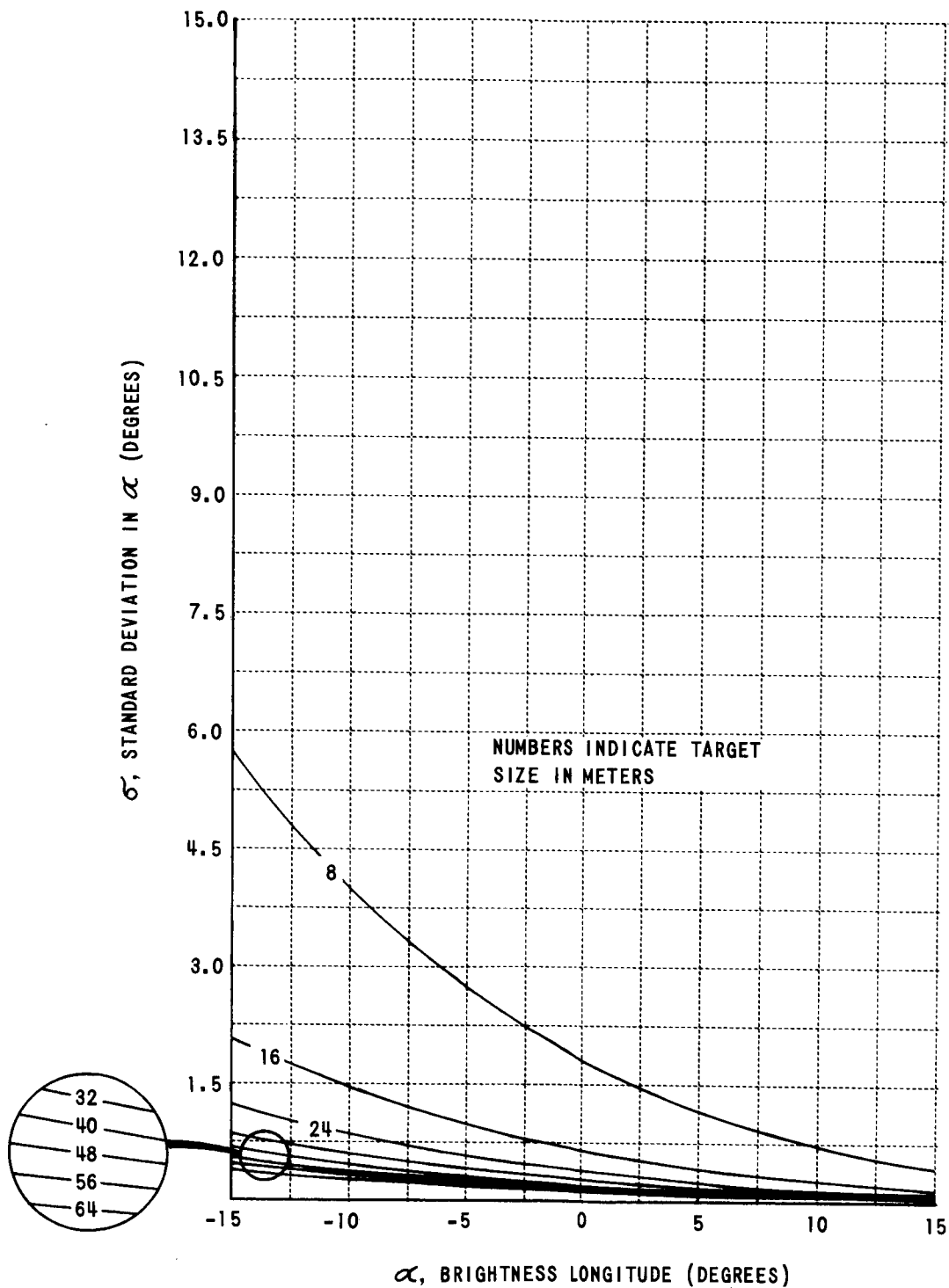


Figure 44 STANDARD DEVIATION IN MEASUREMENT OF BRIGHTNESS LONGITUDE - ORBITER I, MRF 207

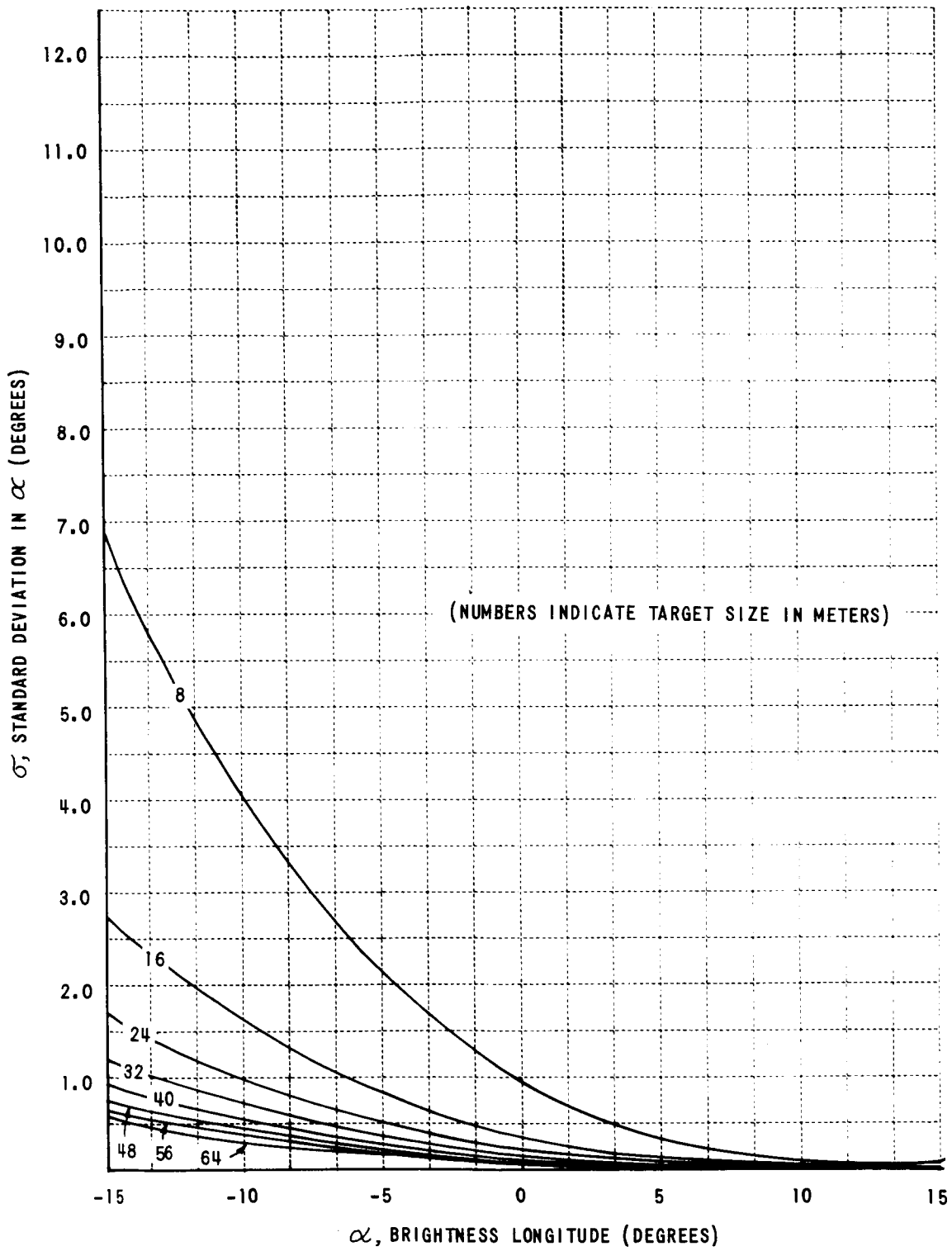


Figure 45 STANDARD DEVIATION IN MEASUREMENT OF BRIGHTNESS LONGITUDE - ORBITER II, MRF 13

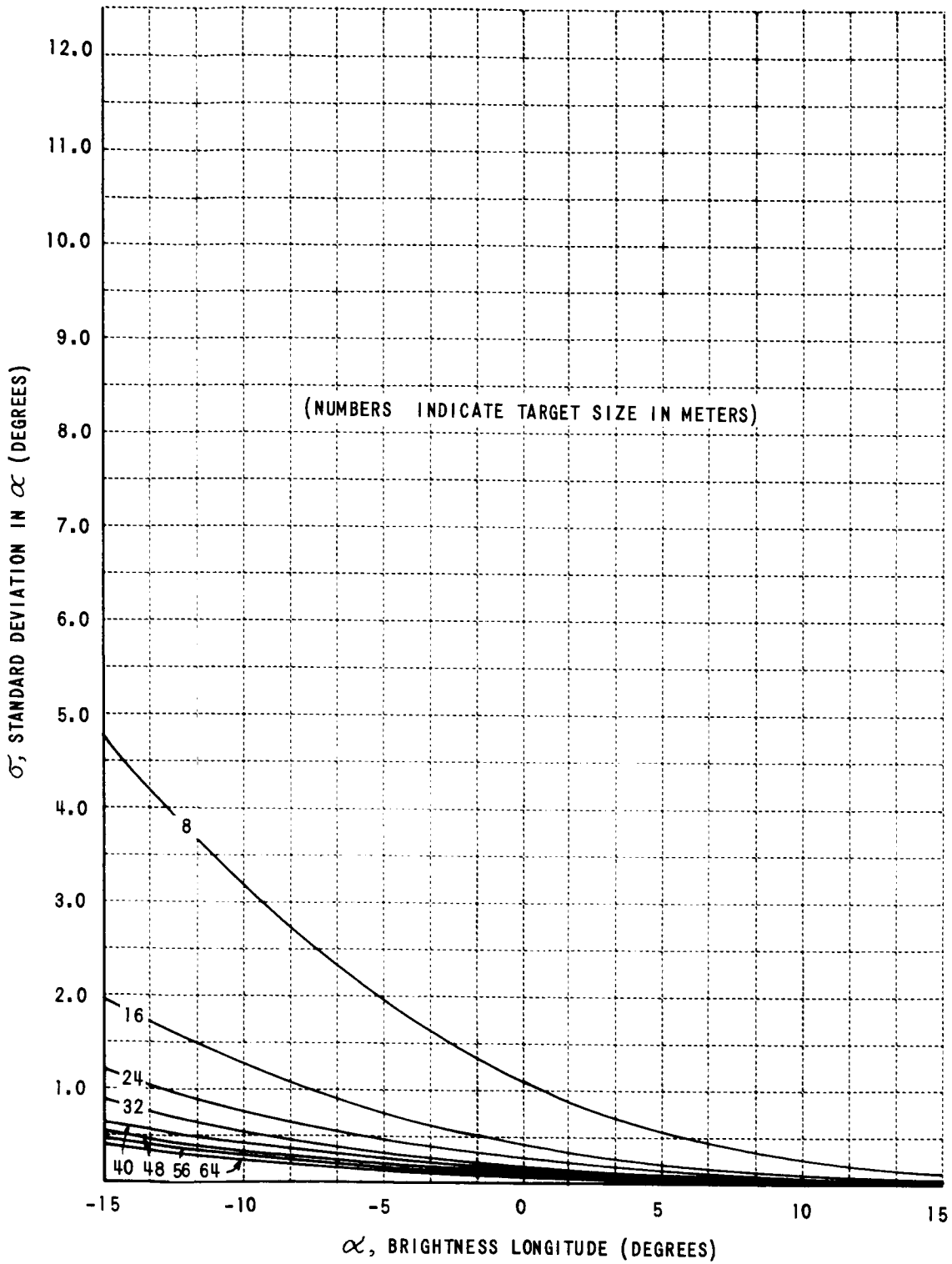


Figure 46 STANDARD DEVIATION IN MEASUREMENT OF BRIGHTNESS LONGITUDE - ORBITER II, MRF 39

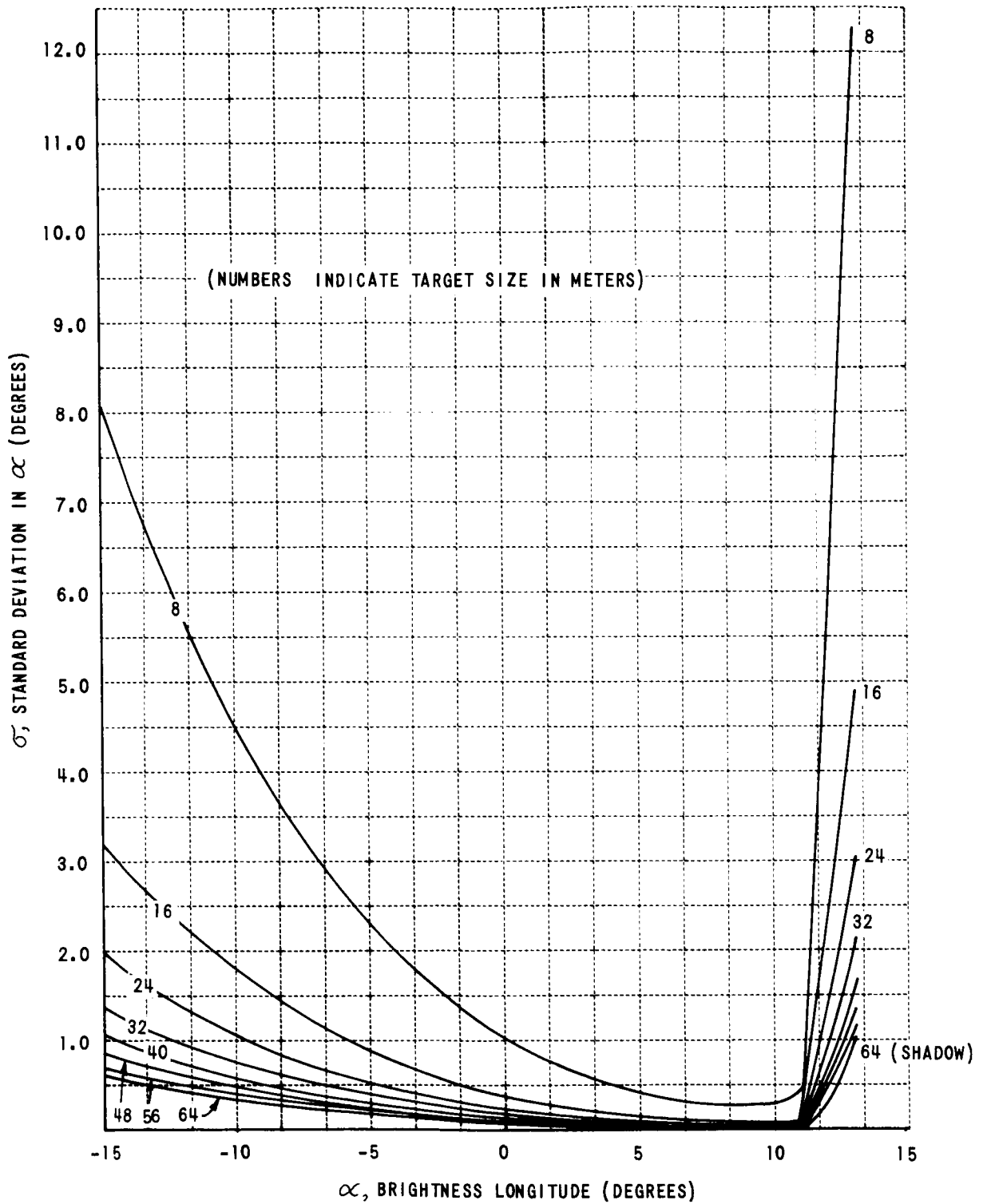


Figure 47 STANDARD DEVIATION IN MEASUREMENT OF BRIGHTNESS LONGITUDE - ORBITER II, MRF 46

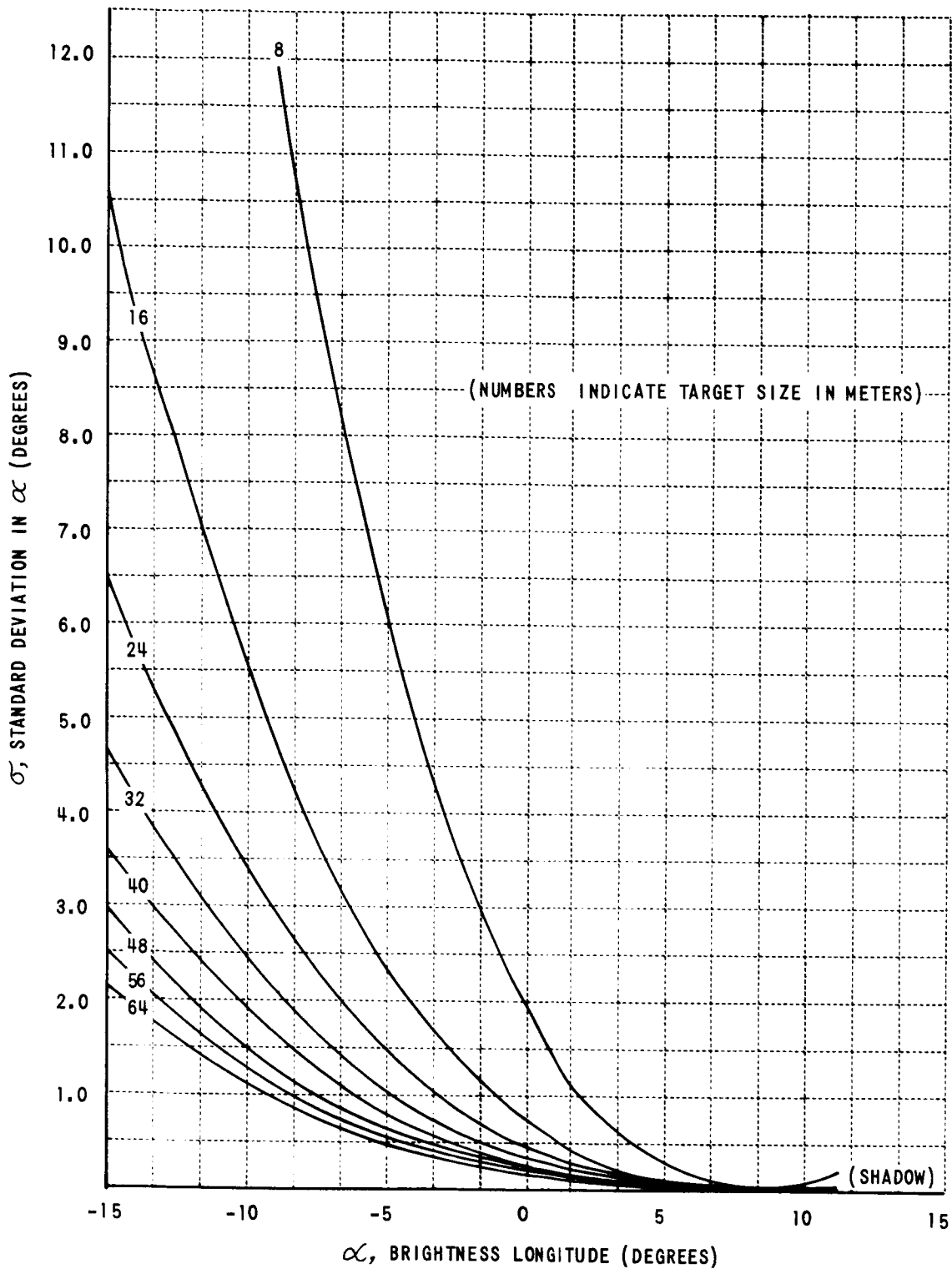


Figure 48 STANDARD DEVIATION IN MEASUREMENT OF BRIGHTNESS LONGITUDE - ORBITER II, MRF 63

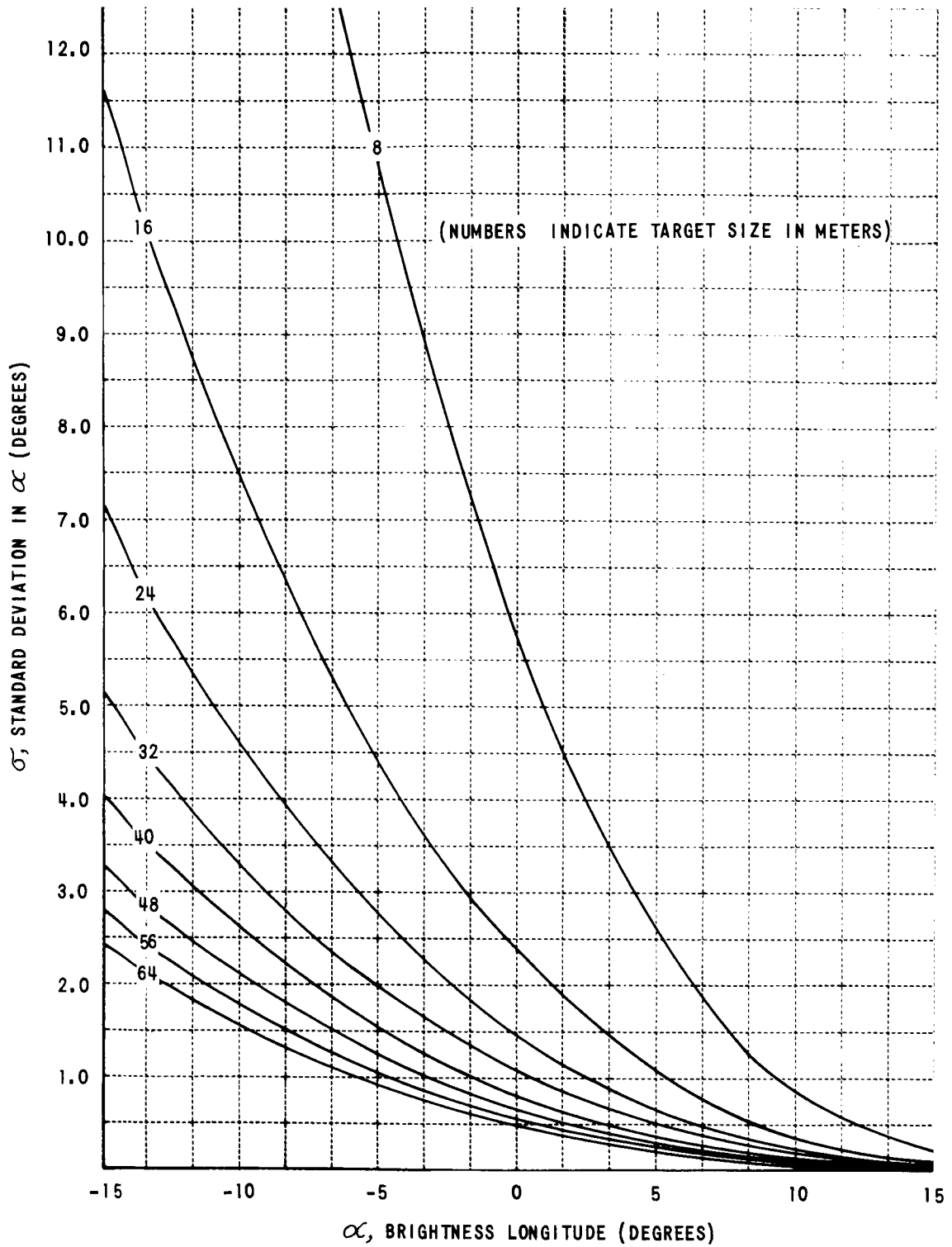


Figure 49 STANDARD DEVIATION IN MEASUREMENT OF BRIGHTNESS LONGITUDE - ORBITER II, MRF 69

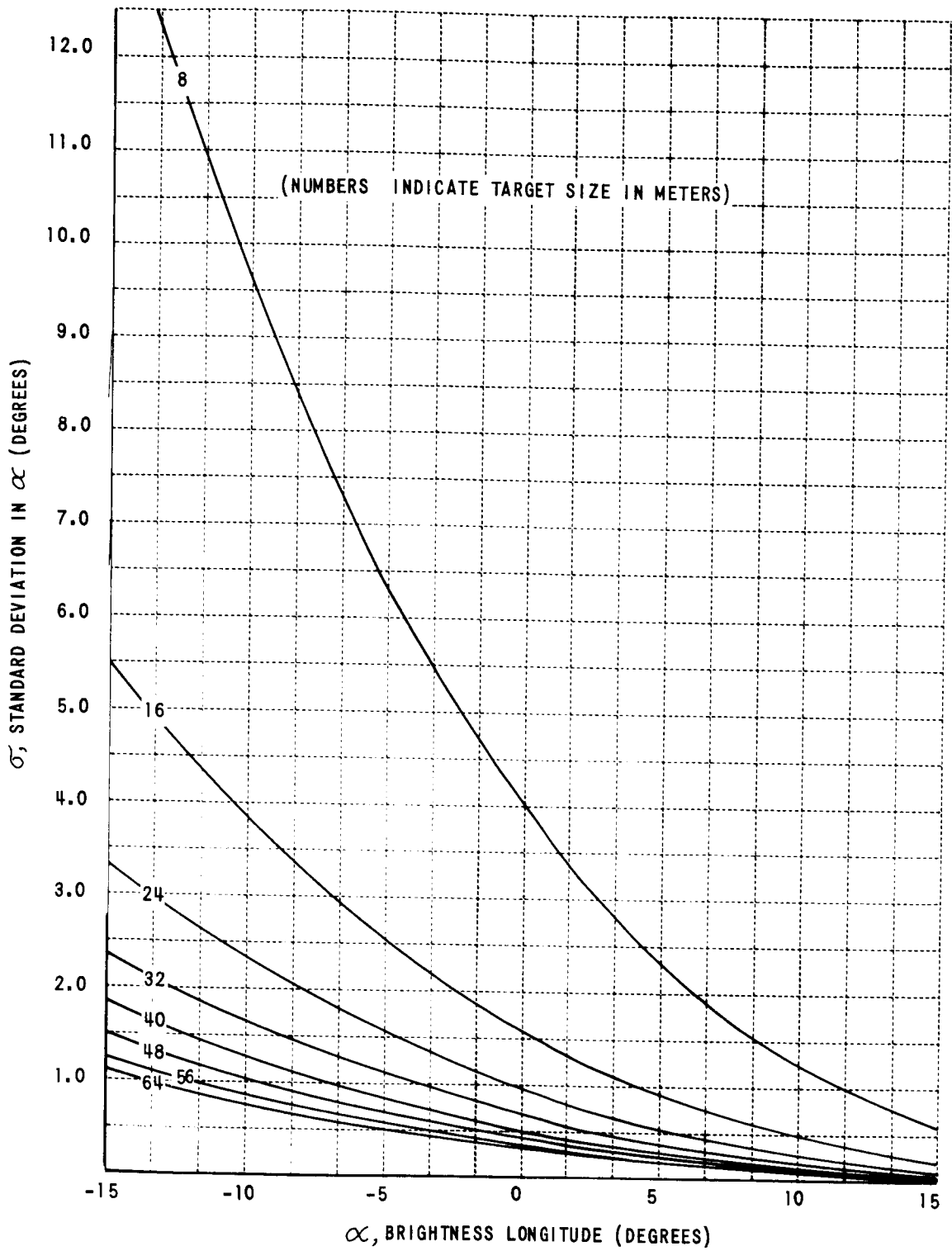


Figure 50 STANDARD DEVIATION IN MEASUREMENT OF BRIGHTNESS LONGITUDE - ORBITER II, MRF 88

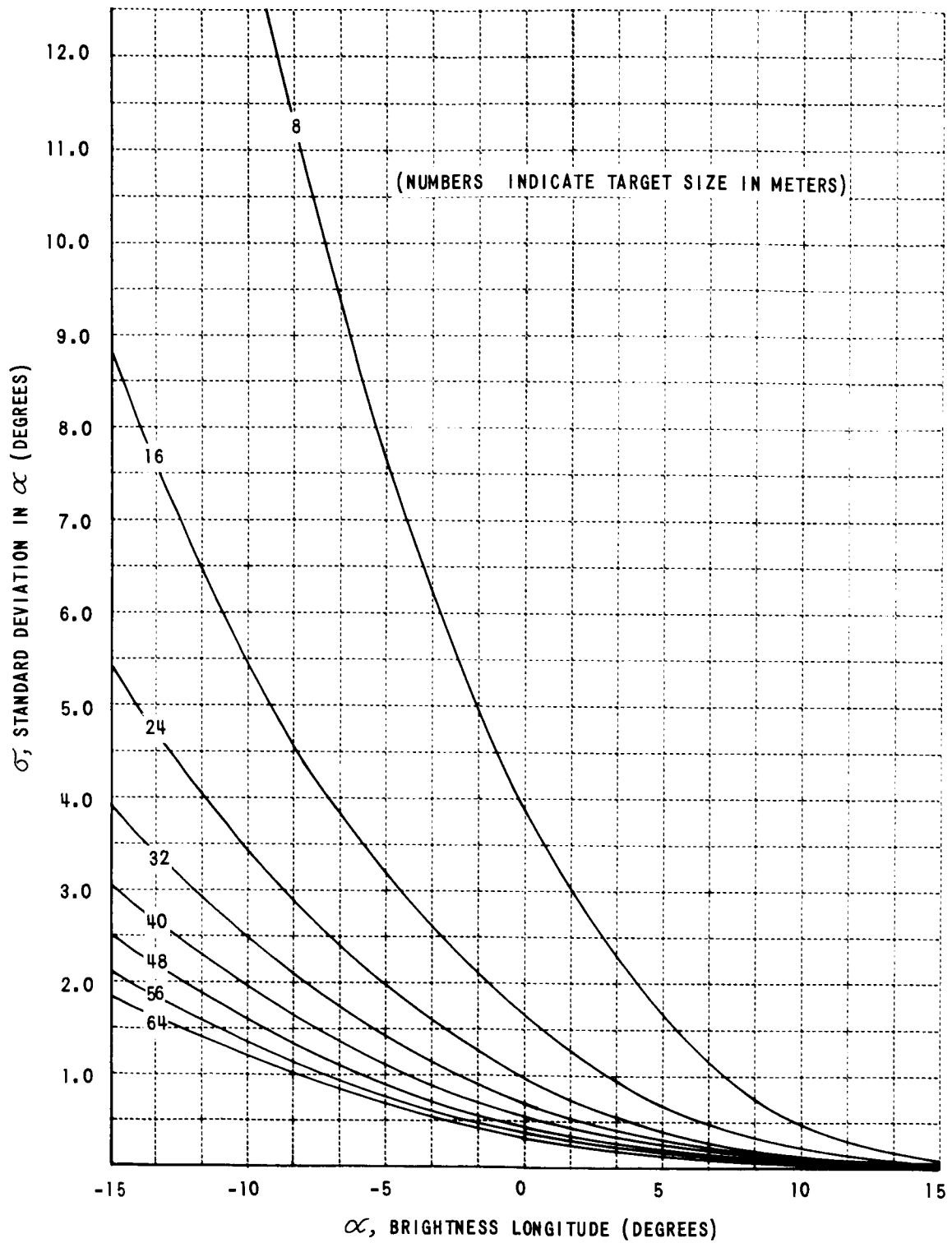


Figure 51 STANDARD DEVIATION IN MEASUREMENT OF BRIGHTNESS LONGITUDE - ORBITER II, MRF 99

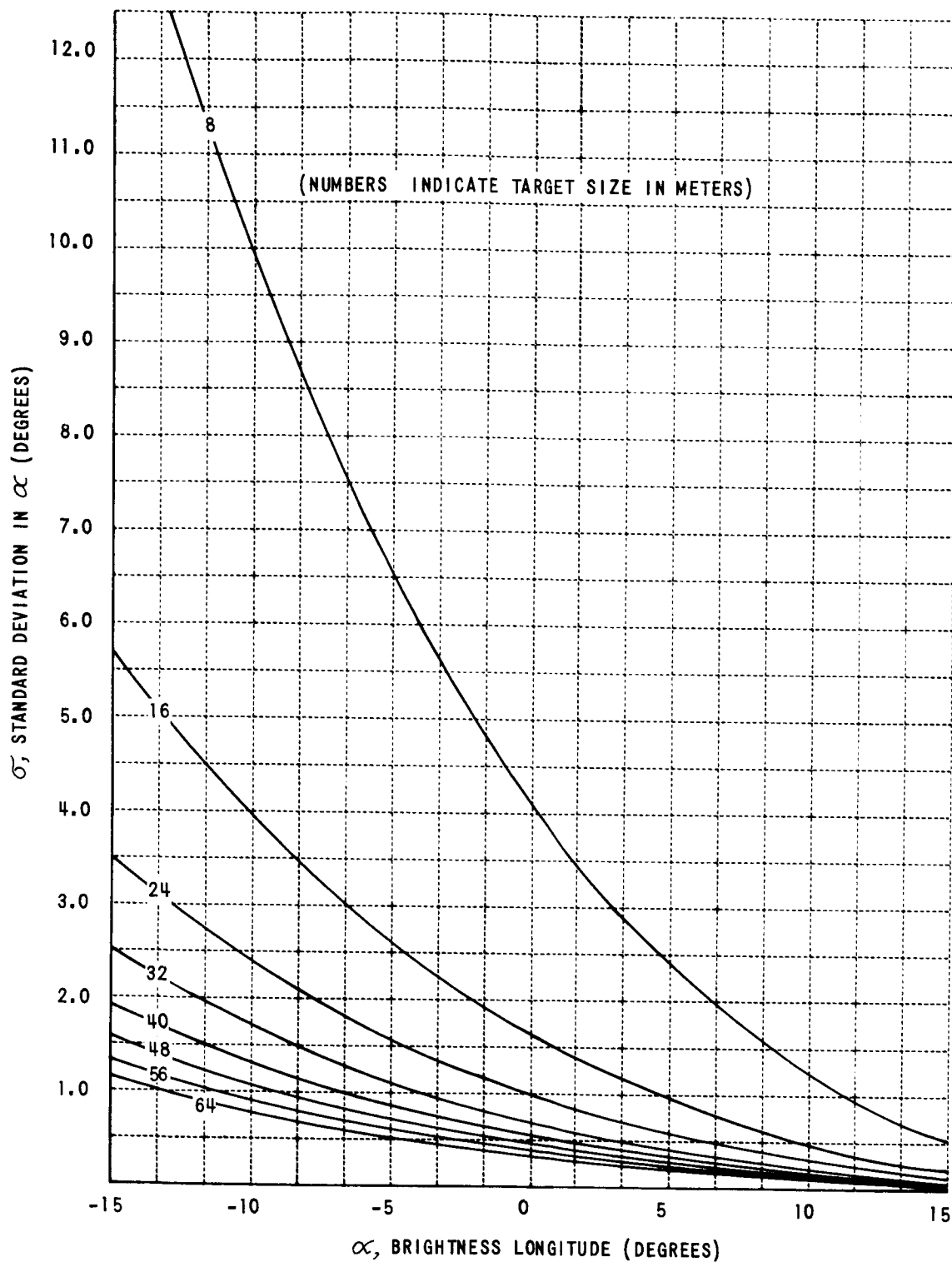


Figure 52 STANDARD DEVIATION IN MEASUREMENT OF BRIGHTNESS LONGITUDE - ORBITER II, MRF 124

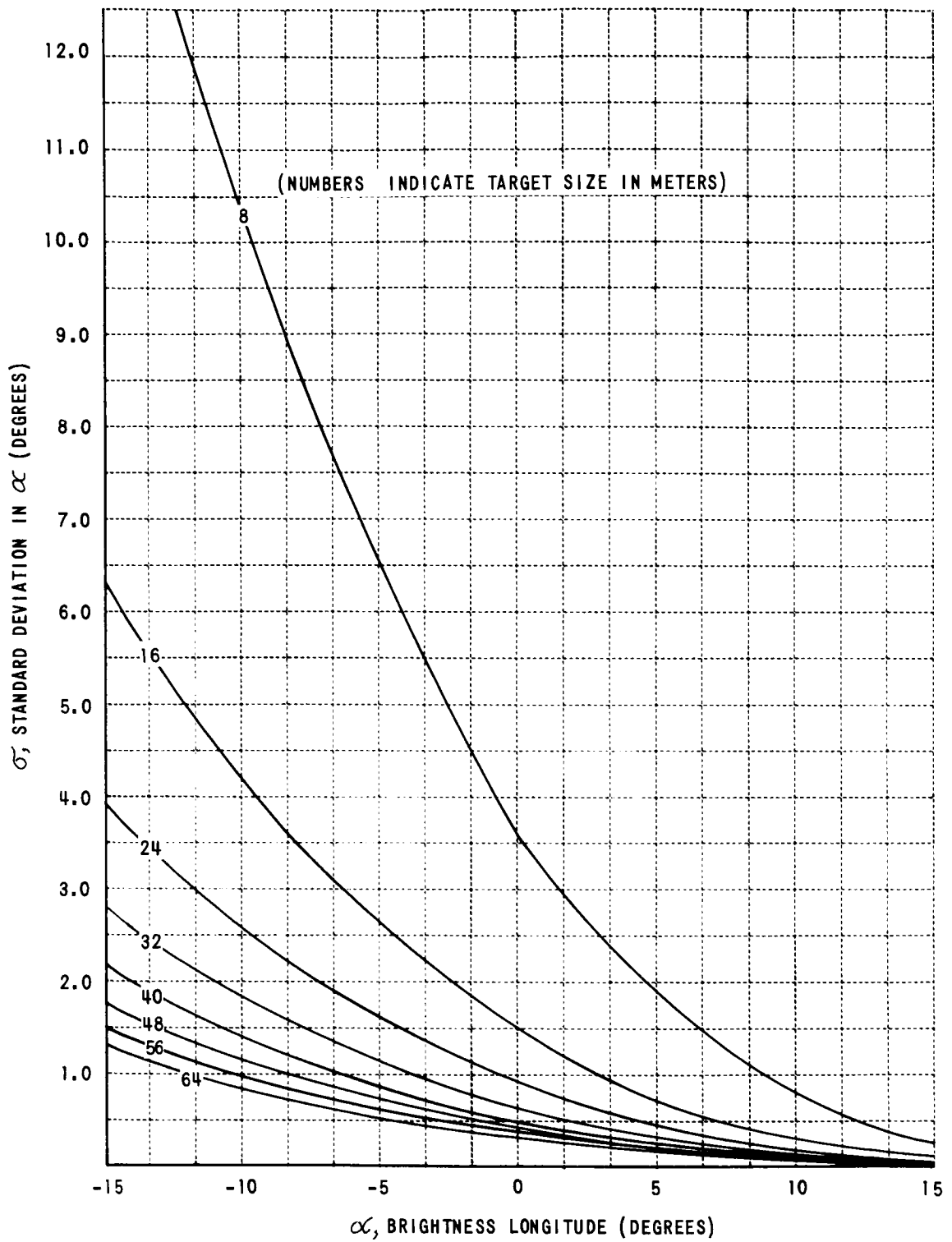


Figure 53 STANDARD DEVIATION IN MEASUREMENT OF BRIGHTNESS LONGITUDE - ORBITER II, MRF 141

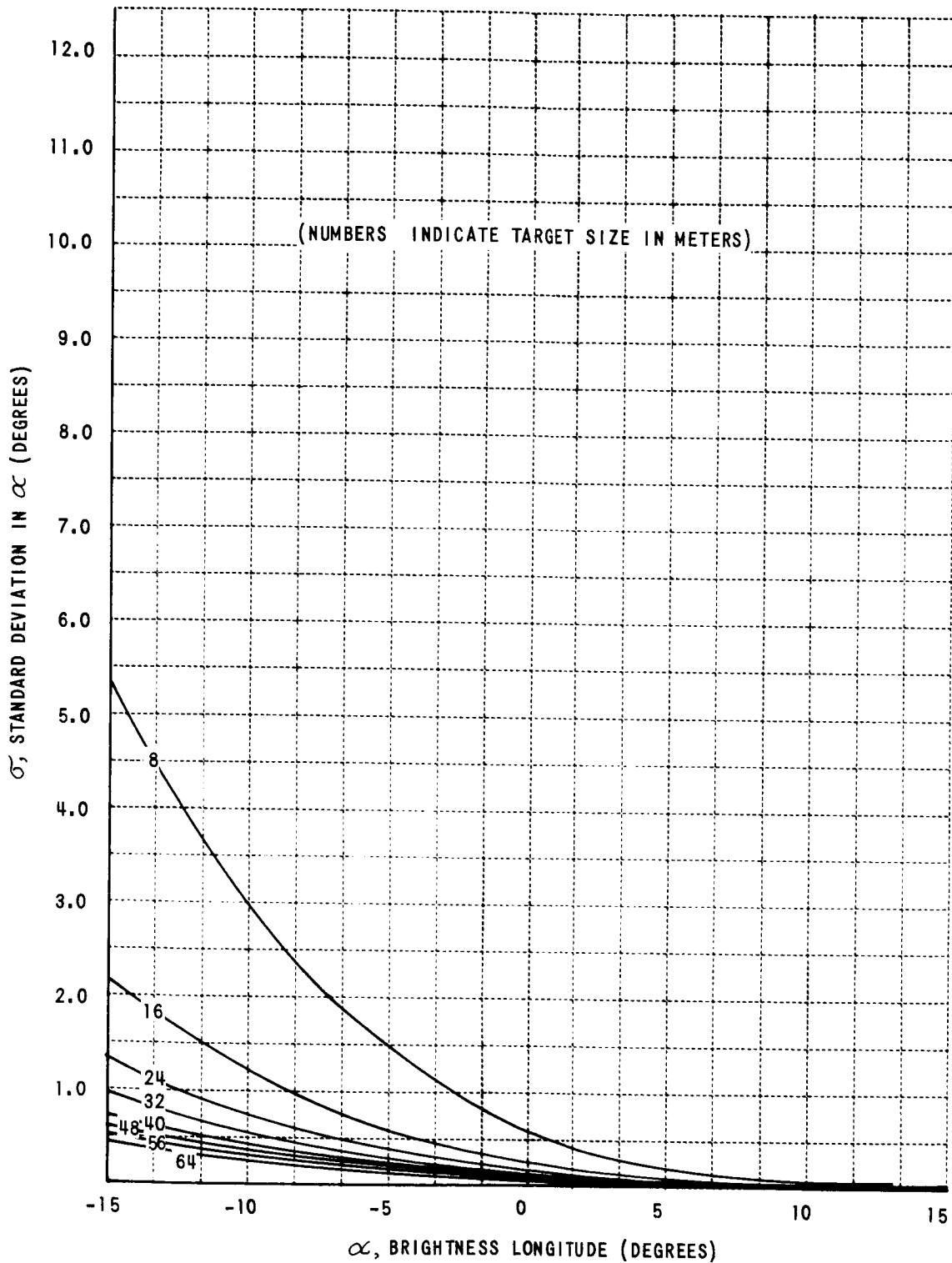


Figure 54 STANDARD DEVIATION IN MEASUREMENT OF BRIGHTNESS LONGITUDE - ORBITER II, MRF 157

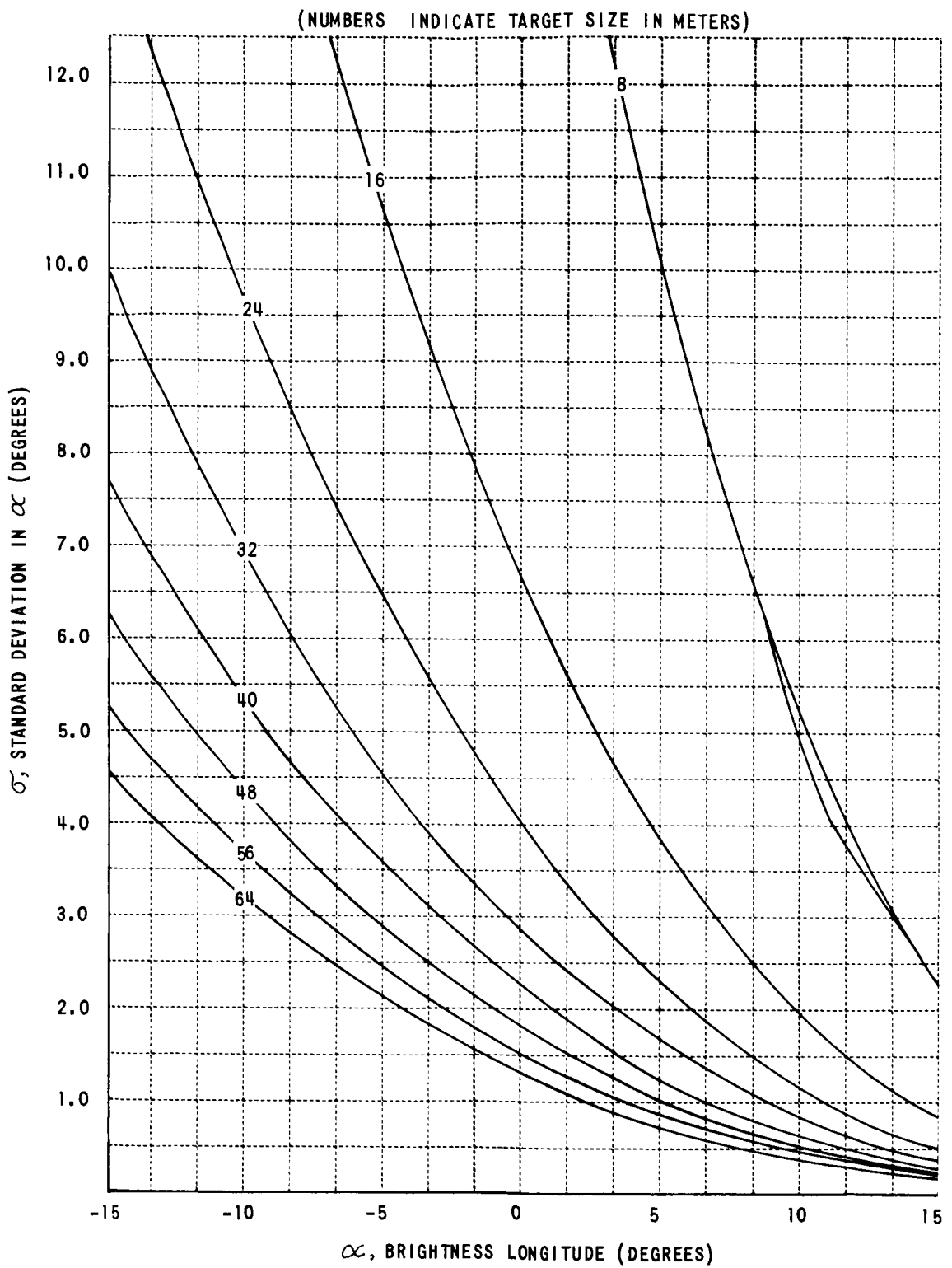


Figure 55 STANDARD DEVIATION IN MEASUREMENT OF BRIGHTNESS LONGITUDE - ORBITER II, MRF 174

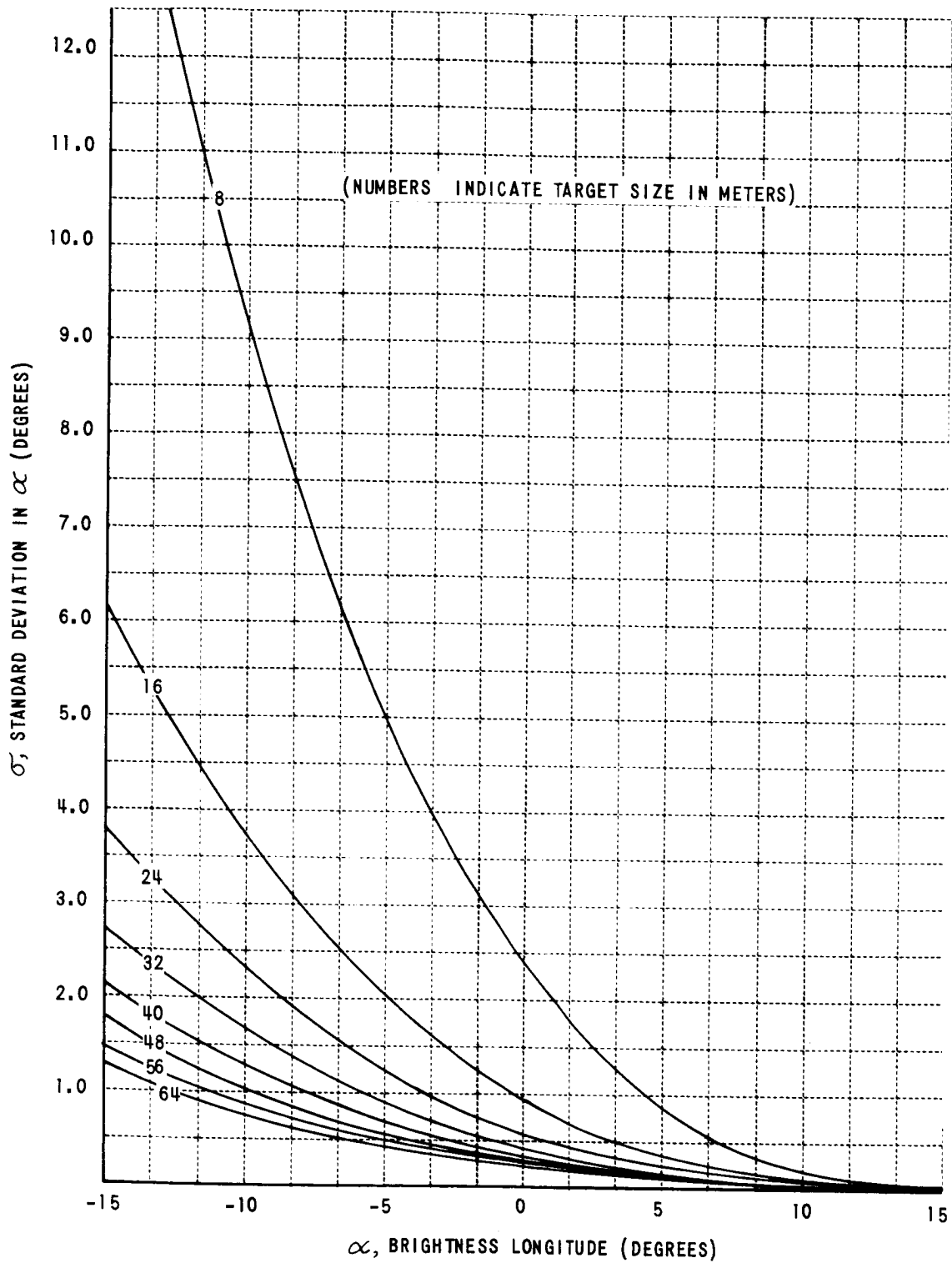


Figure 56 STANDARD DEVIATION IN MEASUREMENT OF BRIGHTNESS LONGITUDE - ORBITER II, MRF 183

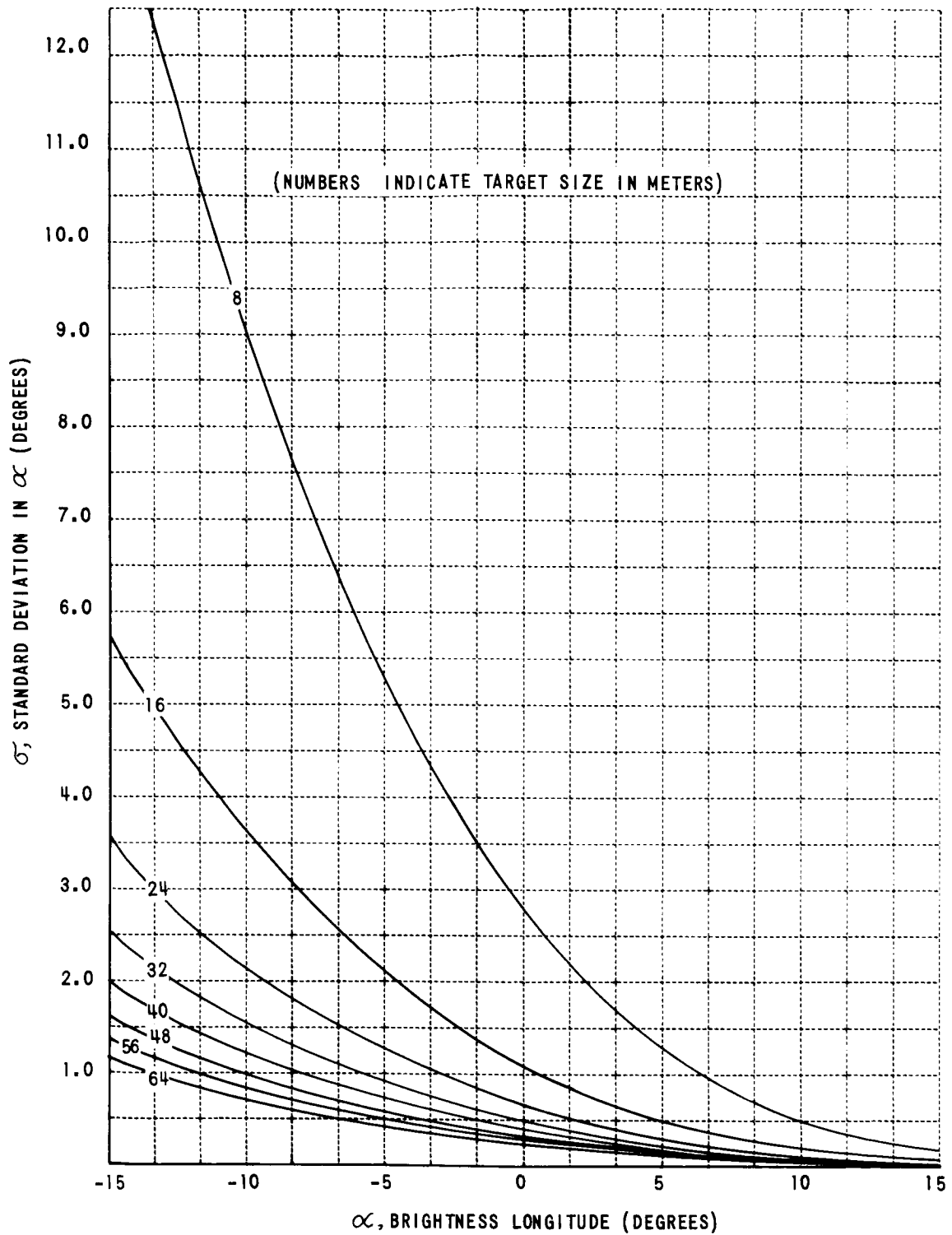


Figure 57 STANDARD DEVIATION IN MEASUREMENT OF BRIGHTNESS LONGITUDE - ORBITER II, MRF 208

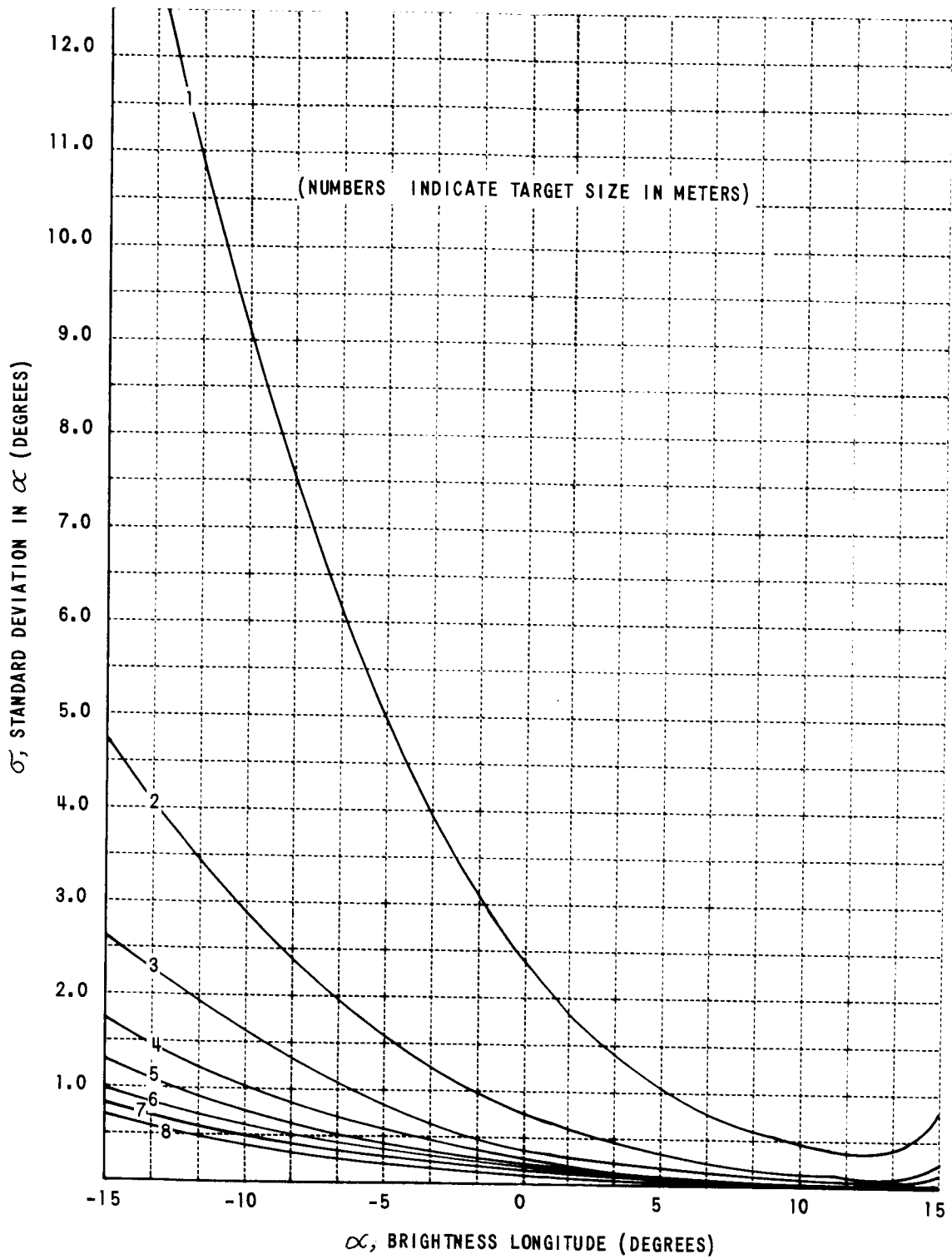


Figure 58 STANDARD DEVIATION IN MEASUREMENT OF BRIGHTNESS LONGITUDE - ORBITER II, HRF 13

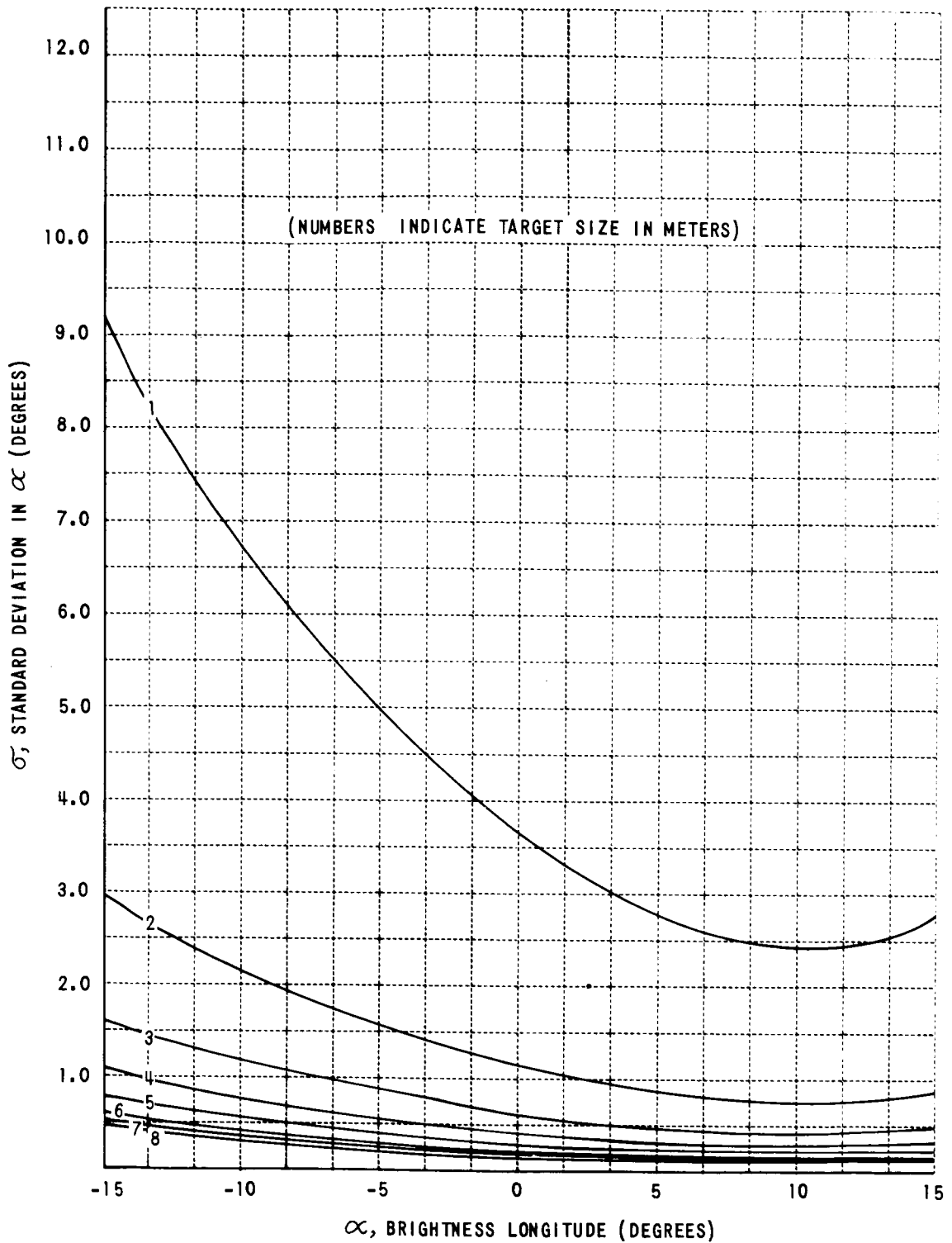


Figure 59 STANDARD DEVIATION IN MEASUREMENT OF BRIGHTNESS LONGITUDE - ORBITER II, HRF 39

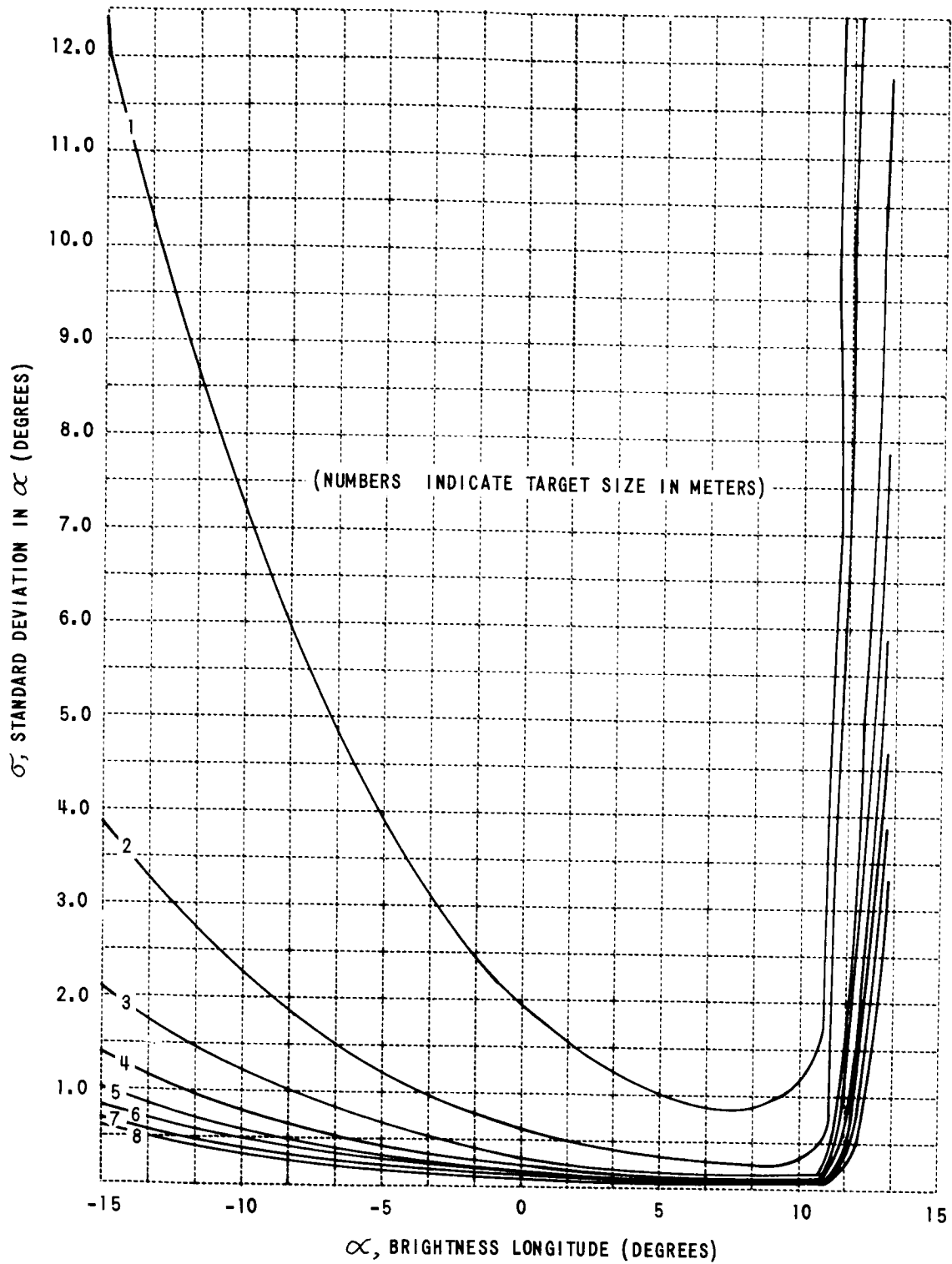


Figure 60 STANDARD DEVIATION IN MEASUREMENT OF BRIGHTNESS LONGITUDE - ORBITER II, HRF 46

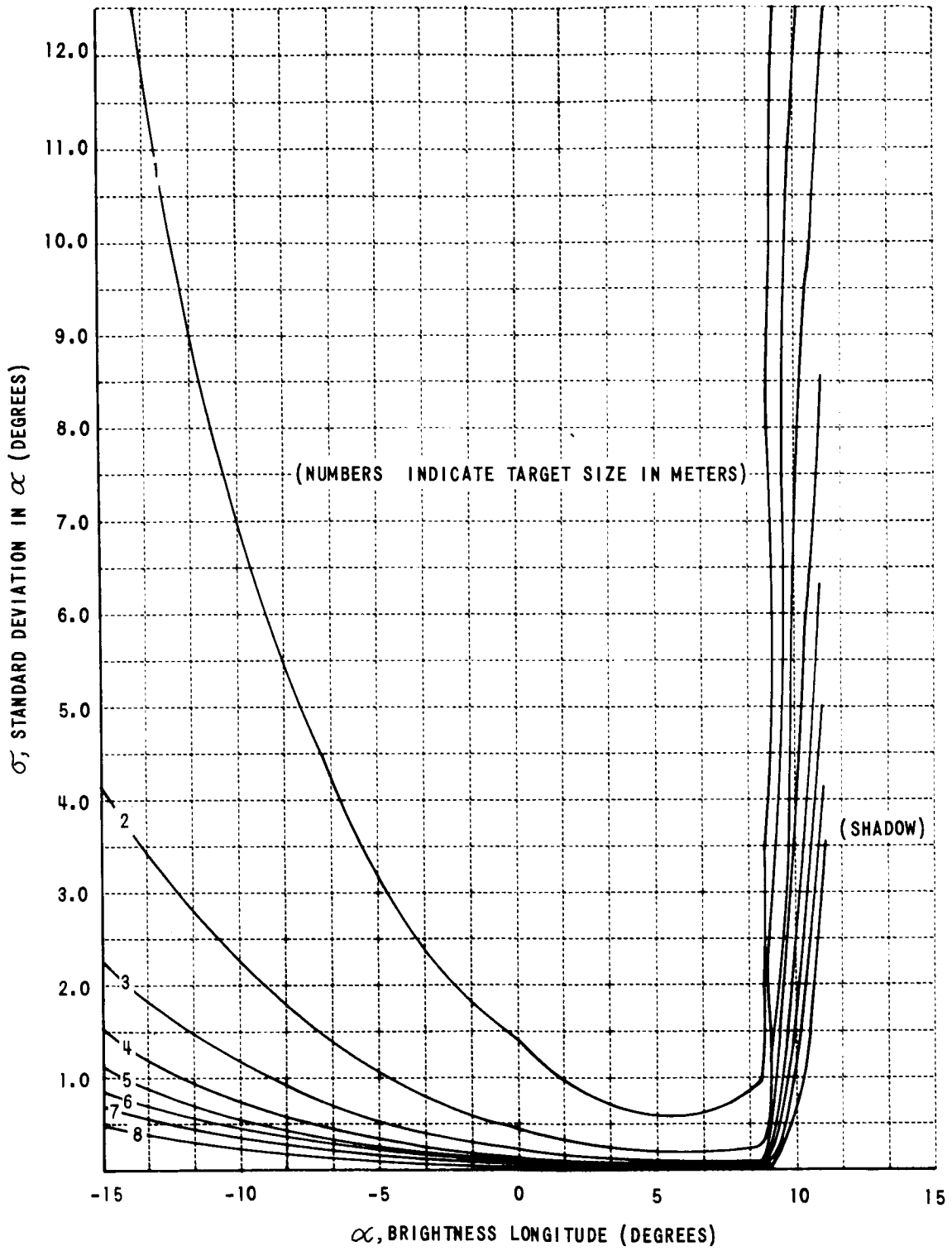


Figure 61 STANDARD DEVIATION IN MEASUREMENT OF BRIGHTNESS LONGITUDE - ORBITER II, HRF 63

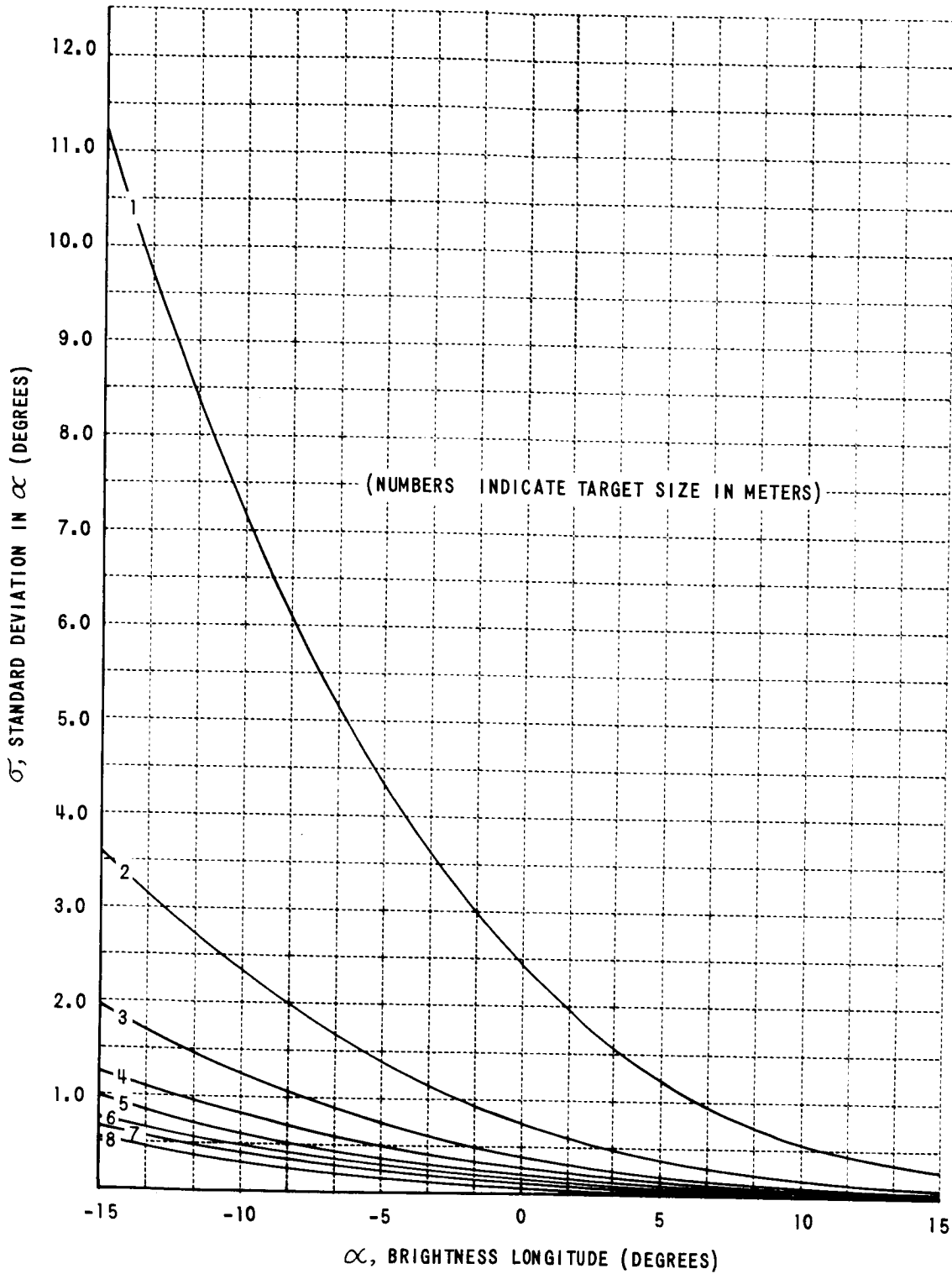


Figure 62 STANDARD DEVIATION IN MEASUREMENT OF BRIGHTNESS LONGITUDE - ORBITER II, HRF 69

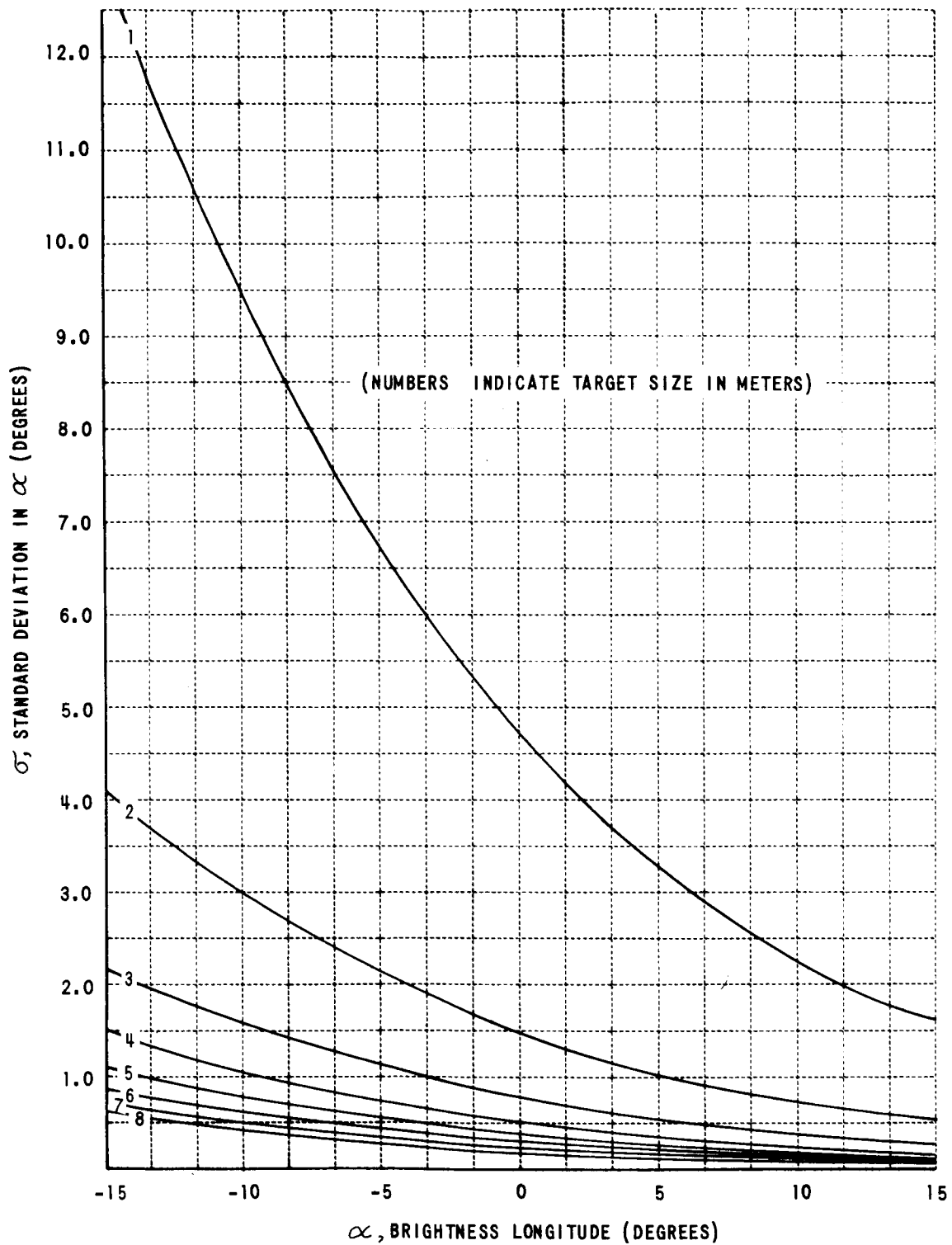


Figure 63 STANDARD DEVIATION IN MEASUREMENT OF BRIGHTNESS LONGITUDE - ORBITER II, HRF 88

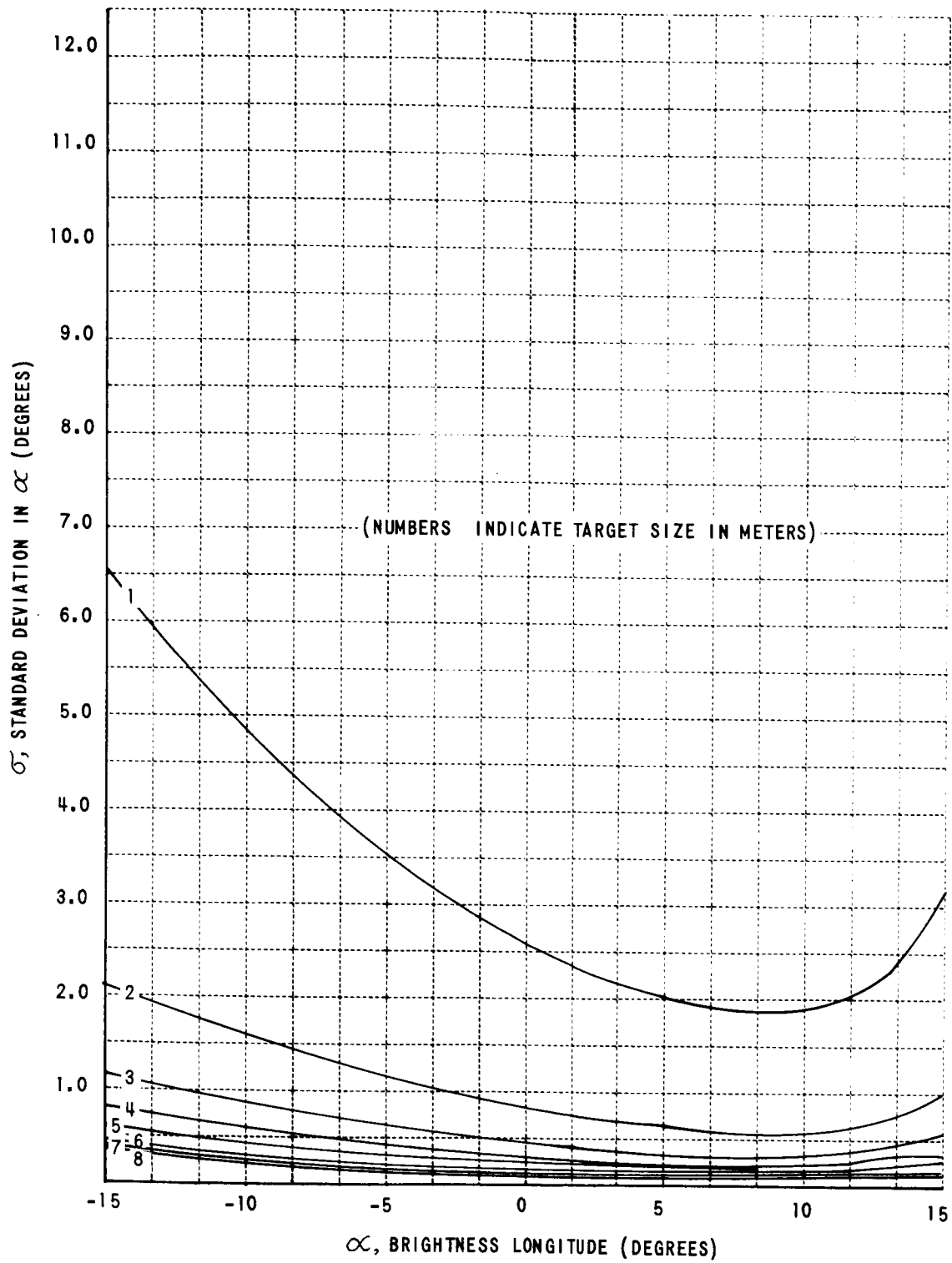


Figure 64 STANDARD DEVIATION IN MEASUREMENT OF BRIGHTNESS LONGITUDE - ORBITER II, HRF 99

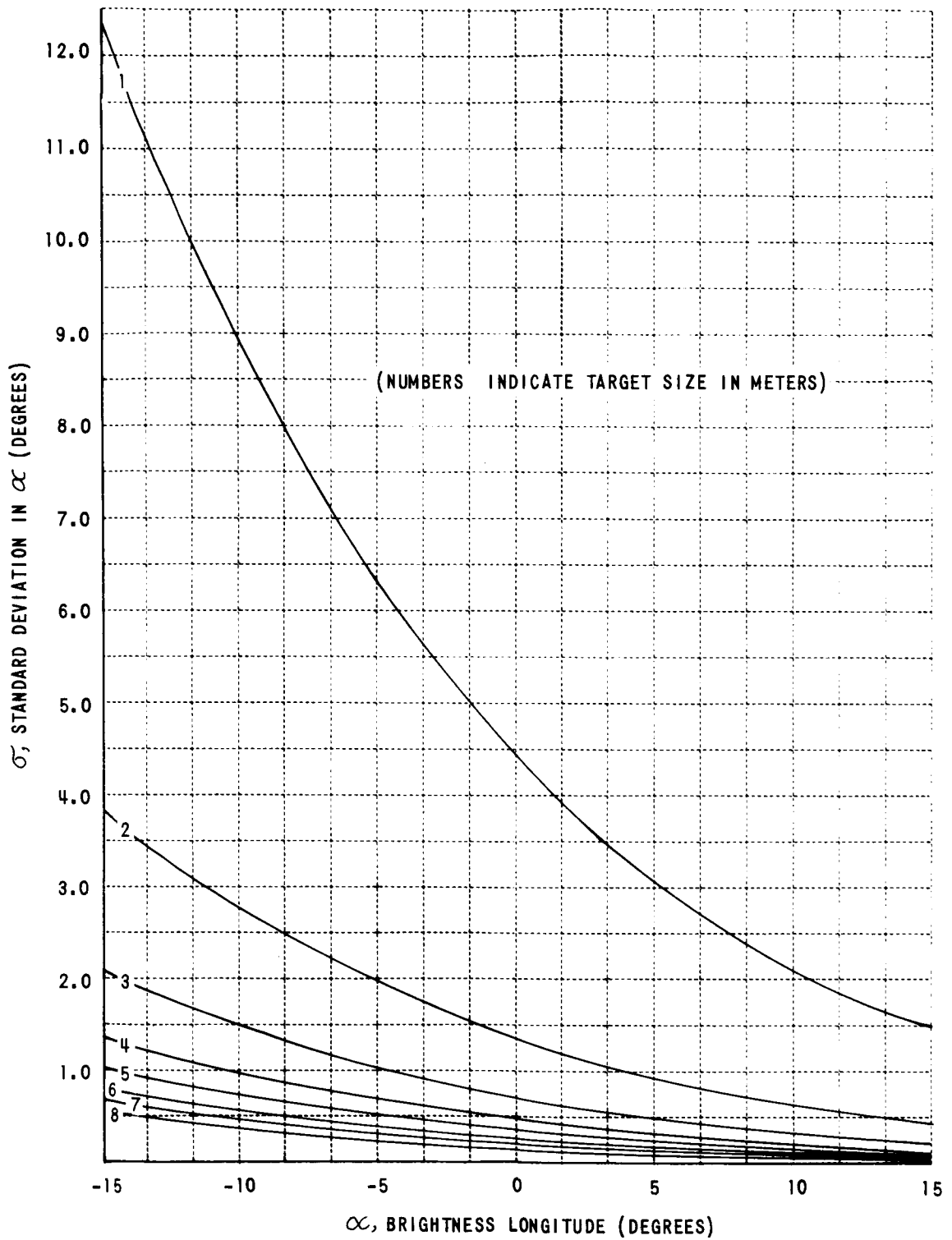


Figure 65 STANDARD DEVIATION IN MEASUREMENT OF BRIGHTNESS LONGITUDE - ORBITER II, HRF 124

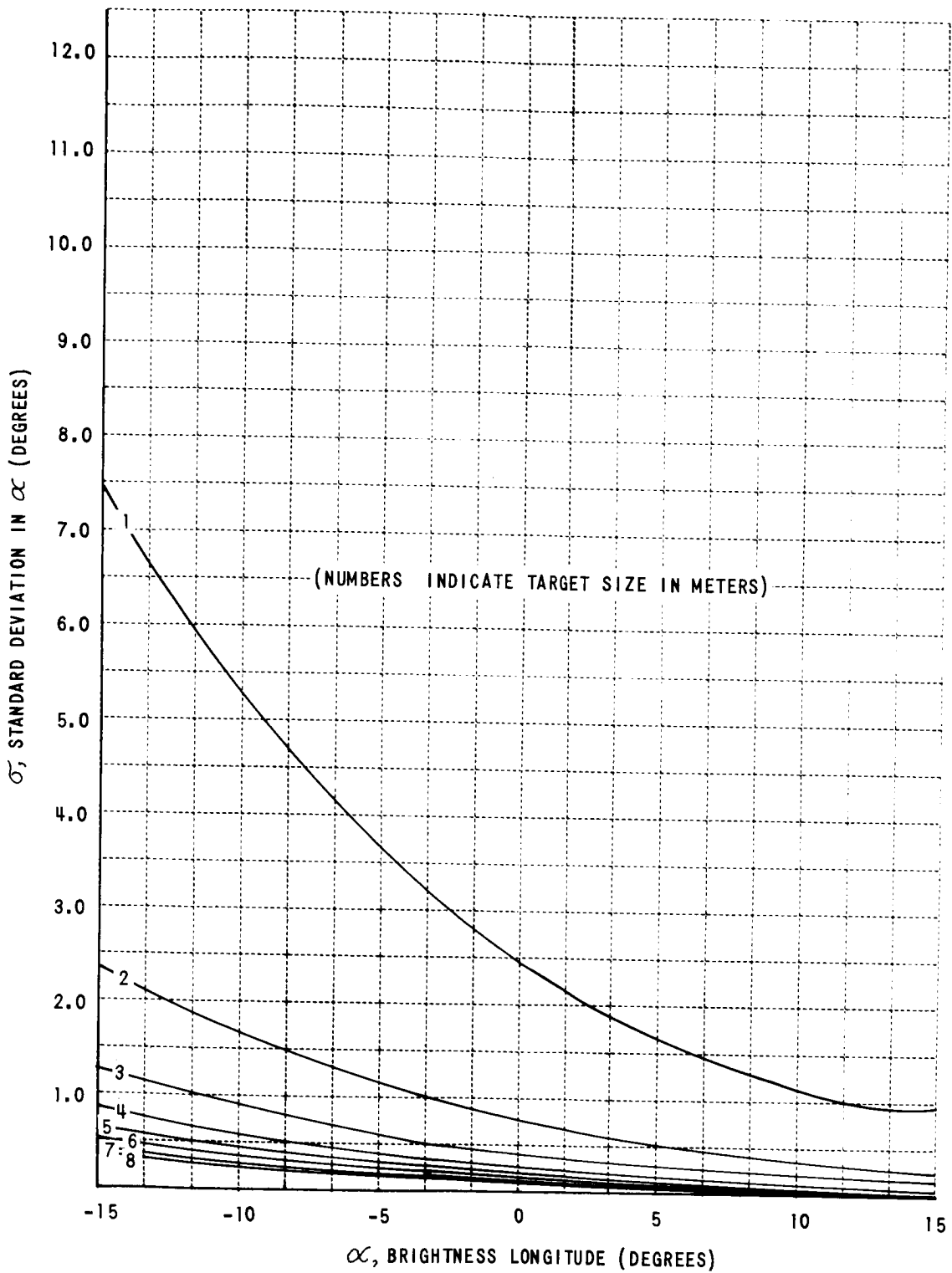


Figure 66 STANDARD DEVIATION IN MEASUREMENT OF BRIGHTNESS LONGITUDE - ORBITER II, HRF 141

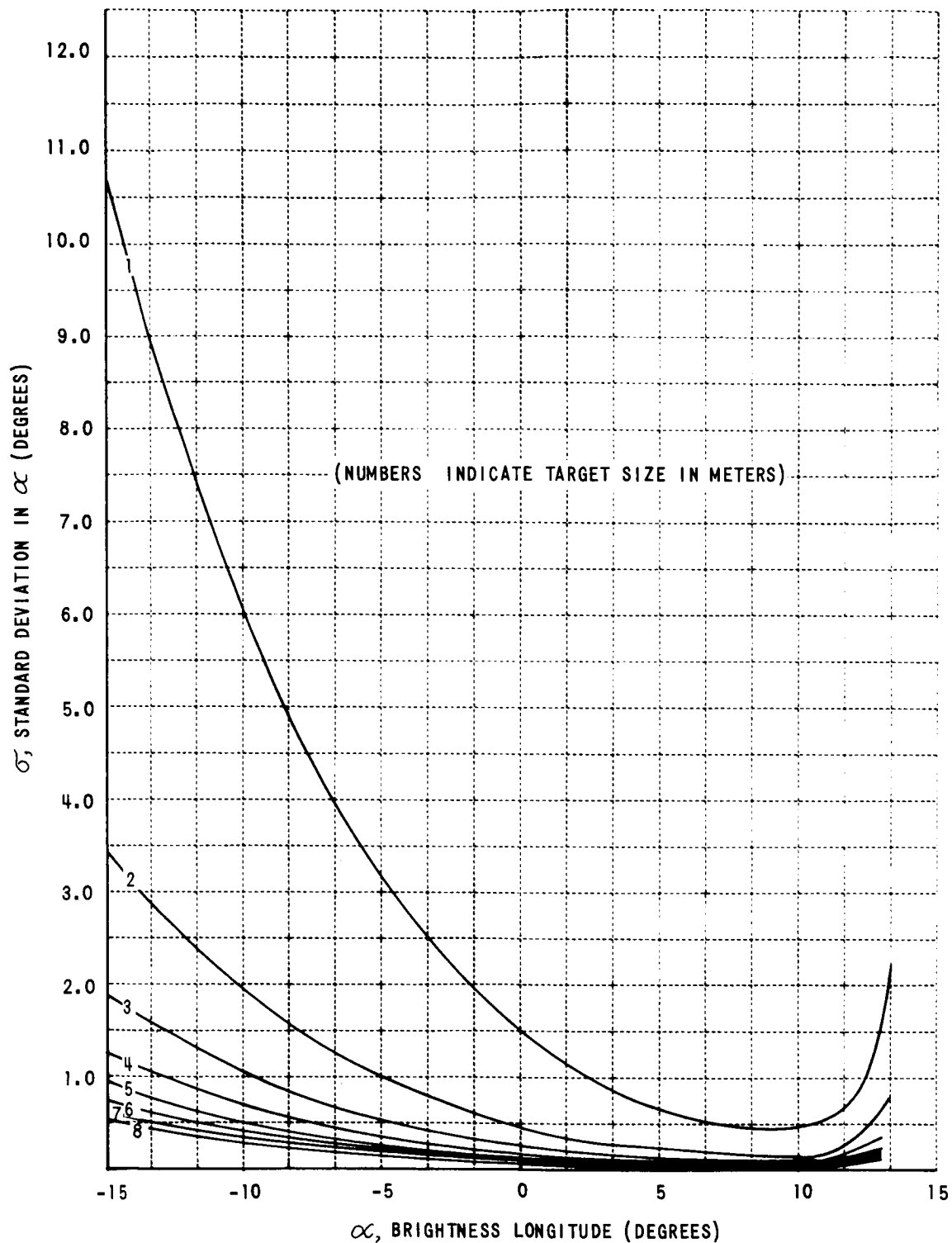


Figure 67 STANDARD DEVIATION IN MEASUREMENT OF BRIGHTNESS LONGITUDE - ORBITER II, HRF 157

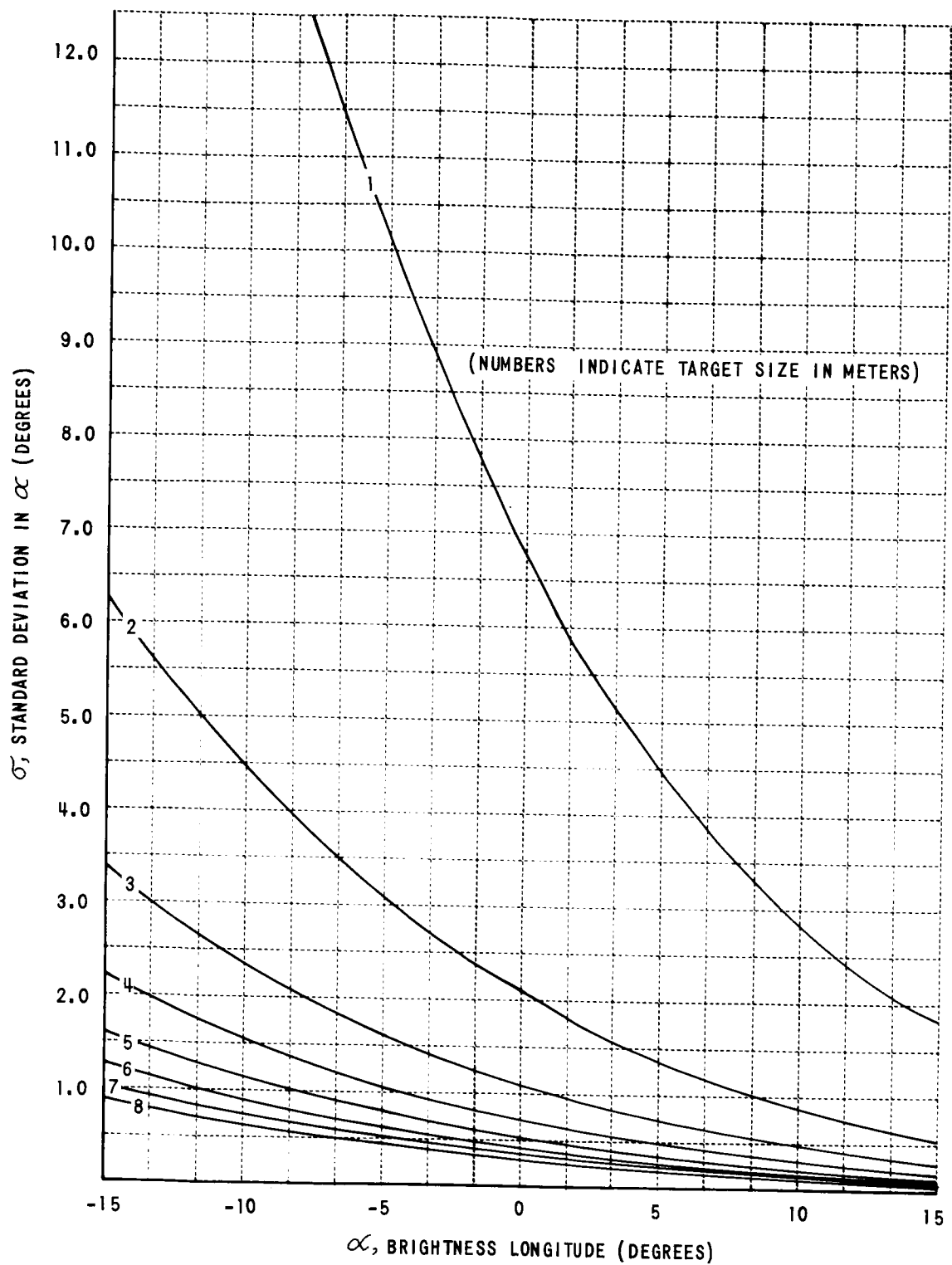


Figure 68 STANDARD DEVIATION IN MEASUREMENT OF BRIGHTNESS LONGITUDE - ORBITER II, HRF 174

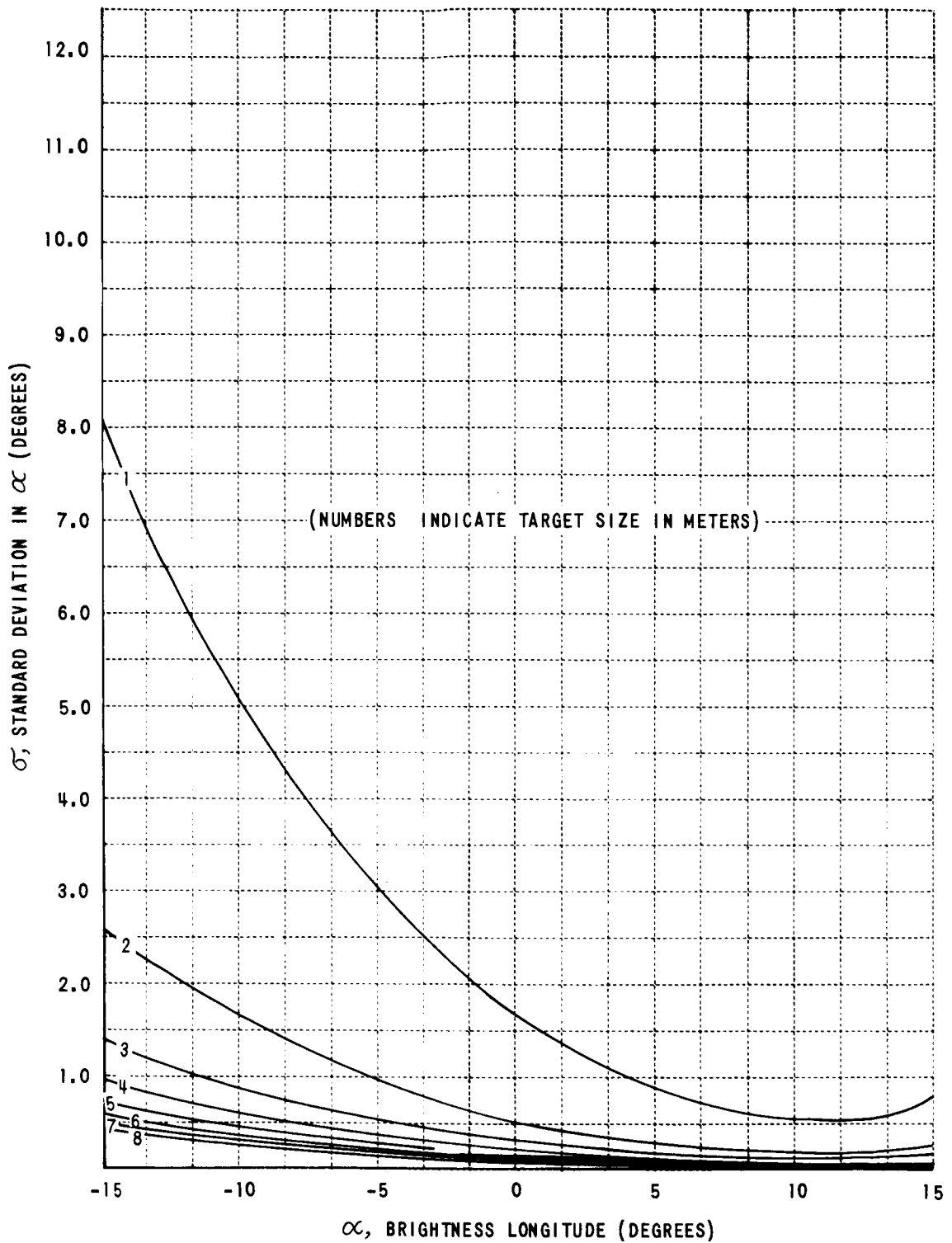


Figure 69 STANDARD DEVIATION IN MEASUREMENT OF BRIGHTNESS LONGITUDE - ORBITER II, HRF 183

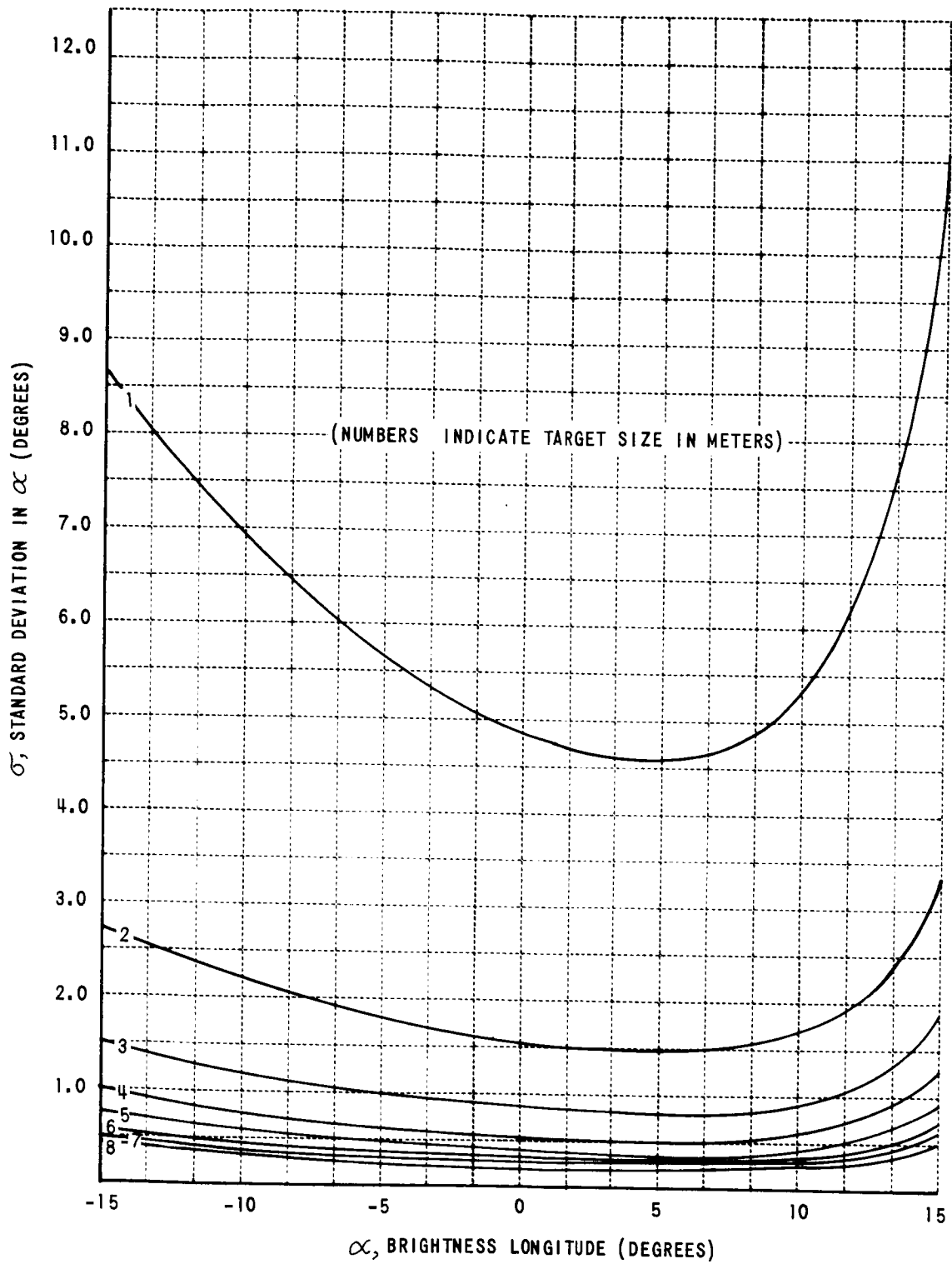


Figure 70 STANDARD DEVIATION IN MEASUREMENT OF BRIGHTNESS LONGITUDE - ORBITER II, HRF 208

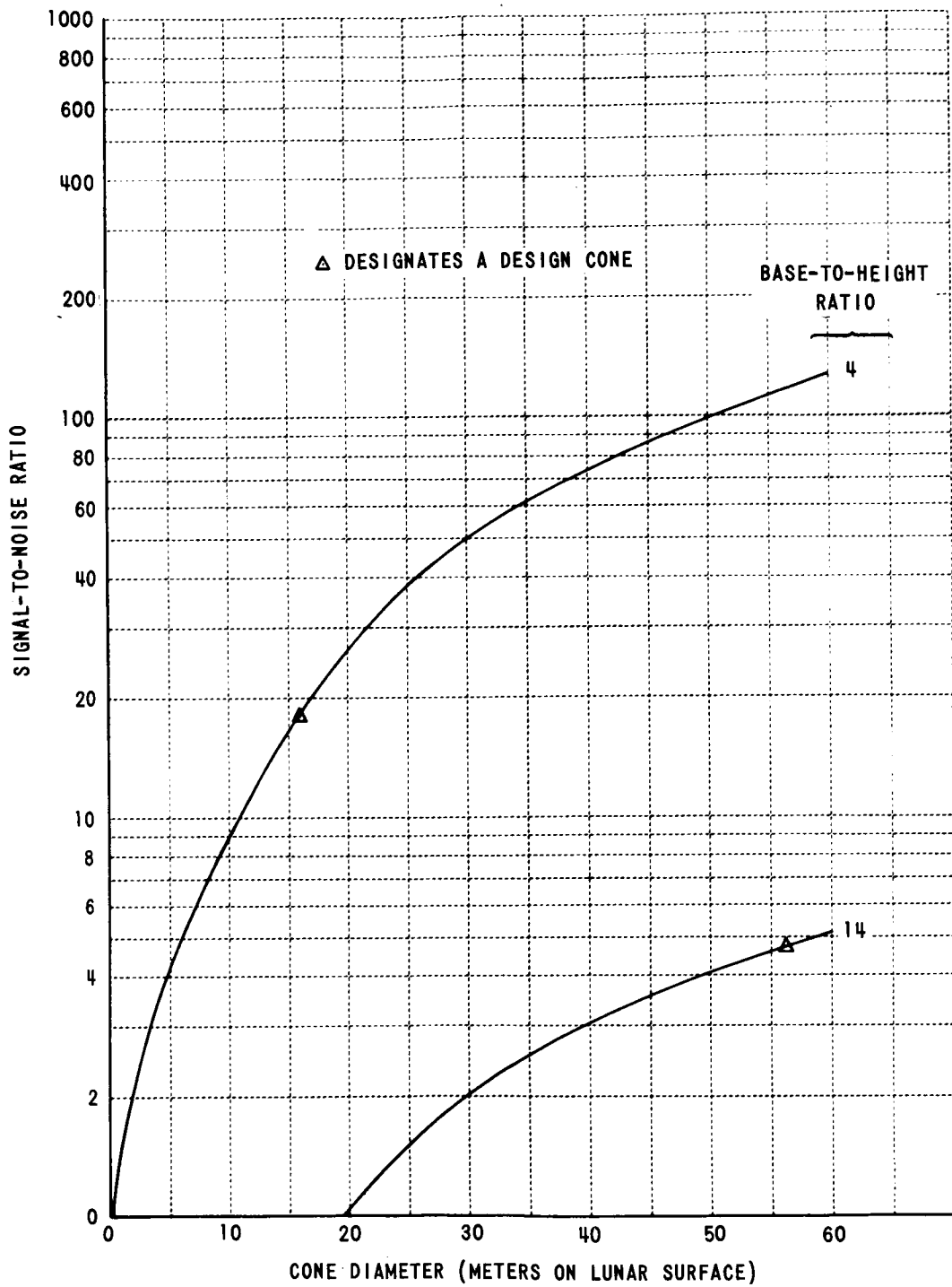


Figure 71 SIGNAL-TO-NOISE RATIO FOR CONE DETECTION - ORBITER I, MRF 61

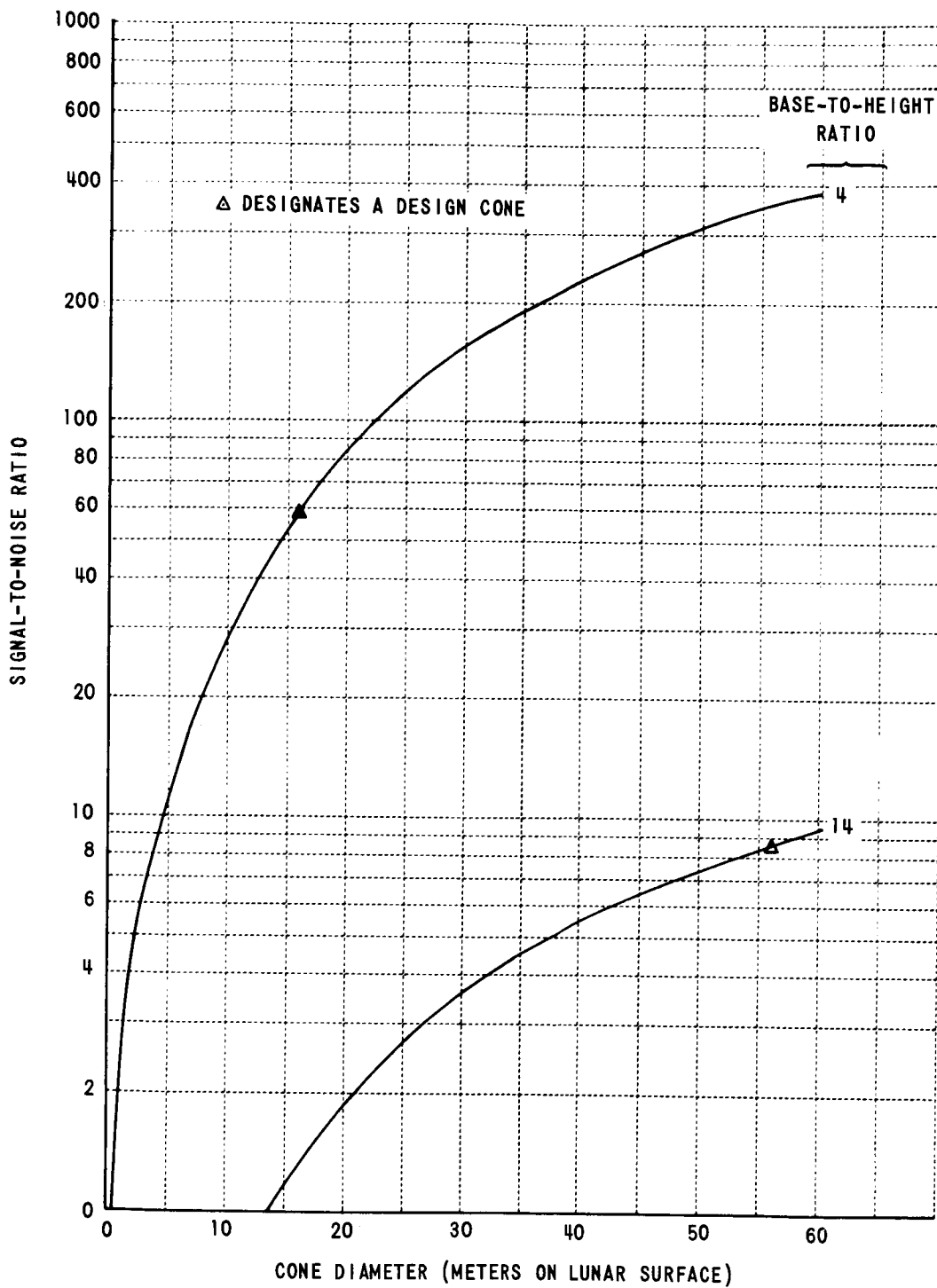


Figure 72 SIGNAL-TO-NOISE RATIO FOR CONE DETECTION - ORBITER I, MRF 85

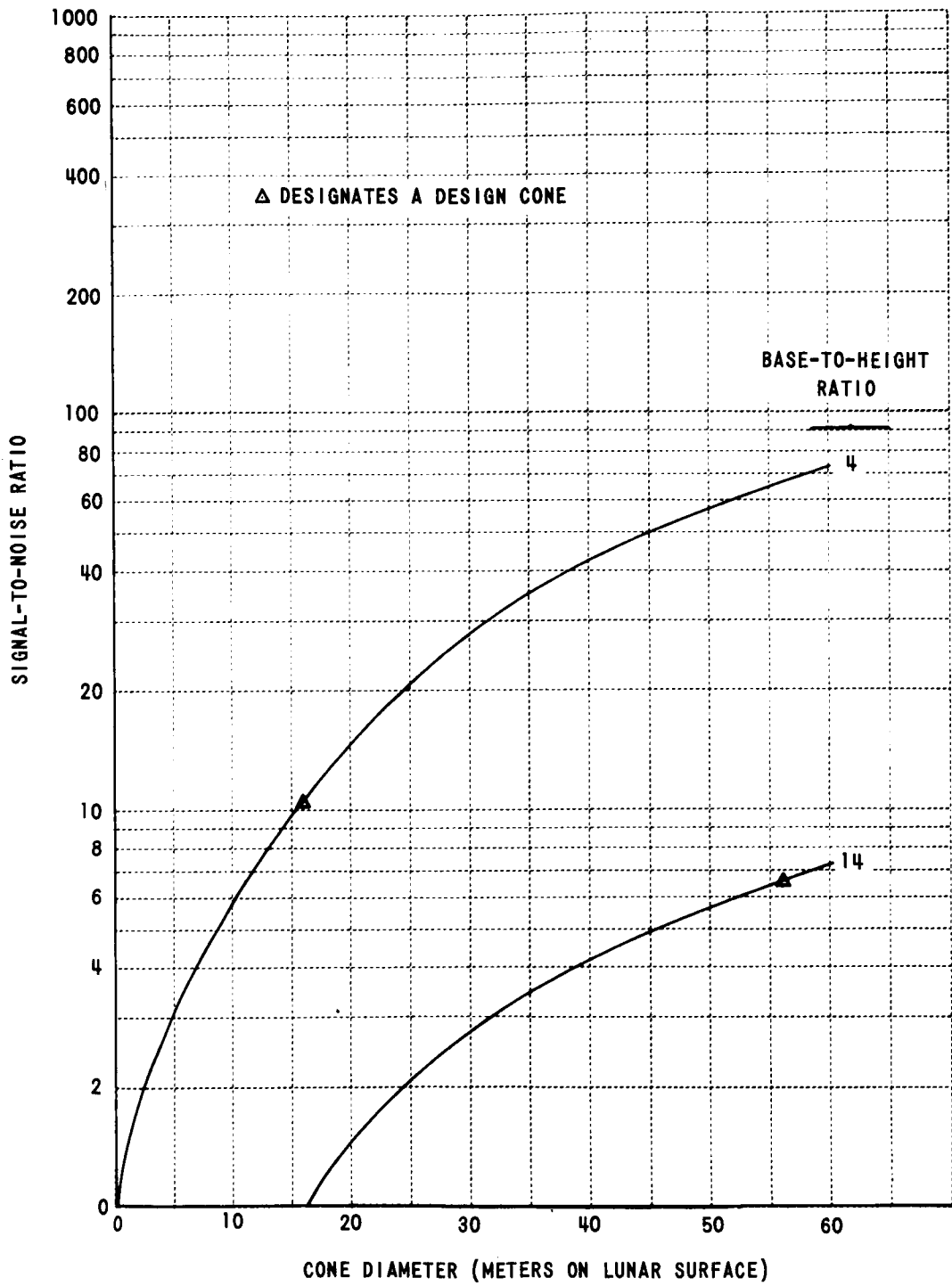


Figure 73 SIGNAL-TO-NOISE RATIO FOR CONE DETECTION - ORBITER I, MRF 144

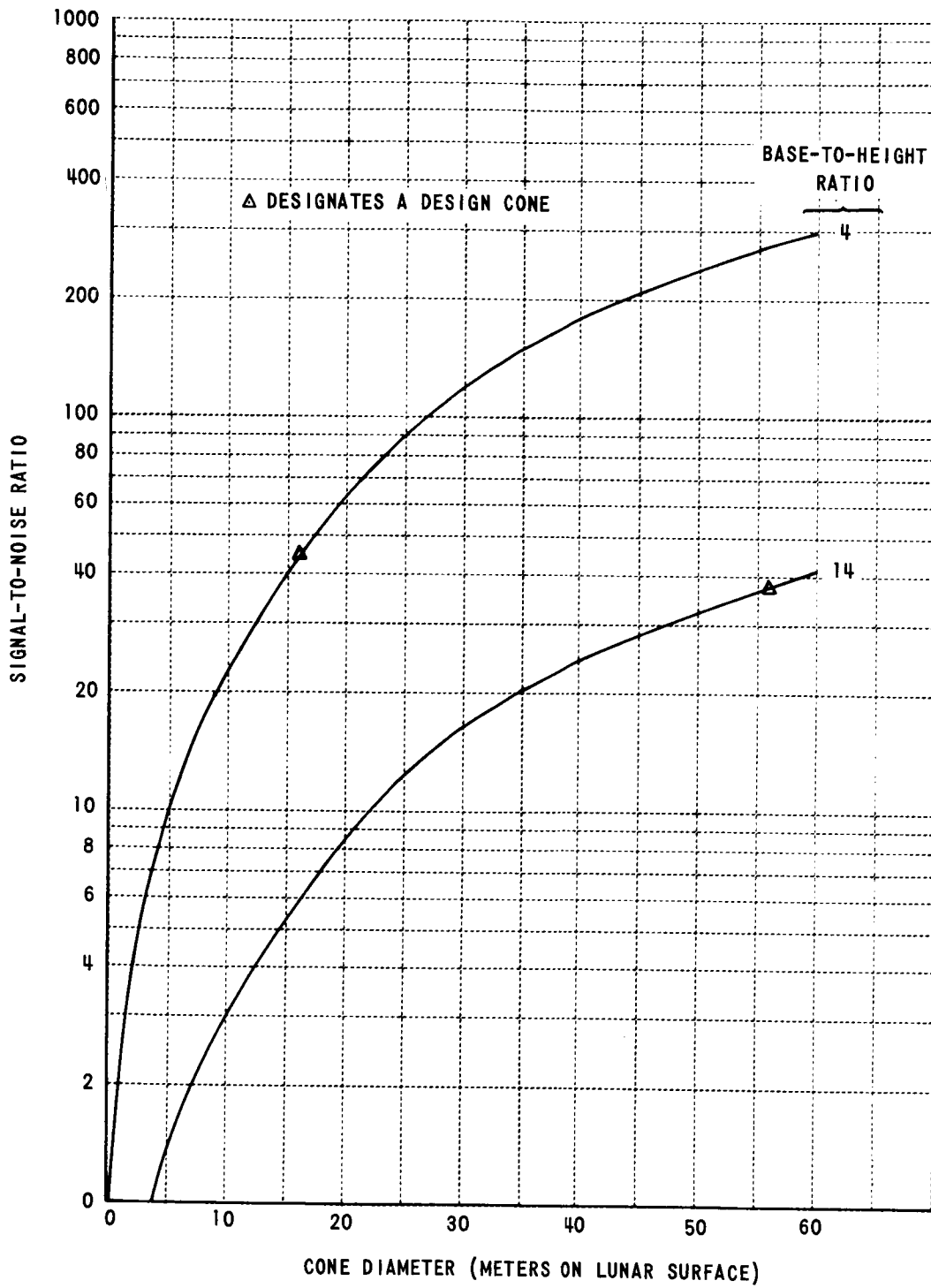


Figure 74 SIGNAL-TO-NOISE RATIO FOR CONE DETECTION - ORBITER I, MRF 207

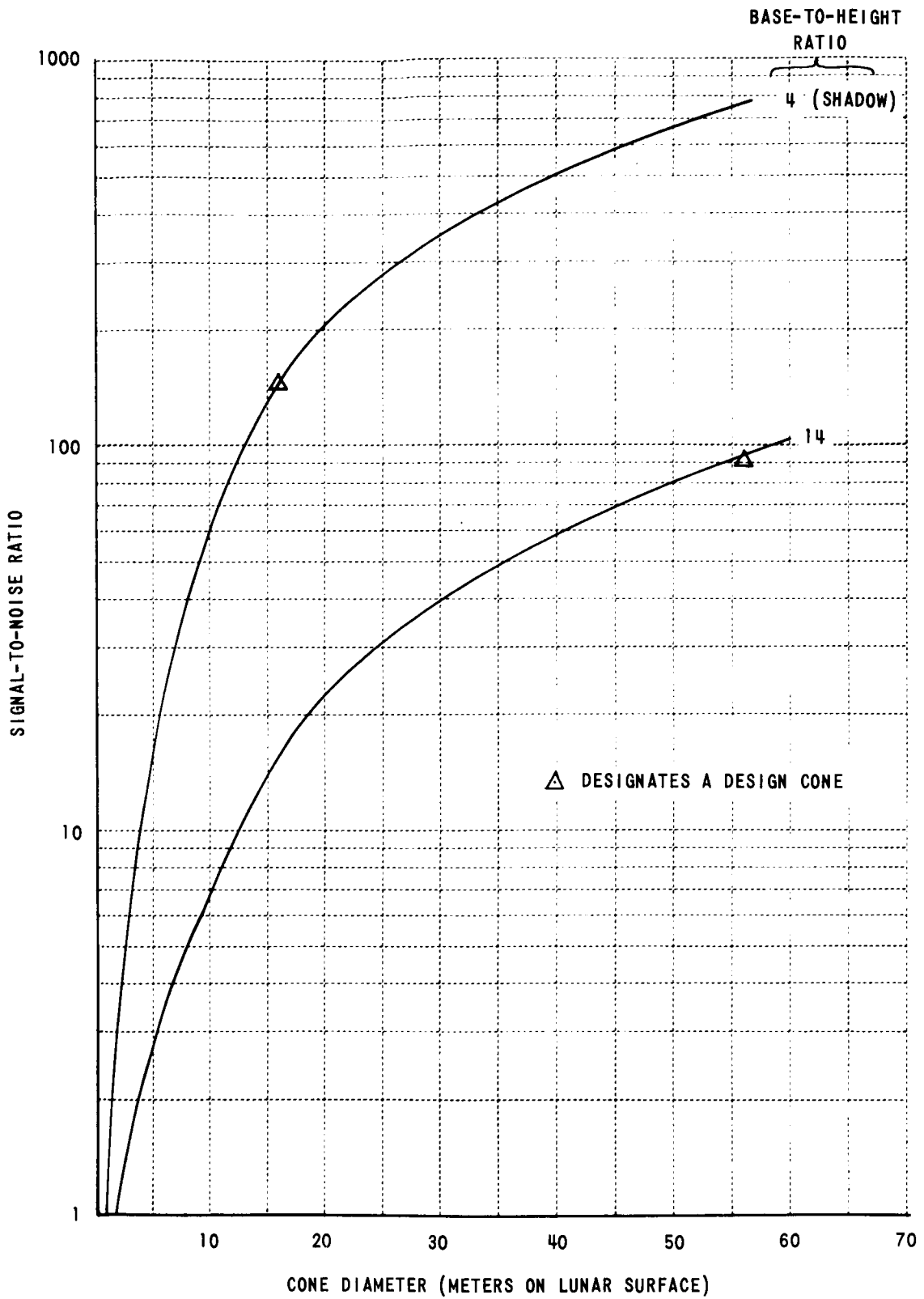


Figure 75 SIGNAL-TO-NOISE RATIO FOR CONE DETECTION - ORBITER II, MRF 13

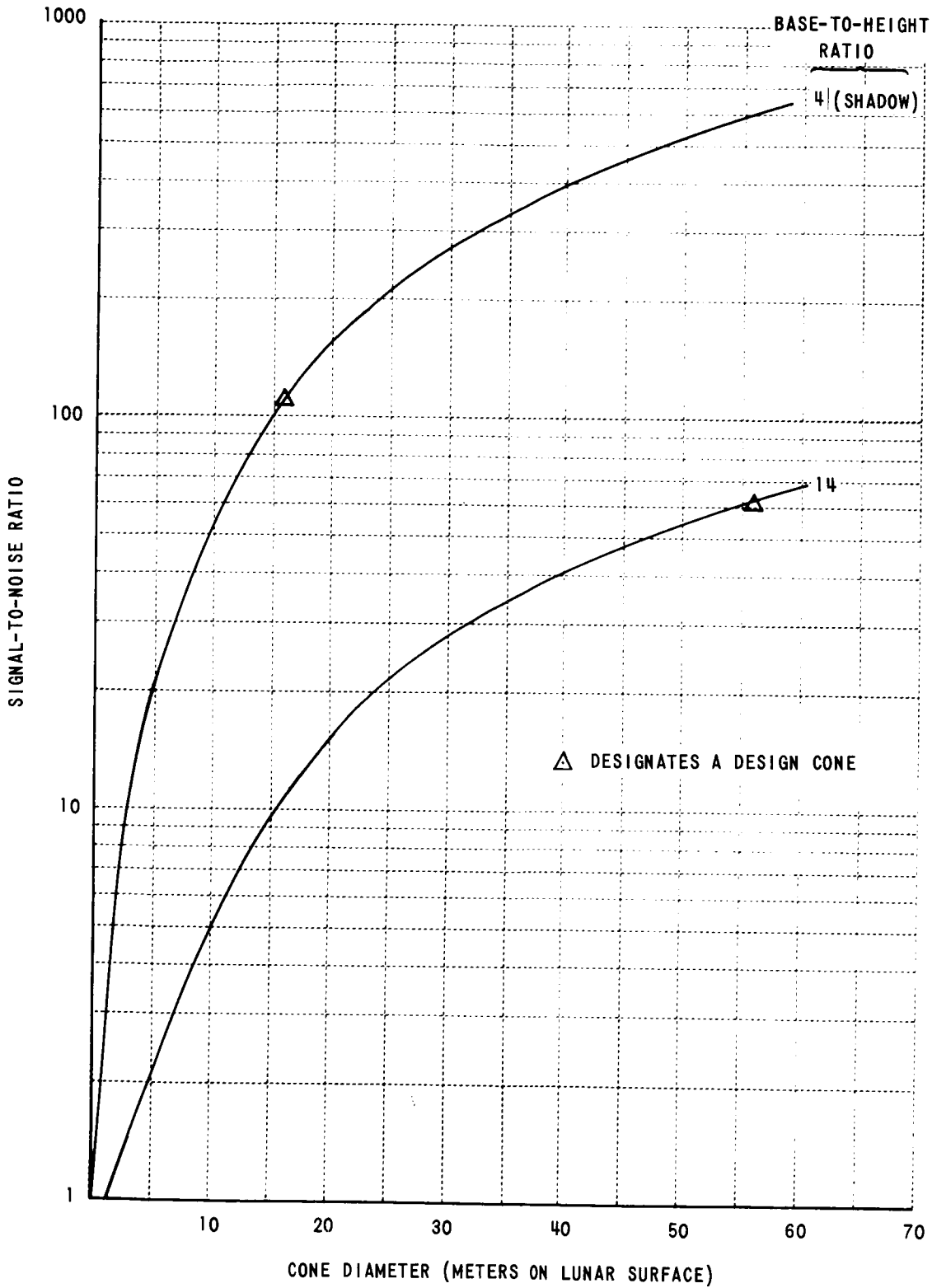


Figure 76 SIGNAL-TO-NOISE RATIO FOR CONE DETECTION - ORBITER II, MRF 39

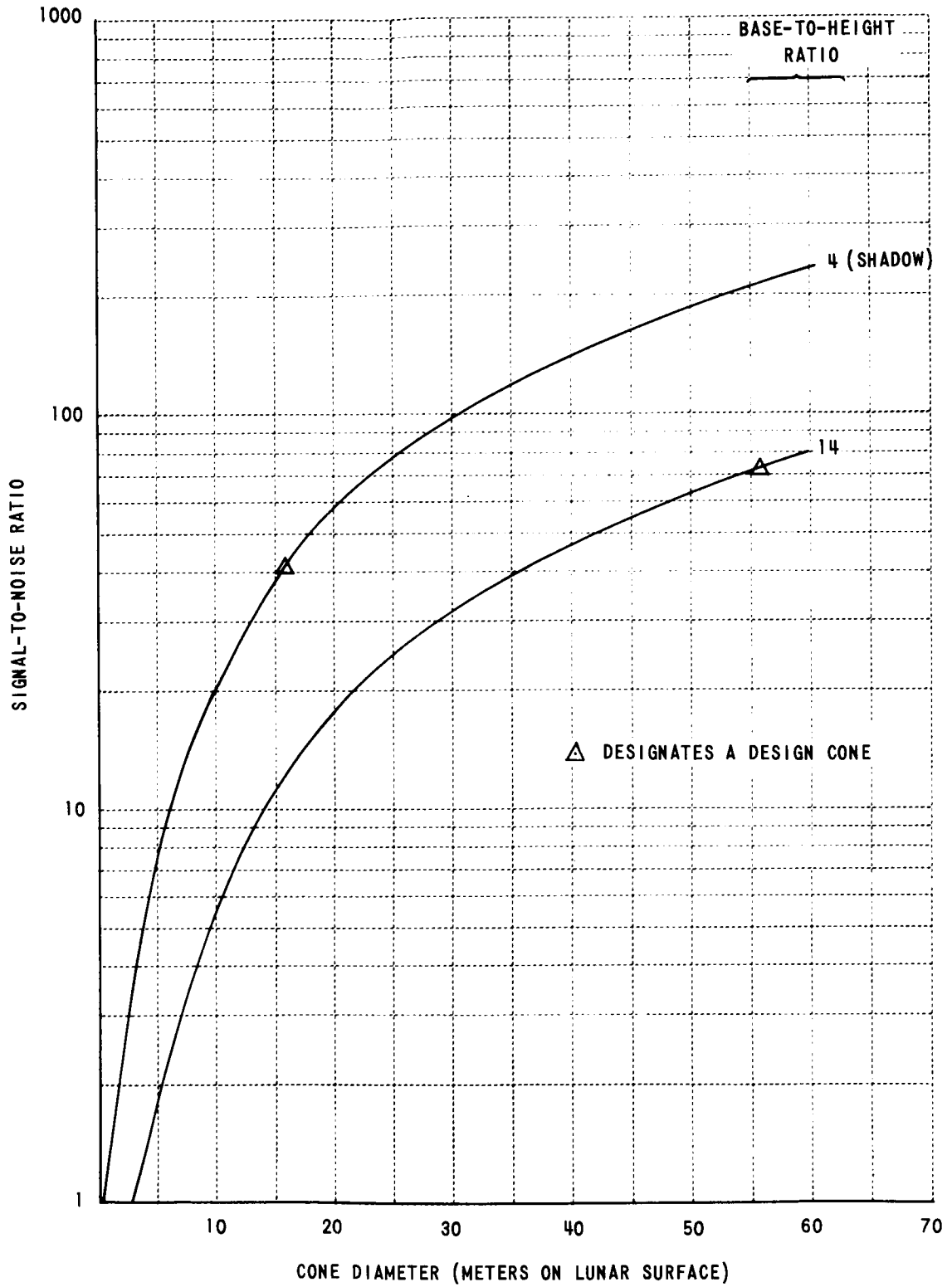


Figure 77 SIGNAL-TO-NOISE RATIO FOR CONE DETECTION - ORBITER II, MRF 46

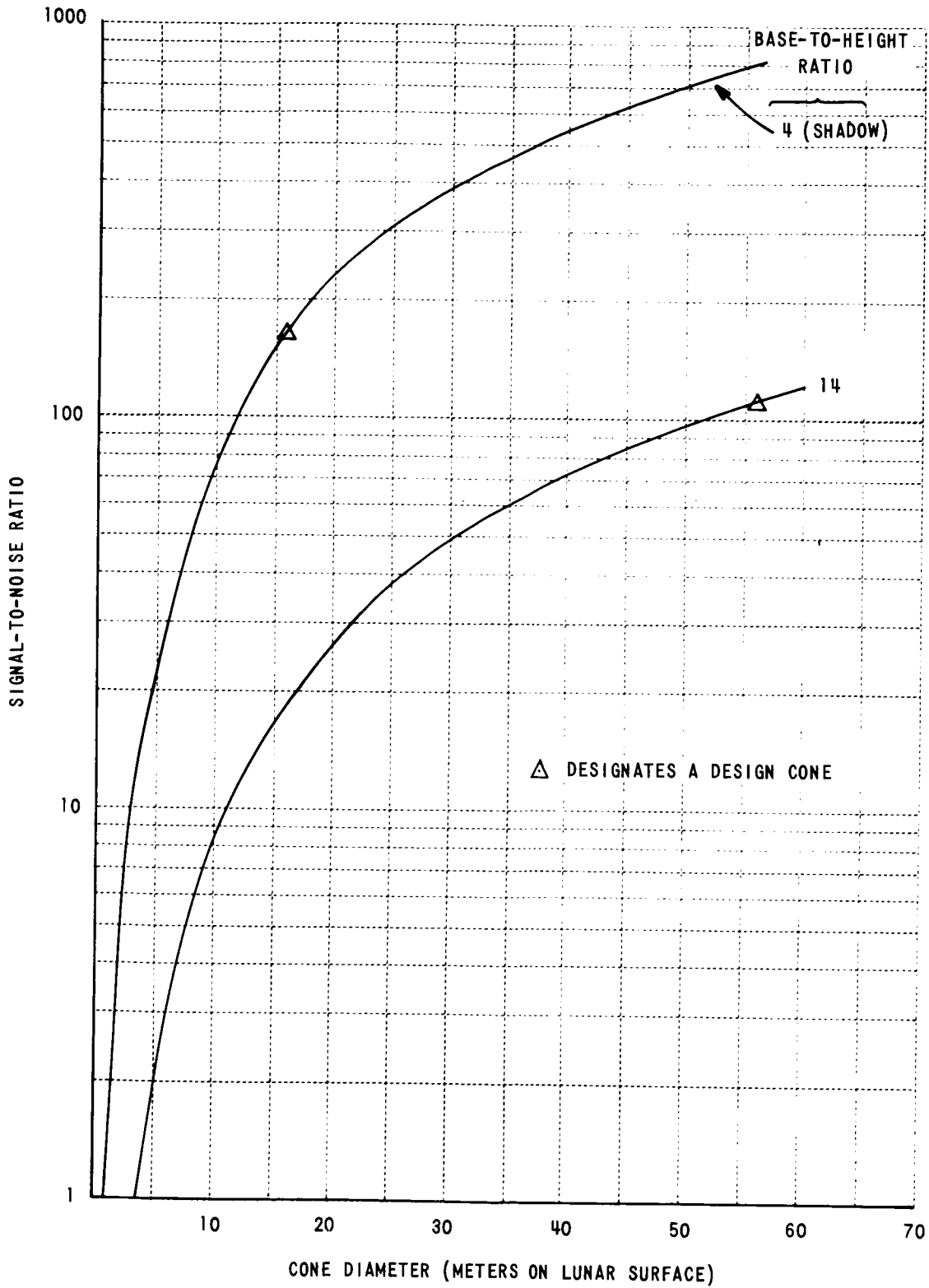


Figure 78 SIGNAL-TO-NOISE RATIO FOR CONE DETECTION - ORBITER II, MRF 63

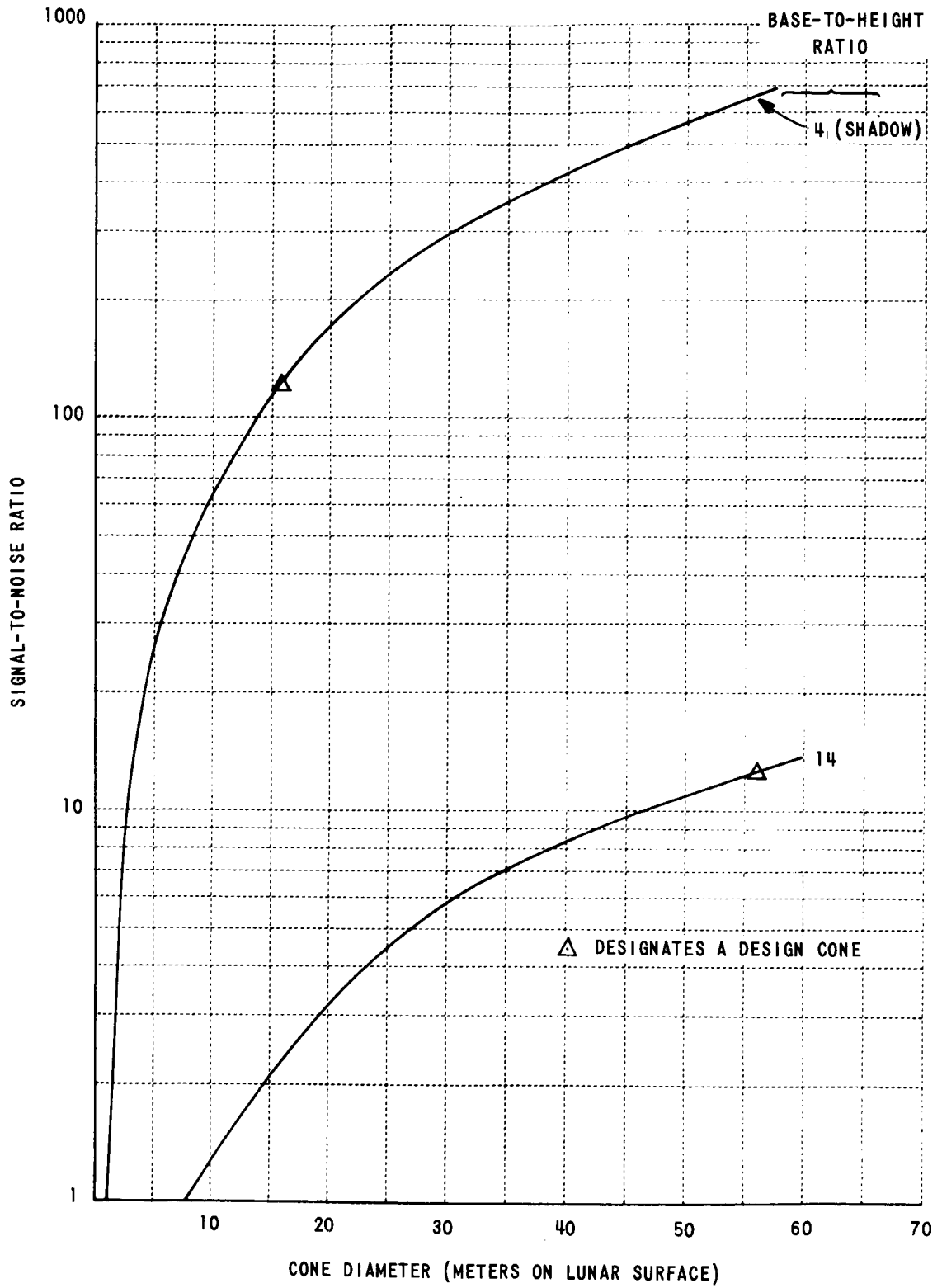


Figure 79 SIGNAL-TO-NOISE RATIO FOR CONE DETECTION - ORBITER II, MRF 69

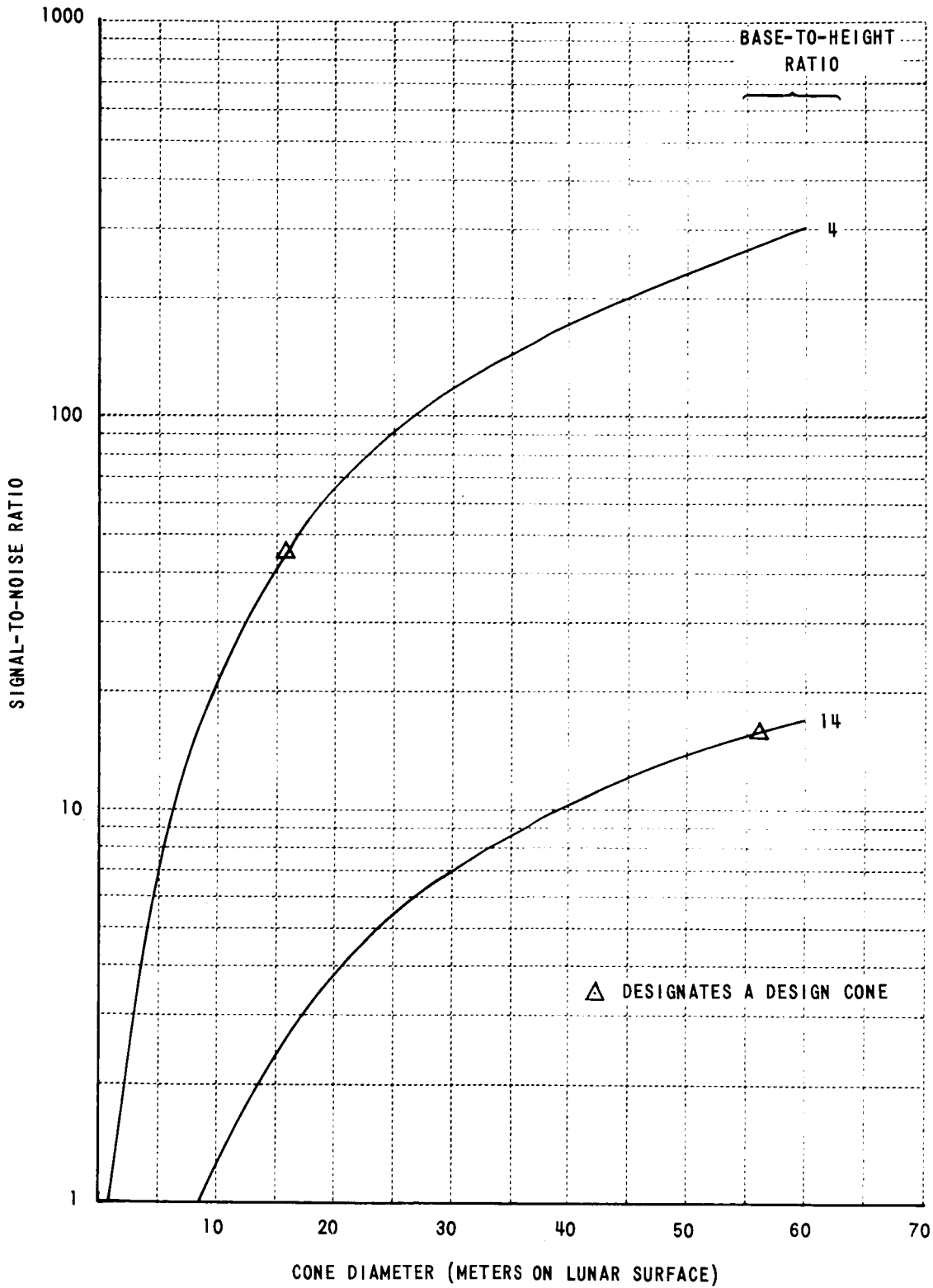


Figure 80 SIGNAL-TO-NOISE RATIO FOR CONE DETECTION - ORBITER II, MRF 88

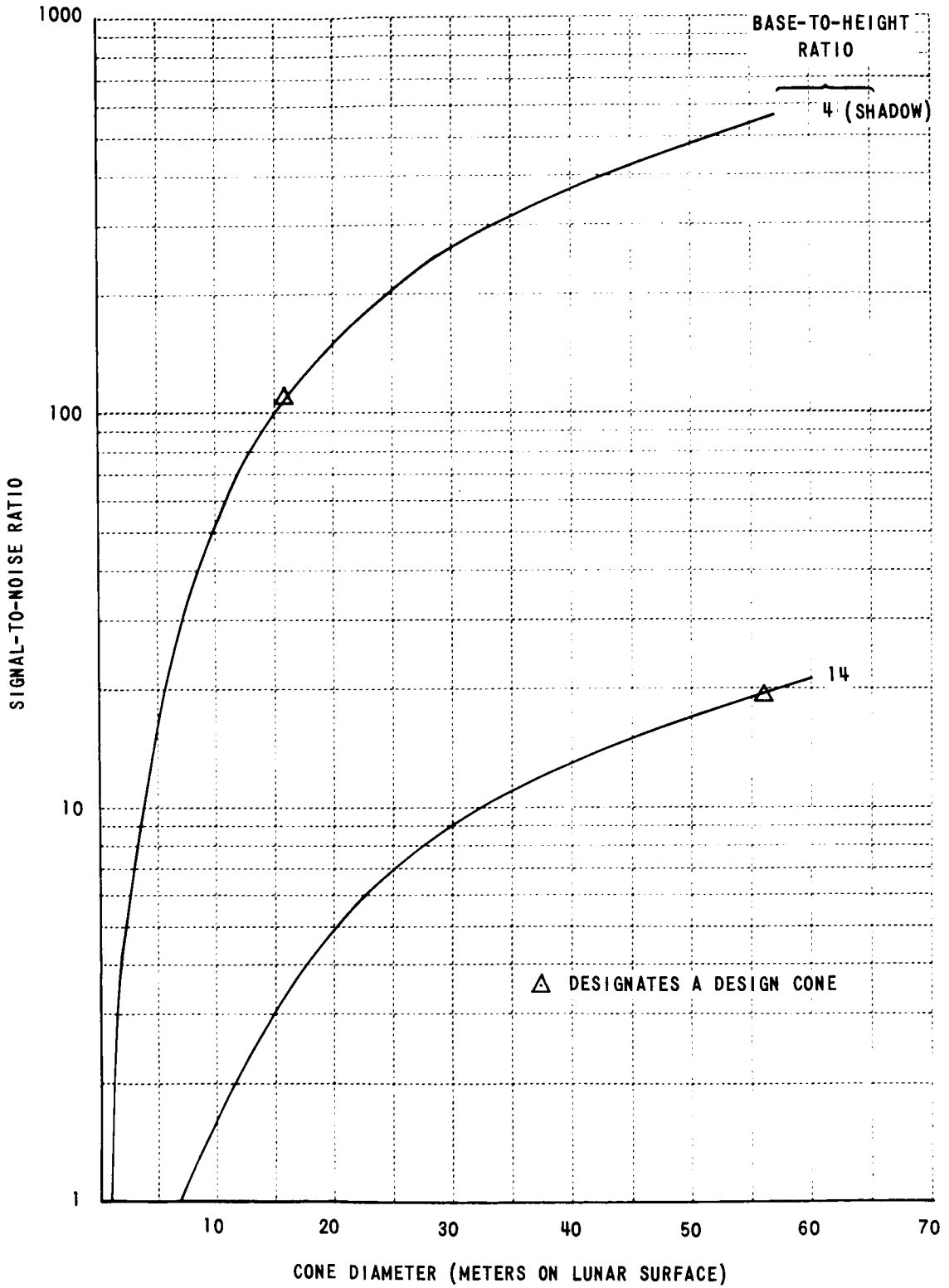


Figure 81 SIGNAL-TO-NOISE RATIO FOR CONE DETECTION - ORBITER II, MRF 99

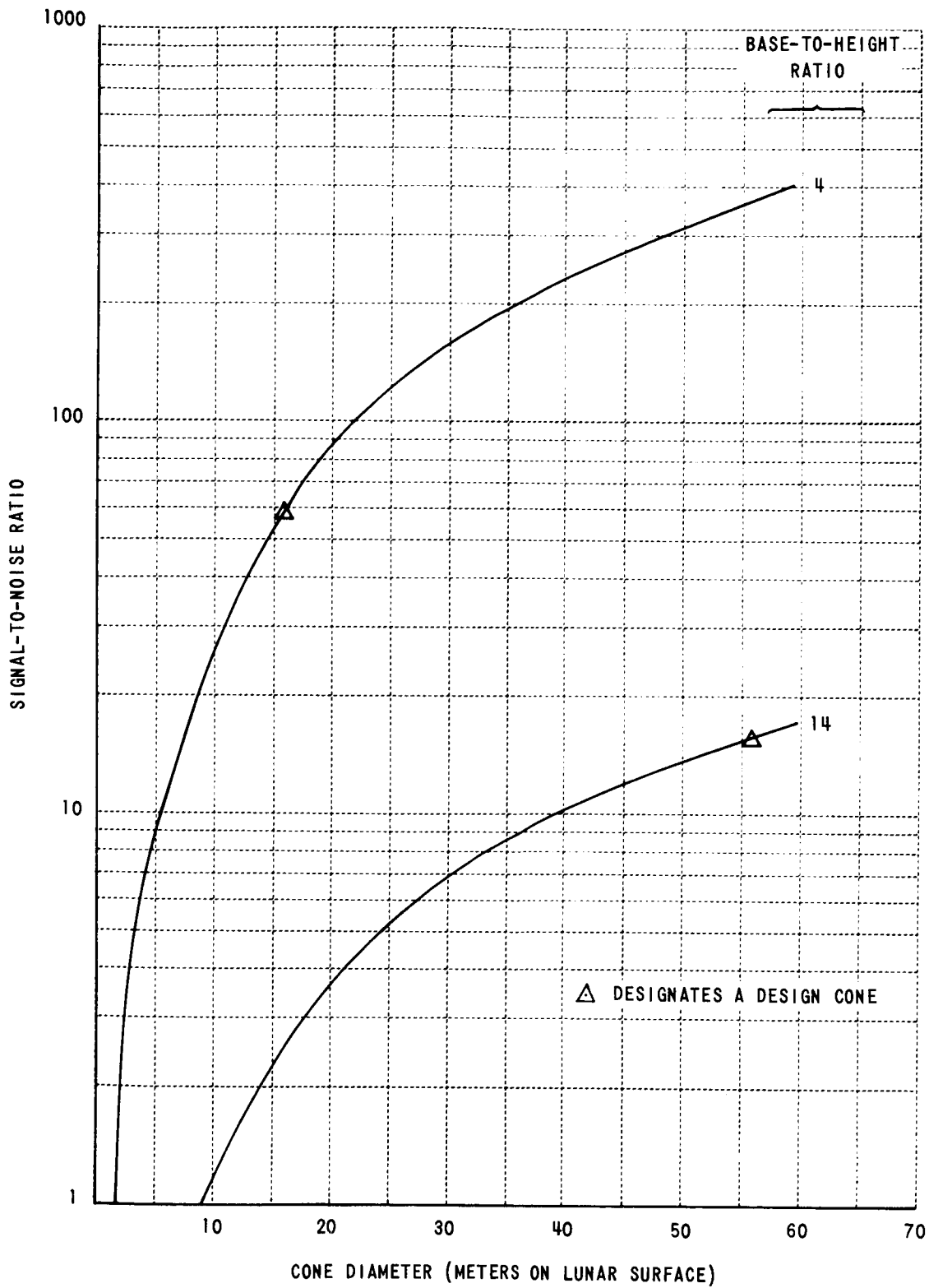


Figure 82 SIGNAL-TO-NOISE RATIO FOR CONE DETECTION - ORBITER II, MRF 124

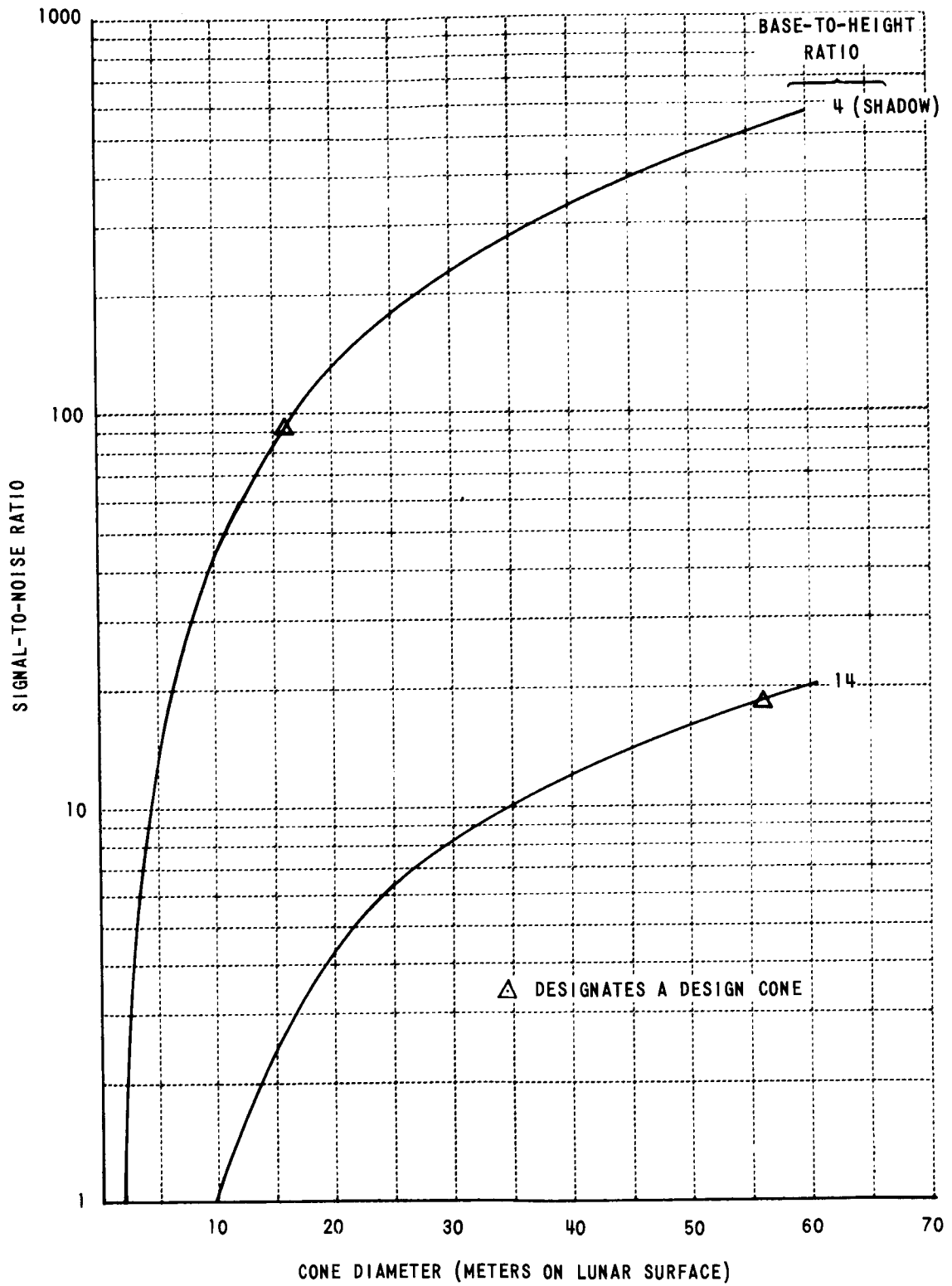


Figure 83 SIGNAL-TO-NOISE RATIO FOR CONE DETECTION - ORBITER II, MRF 141

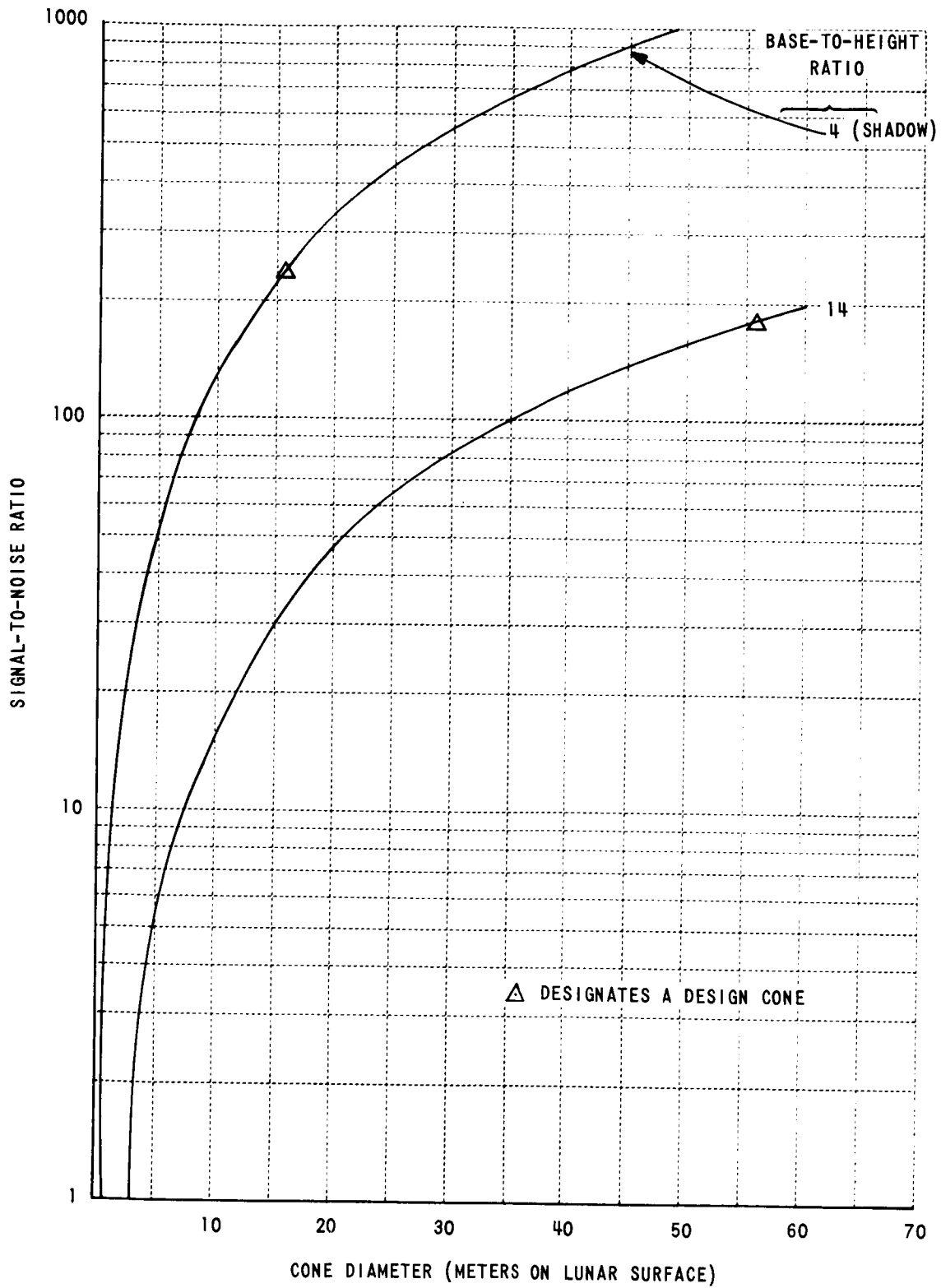


Figure 84 SIGNAL-TO-NOISE RATIO FOR CONE DETECTION - ORBITER II, MRF 157

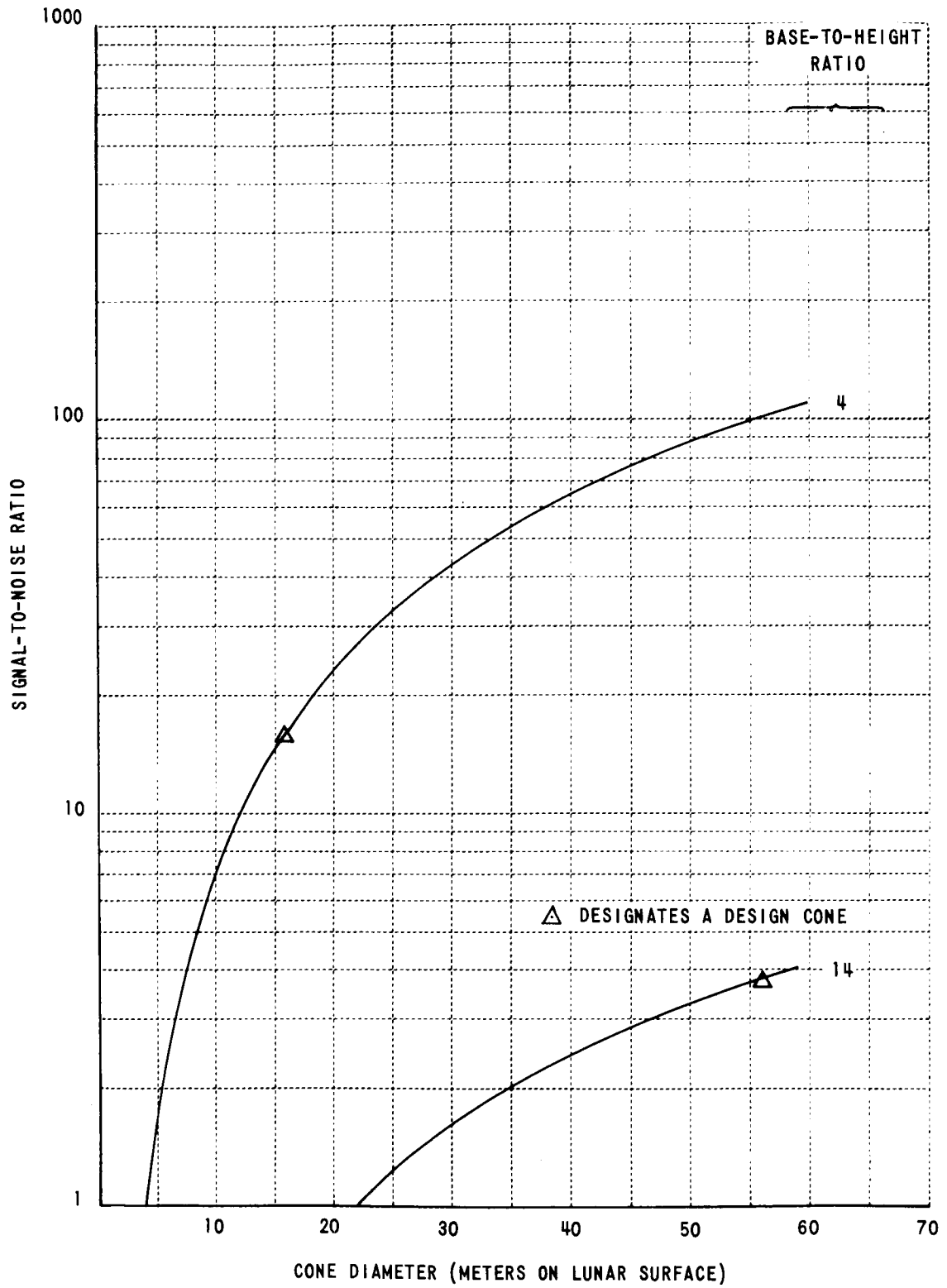


Figure 85 SIGNAL-TO-NOISE RATIO FOR CONE DETECTION - ORBITER II, MRF 174

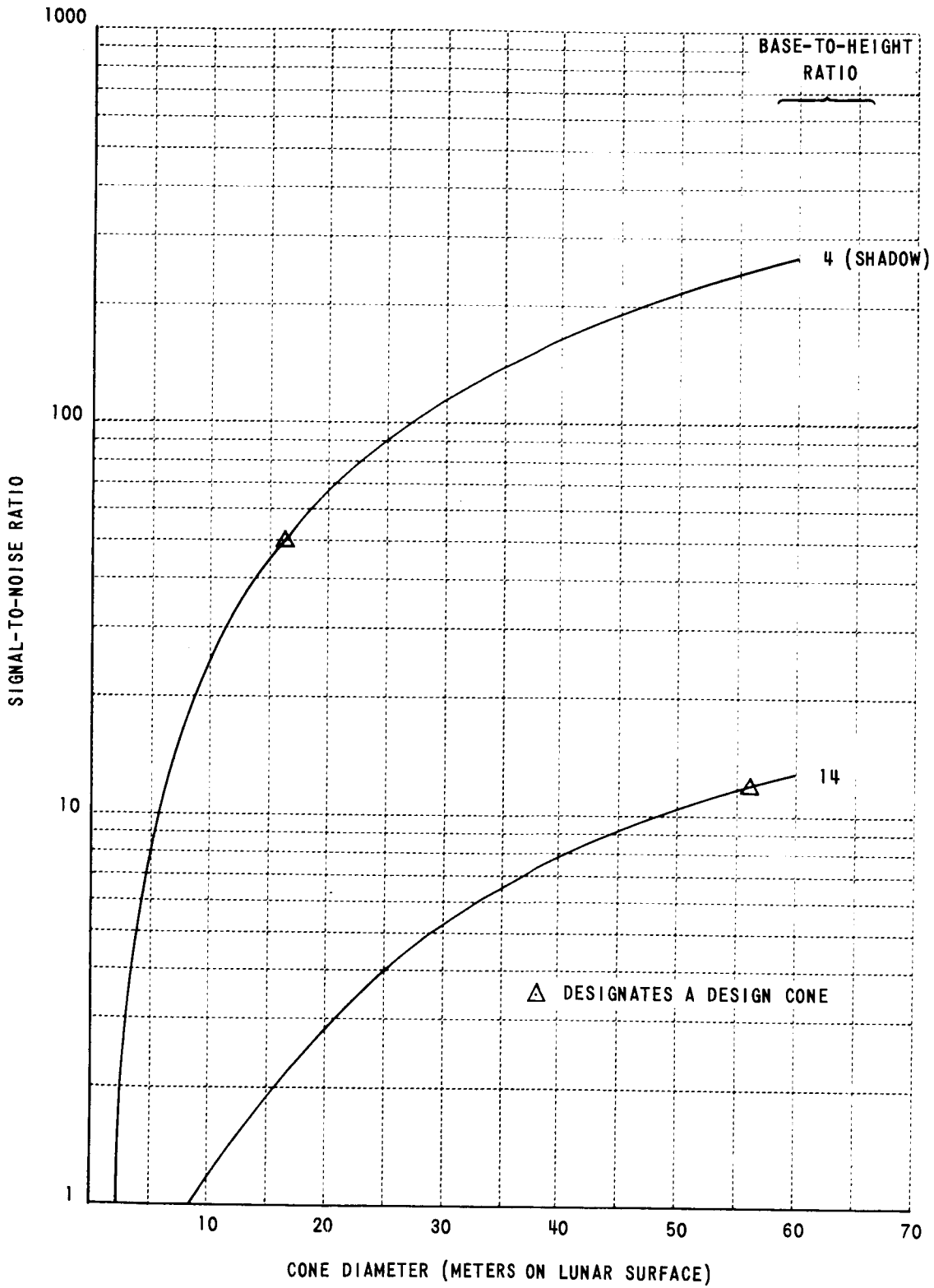


Figure 86 SIGNAL-TO-NOISE RATIO FOR CONE DETECTION - ORBITER II, MRF 183

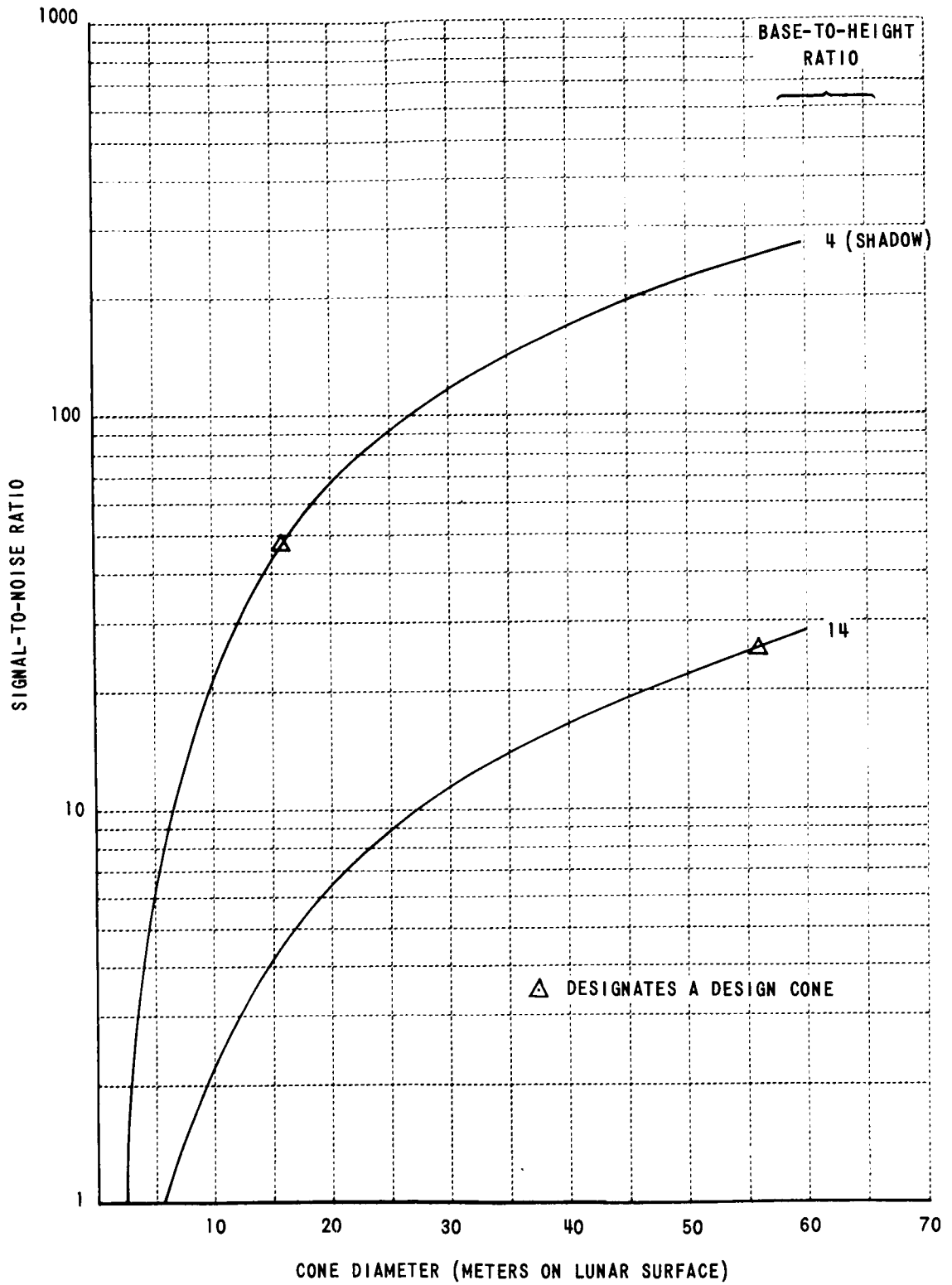


Figure 87 SIGNAL-TO-NOISE RATIO FOR CONE DETECTION - ORBITER II, MRF 208

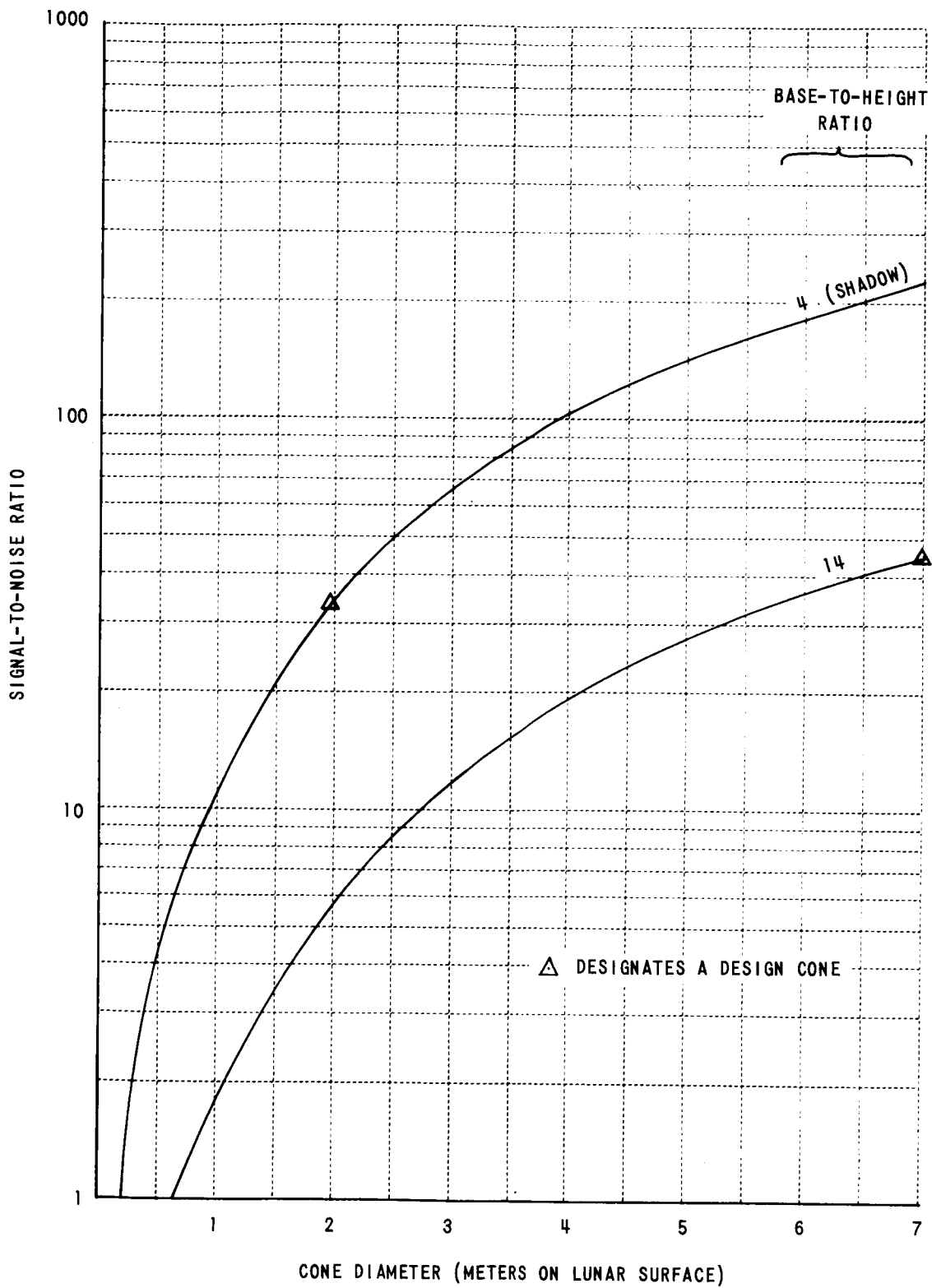


Figure 88 SIGNAL-TO-NOISE RATIO FOR CONE DETECTION - ORBITER II, HRF 13

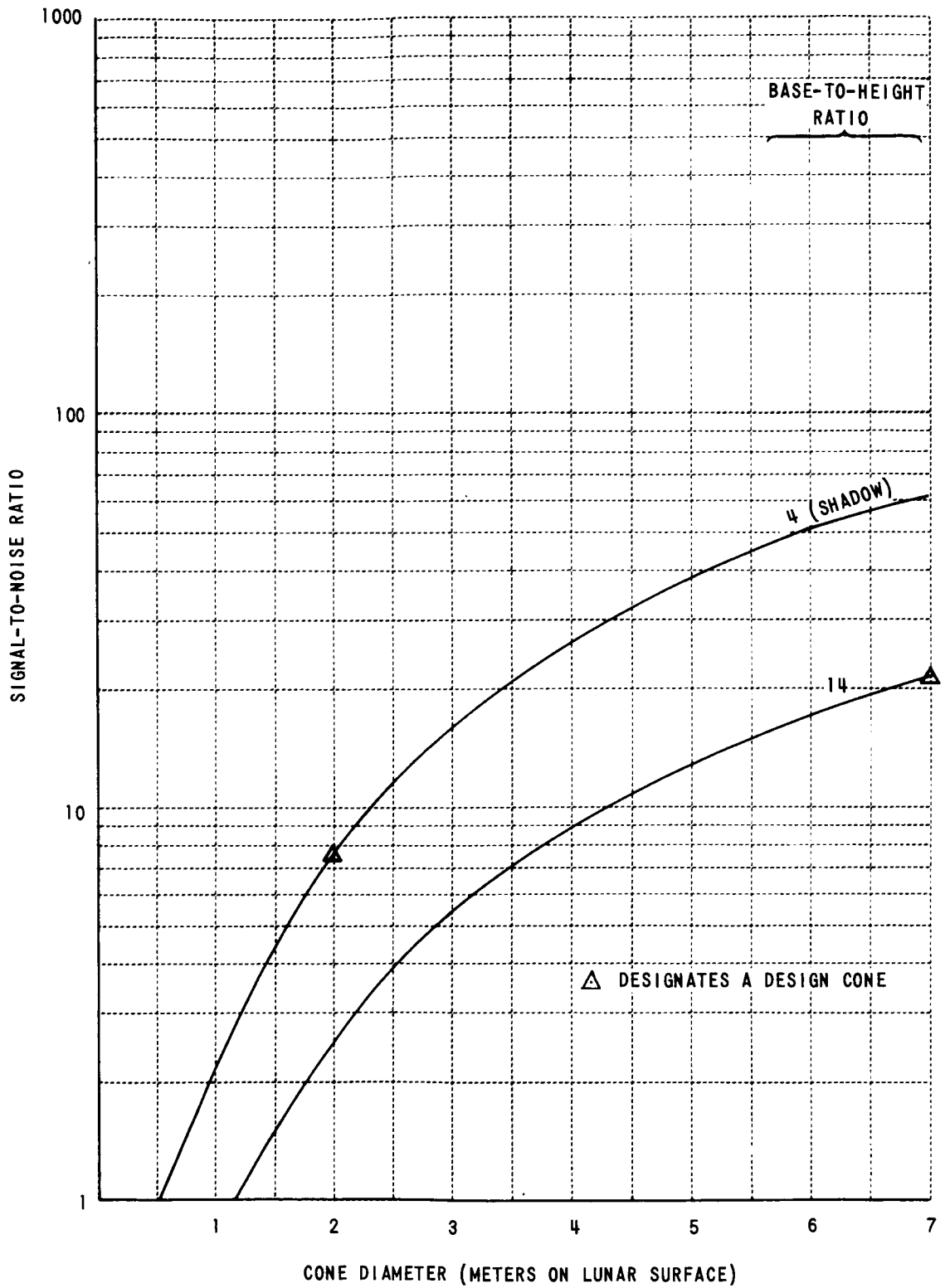


Figure 89 SIGNAL-TO-NOISE RATIO FOR CONE DETECTION - ORBITER II, HRF 39

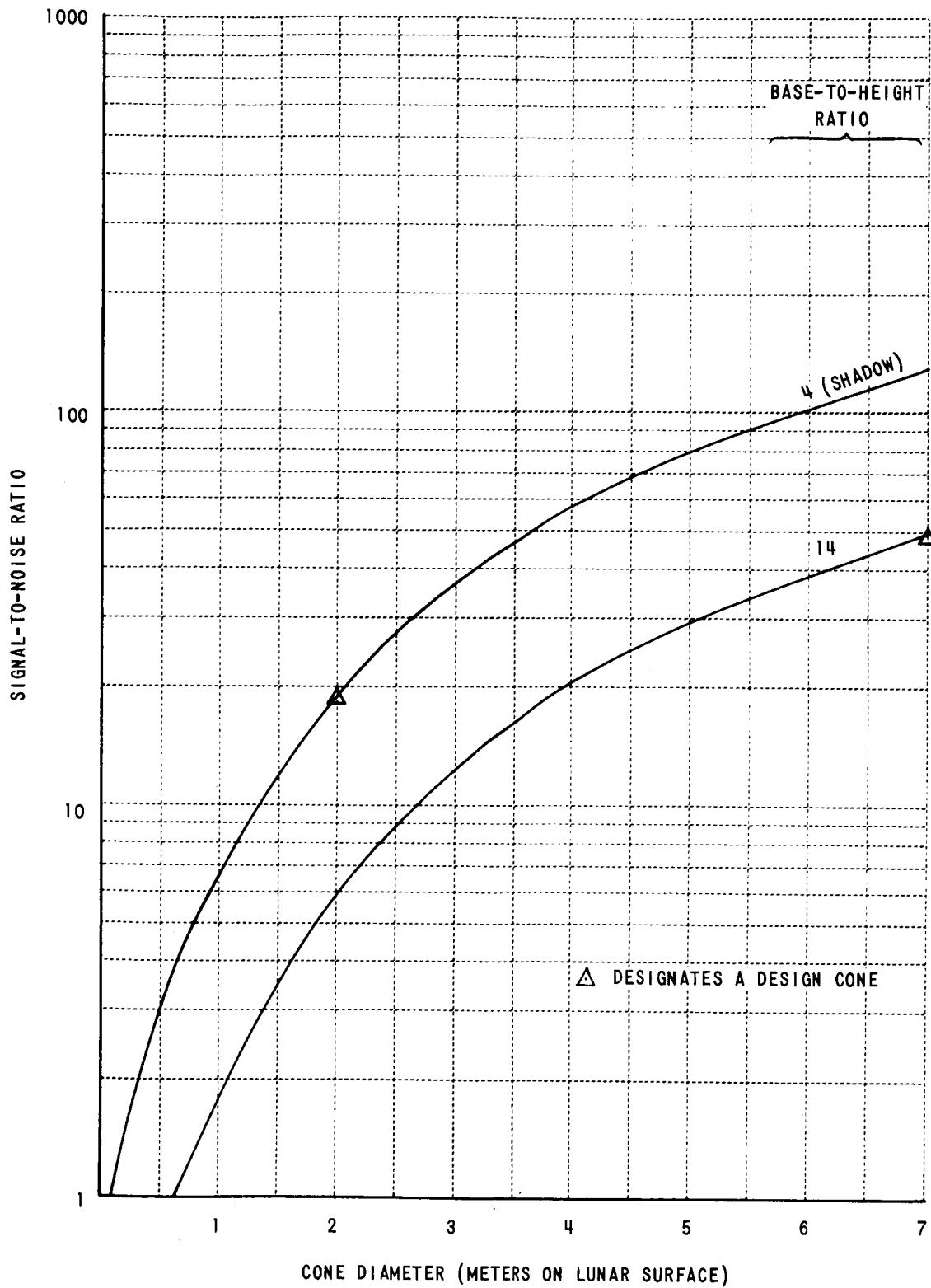


Figure 90 SIGNAL-TO-NOISE RATIO FOR CONE DETECTION - ORBITER II, HRF 46

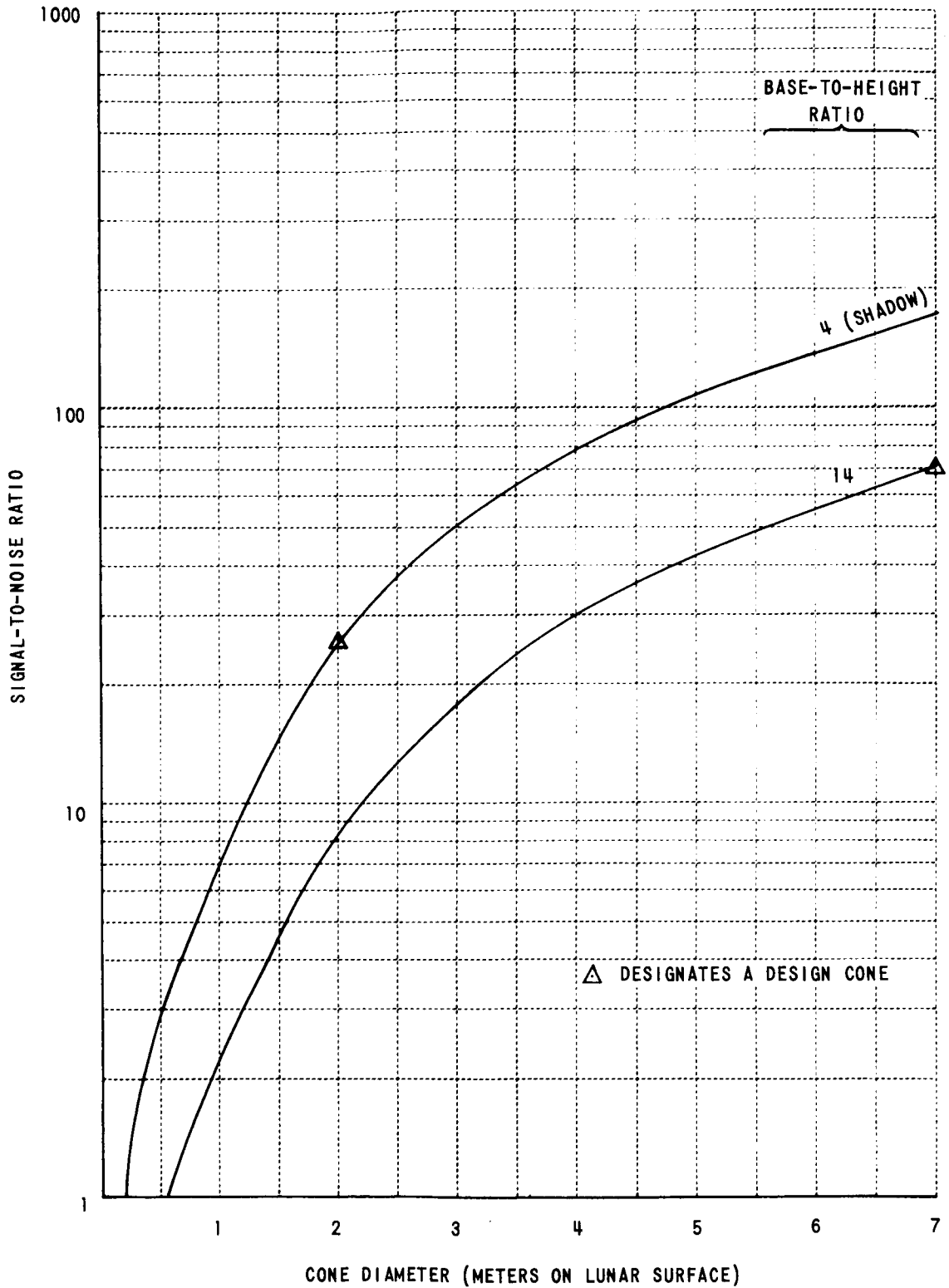


Figure 91 SIGNAL-TO-NOISE RATIO FOR CONE DETECTION - ORBITER II, HRF 63

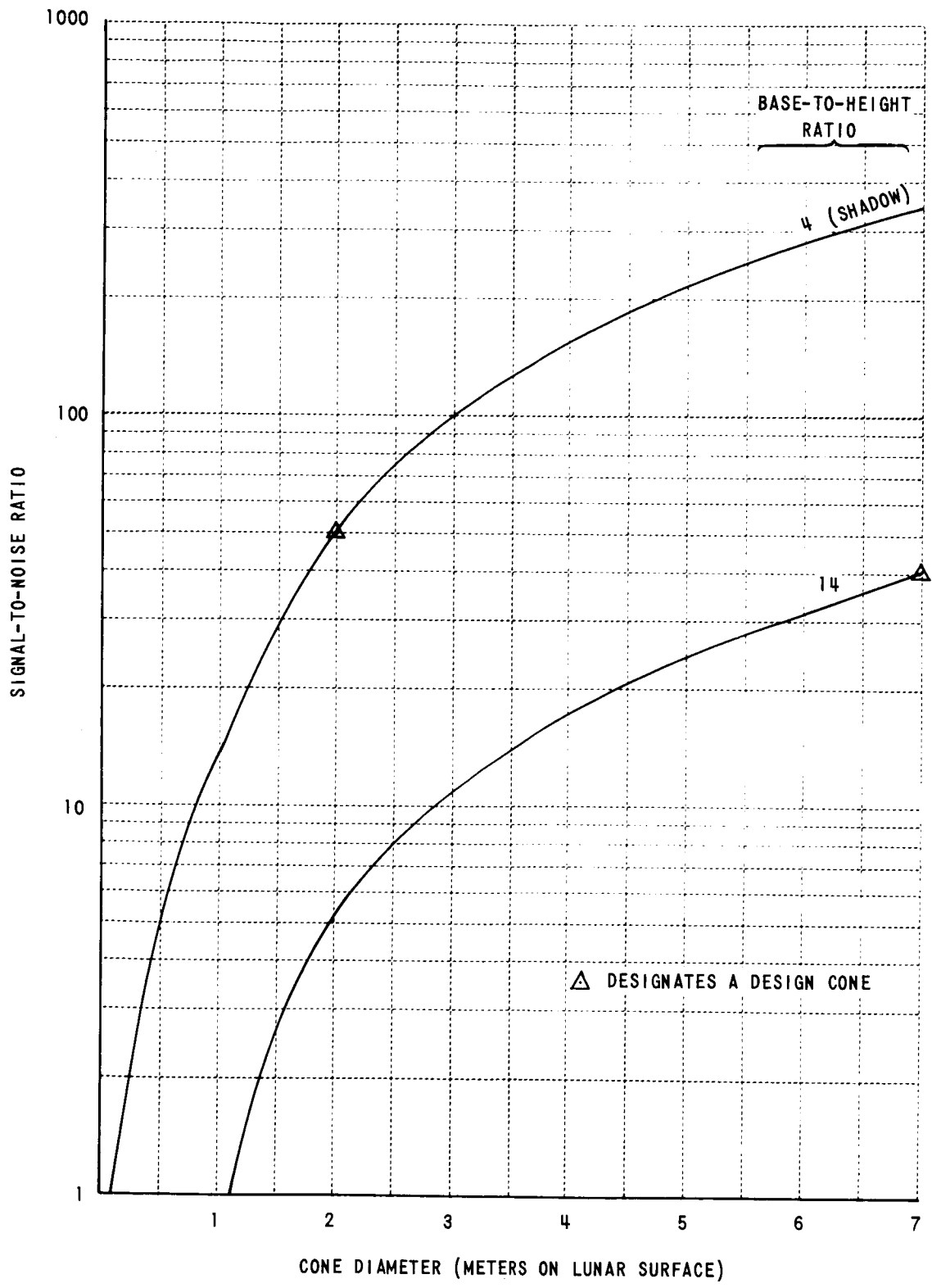


Figure 92 SIGNAL-TO-NOISE RATIO FOR CONE DETECTION - ORBITER II, HRF 63

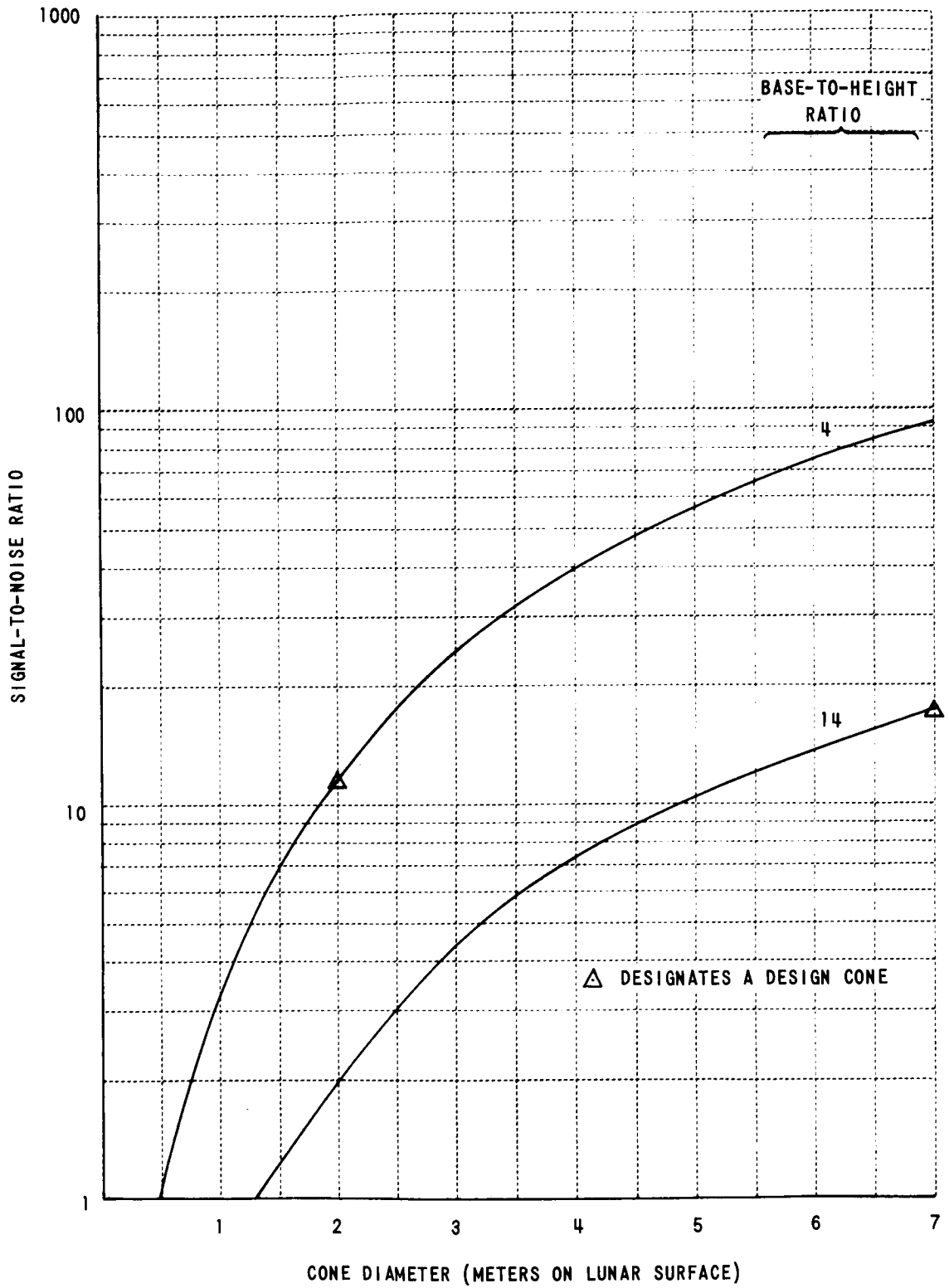


Figure 93. SIGNAL-TO-NOISE RATIO FOR CONE DETECTION - ORBITER II, HRF 69

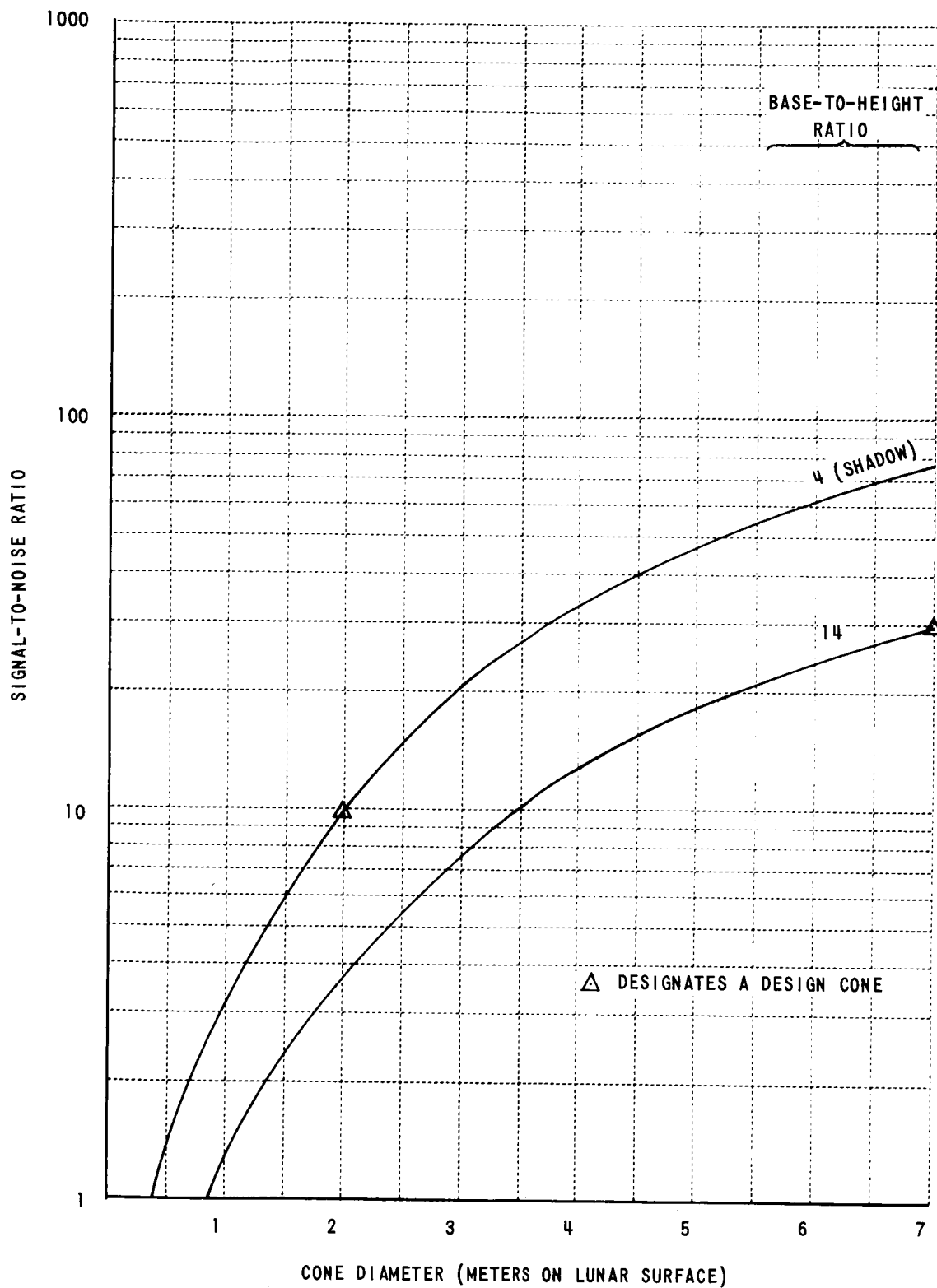


Figure 94 SIGNAL-TO-NOISE RATIO FOR CONE DETECTION - ORBITER II, HRF 88

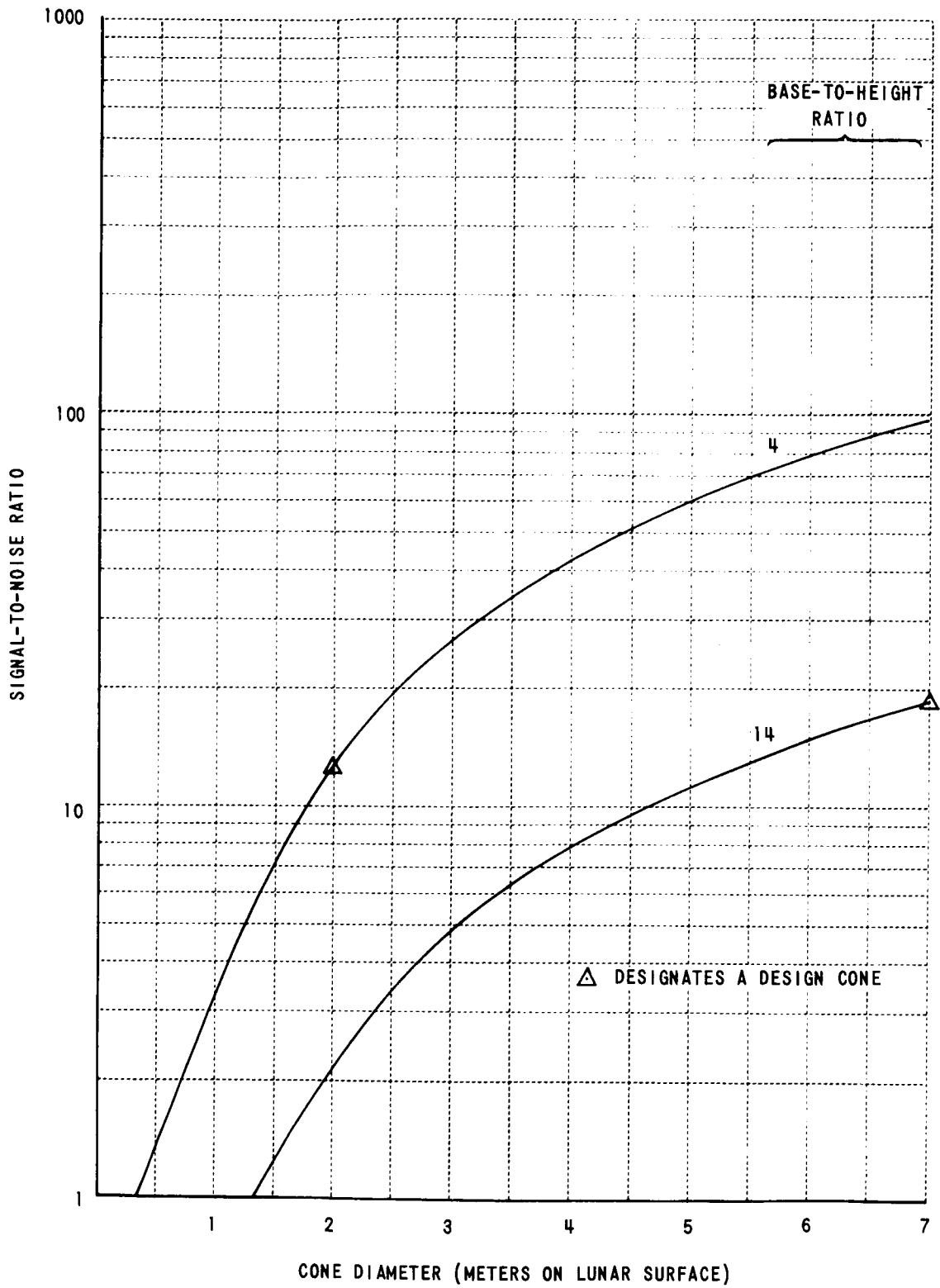


Figure 95 SIGNAL-TO-NOISE RATIO FOR CONE DETECTION - ORBITER II, HRF 99

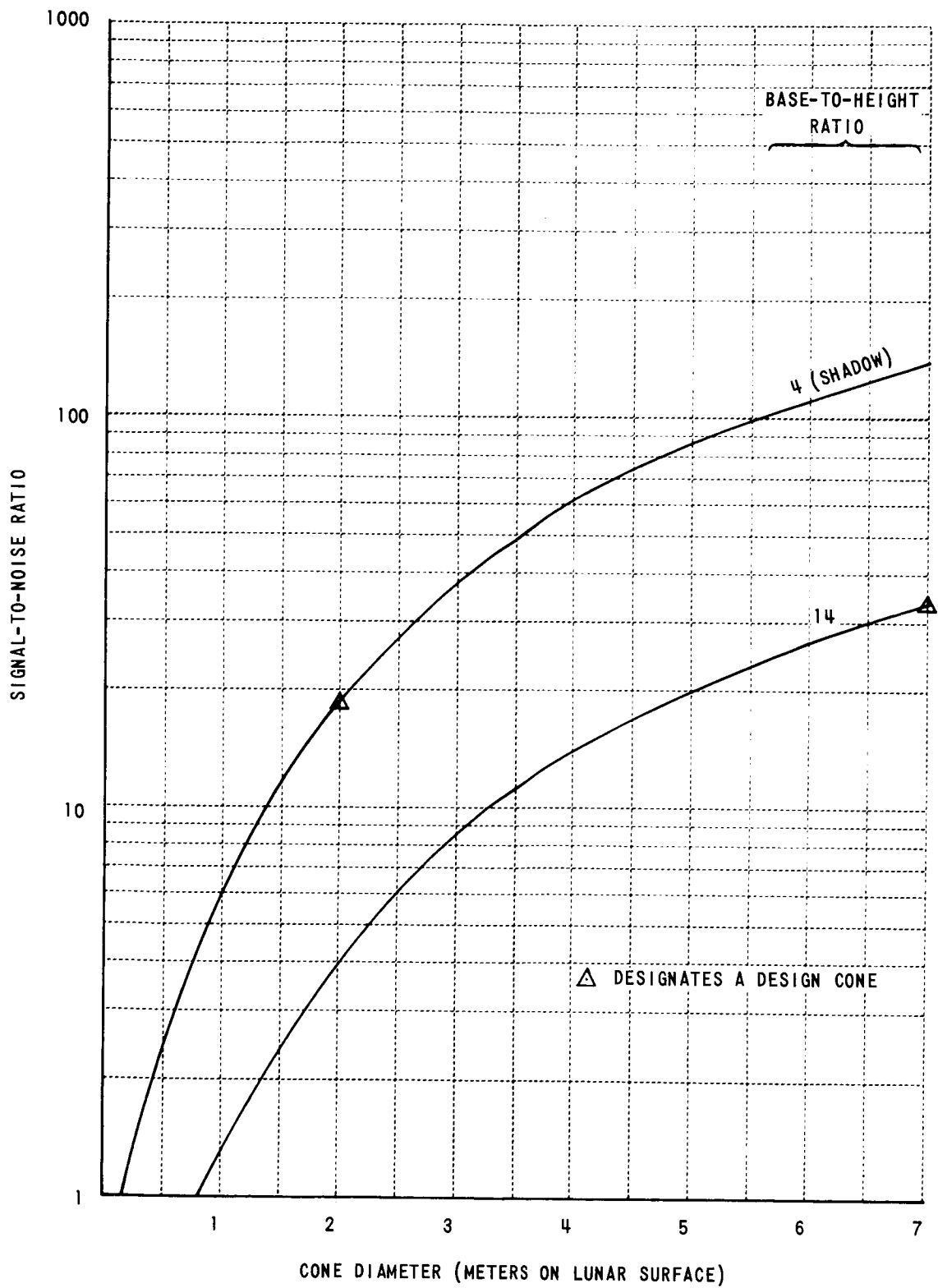


Figure 96 SIGNAL-TO-NOISE RATIO FOR CONE DETECTION - ORBITER II, HRF 141

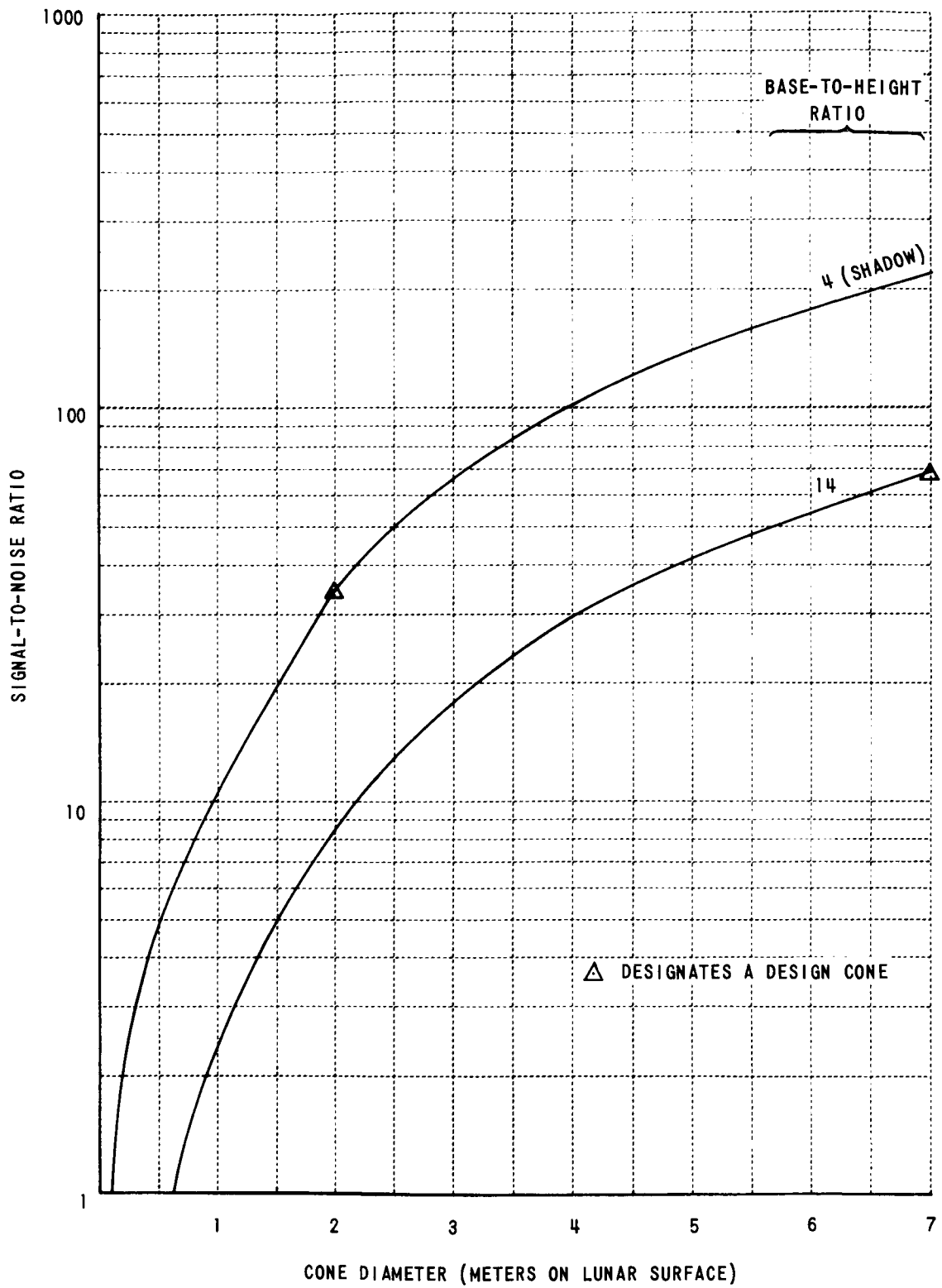


Figure 97 SIGNAL-TO-NOISE RATIO FOR CONE DETECTION - ORBITER II, HRF 157

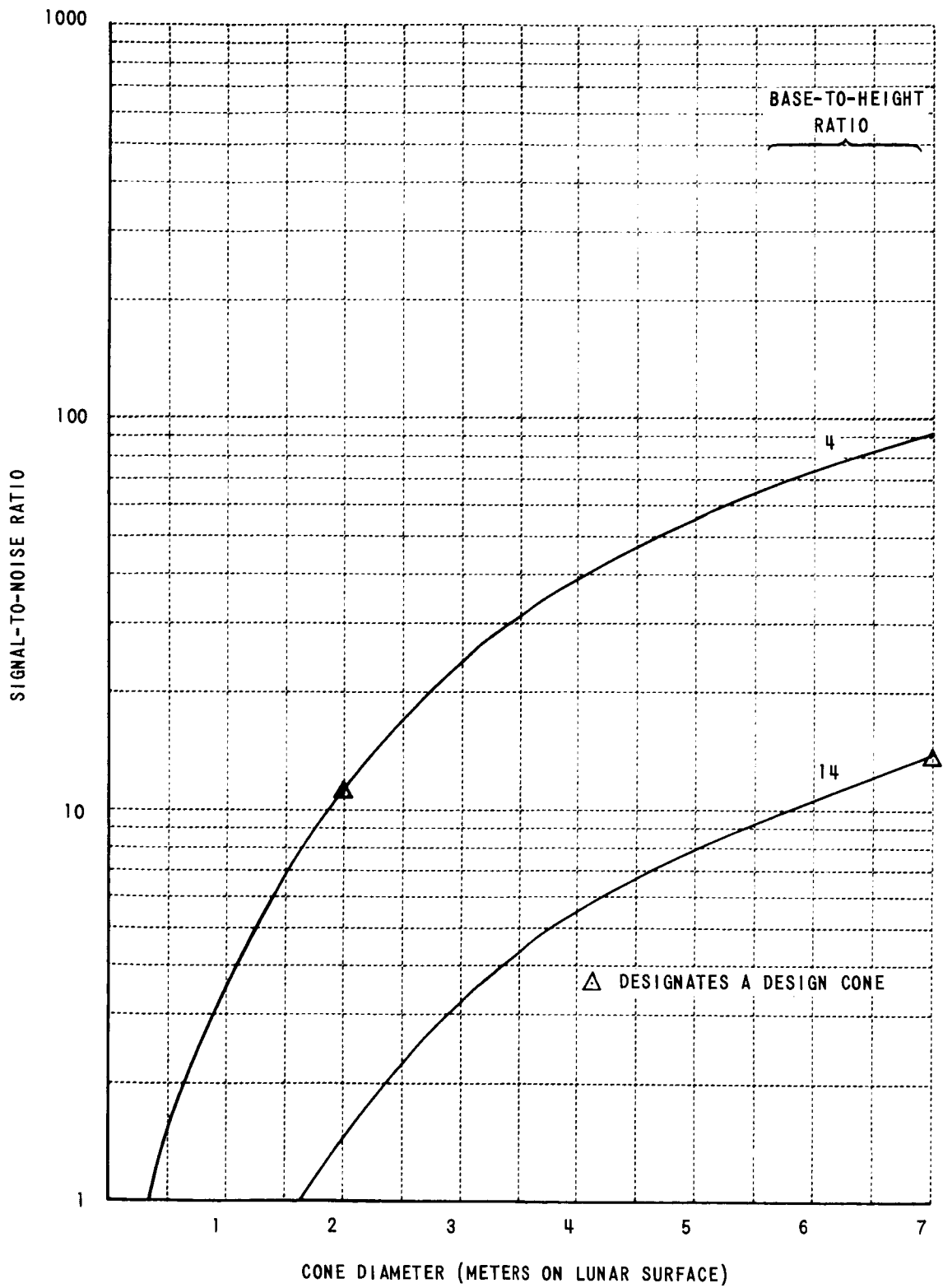


Figure 98 SIGNAL-TO-NOISE RATIO FOR CONE DETECTION - ORBITER II, HRF 174

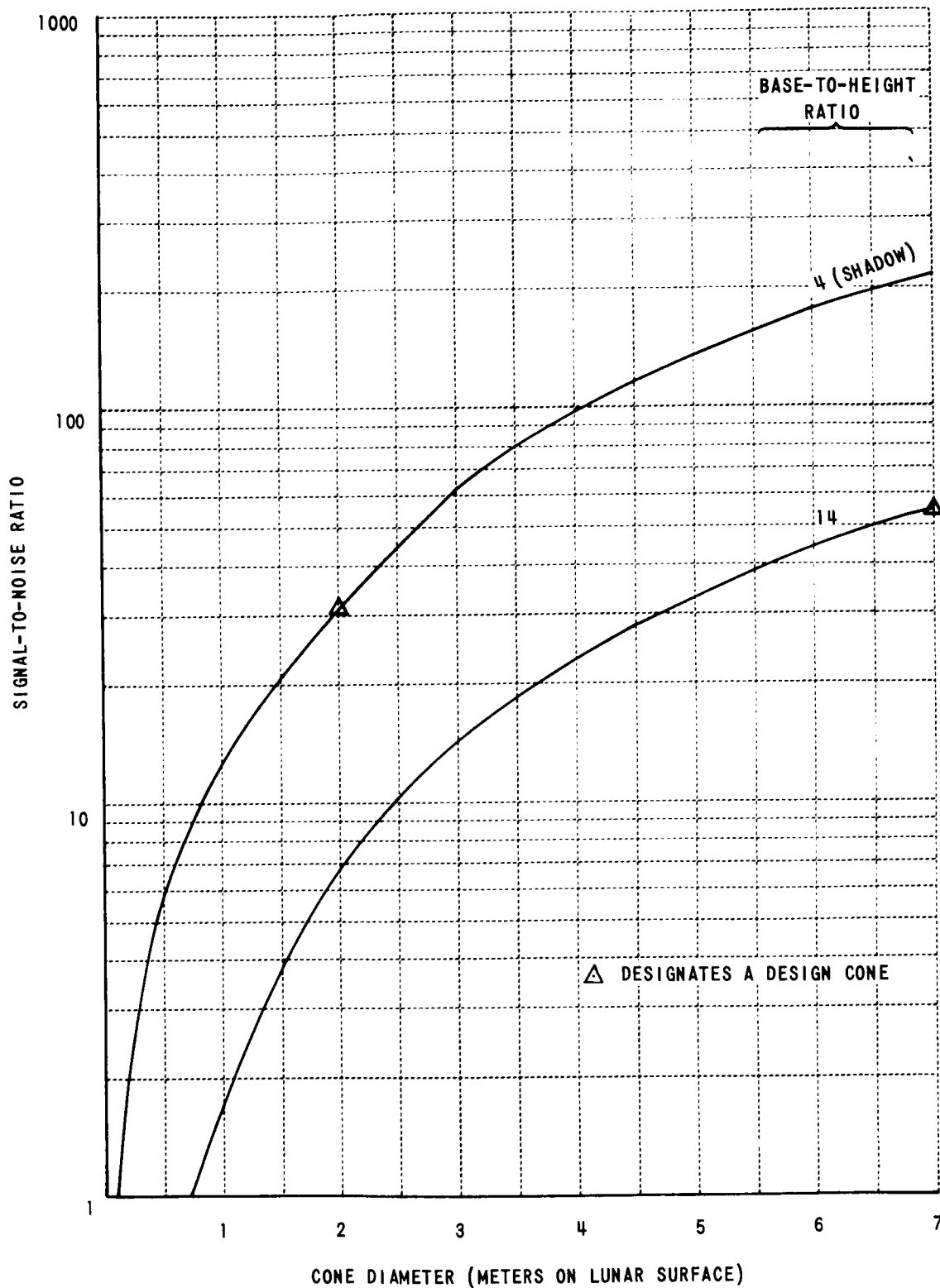


Figure 99 SIGNAL-TO-NOISE RATIO FOR CONE DETECTION - ORBITER II, HRF 183

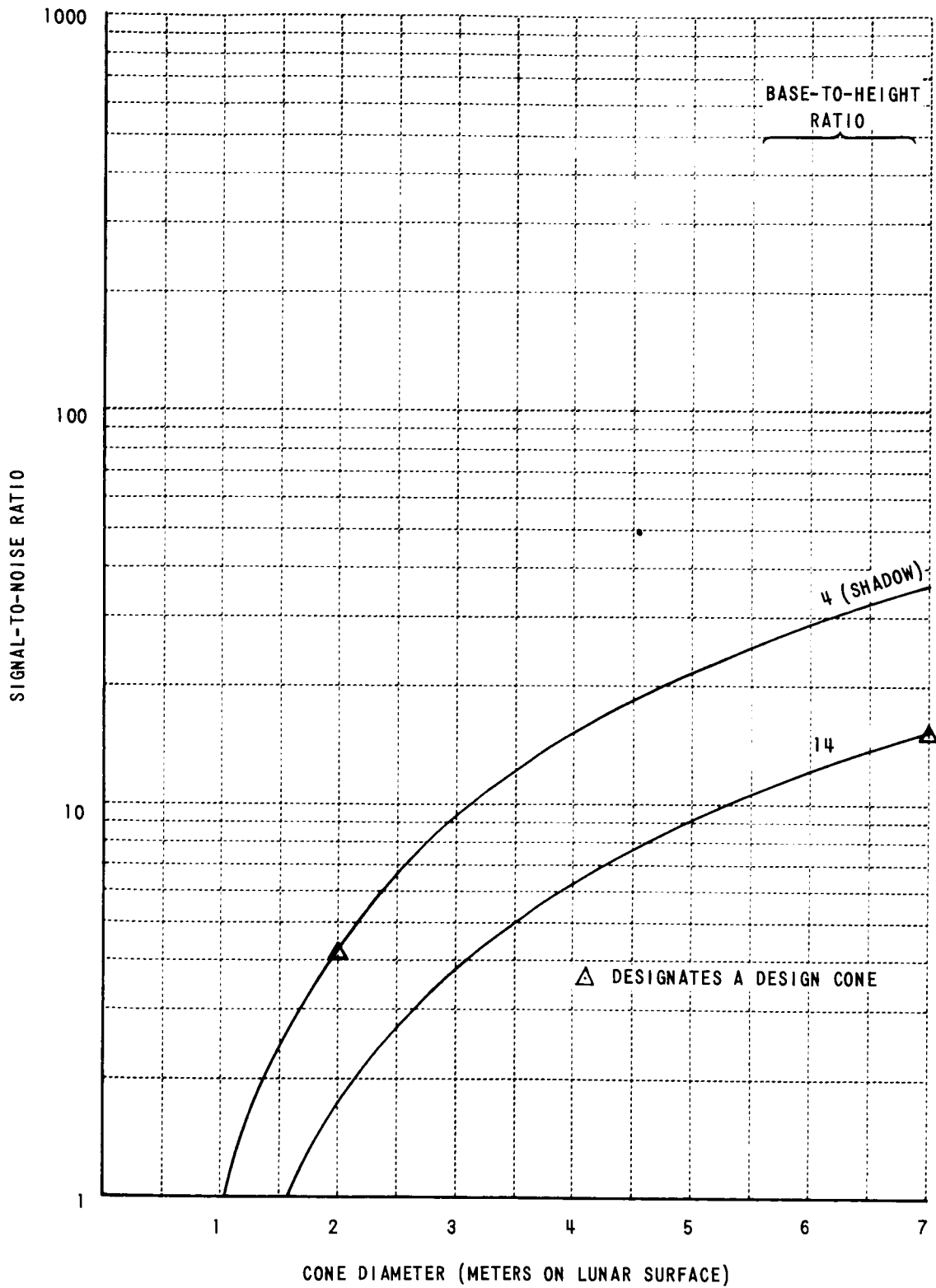


Figure 100 SIGNAL-TO-NOISE RATIO FOR CONE DETECTION - ORBITER II, HRF 208

PRECEDING PAGE BLANK NOT FILMED.

REFERENCES

1. Kinzly, R. E. ; Roetling, P. G. ; and Holladay, T.M. : Project SLOPE, Study of Lunar Orbiter Photographic Evaluation, Phase I Final Report. NASA CR-66158, May 20, 1966.
  2. Kinzly, R. E. ; and Mazurowski, M. J. : Project SLOPE, Study of Lunar Orbiter Photographic Evaluation, Phase II Final Report. NASA CR-66493, April 1, 1967.
  3. Mazurowski, M. J. ; and Holladay, T. M. : Project SLOPE, Study of Lunar Orbiter Photographic Evaluation, Phase III Final Report. NASA CR-66495, September 15, 1967.
- Coltman, J. W. : The Specification of Imaging Properties by Response to a Sine Wave Input. J. Opt. Soc. Am. , Vol. 44, No. 6, June 1954, p. 468.